

**Efficient microscale screening of various
Haematococcus pluvialis strains
for growth and astaxanthin production**

Inaugural-Dissertation

zur

Erlangung des Doktorgrades
der Mathematisch-Naturwissenschaftlichen Fakultät
der Universität zu Köln



vorgelegt von

Zehra Çebi

aus Köln

Köln, 2017

Berichtersteller: Prof. Dr. Michael Melkonian
(Gutachter) Prof Dr. Burkhard Becker

Tag der mündlichen Prüfung: 23.01.2017



Zusammenfassung

Das Ketocarotenoid Astaxanthin wird in der Natur von einigen Algen, Pflanzen, Pilzen und Bakterien synthetisiert. Hierbei besitzt die Grünalge *Haematococcus pluvialis* mit bis zu 4% des Trockengewichtes die höchste Kapazität Astaxanthin zu akkumulieren. Kommerziell wird natürliches Astaxanthin aus *H. pluvialis* als pharmazeutisch-funktionelles Lebensmittel für den Menschen und hauptsächlich als Färbemittel in der Aquakultur verwendet. Aufgrund hoher Produktionskosten von natürlichem Astaxanthin aus *H. pluvialis* wird der kommerzielle Astaxanthinmarkt von dem synthetischen Analogon dominiert. Da jedoch die Nachfrage für natürliches Astaxanthin stetig steigt, laufen die Bestrebungen zur Verbesserung von Massenkultursystemen für *H. pluvialis*, insbesondere auf technischer Ebene, auf Hochtouren, um die Produktionskosten zu senken und damit die Konkurrenzfähigkeit von natürlichem Astaxanthin auf dem Carotenoidmarkt zu erhöhen.

Der Fokus dieser Doktorarbeit liegt auf der Verbesserung der *H. pluvialis* Produktivität auf biologischer Ebene, nämlich durch Selektion und genetische Manipulation eines effizienten *H. pluvialis* Stammes. Hierfür wurden 26 Stämme mit geographisch unterschiedlicher Herkunft im Mikromaßstab analysiert. Schnell wachsende Stämme wurden entweder verschiedenen Stressfaktoren ausgesetzt, um die Astaxanthinproduktion zu induzieren, oder durch EMS Mutagenese manipuliert, um sowohl das Wachstum als auch die Astaxanthinproduktion zu verbessern. Zudem wurden phylogenetische Analysen durchgeführt.

Die Versuchsansätze im Mikromaßstab konnten sowohl für das Selektieren effizient wachsender Stämme als auch für das Selektieren von Stressfaktoren für eine effiziente Astaxanthinproduktion erfolgreich eingesetzt werden. Hierbei wurden fünf

effizient wachsende Stämme mit einem maximalen $AUC_{\text{exp}} / AUC_{\text{total}}$ Verhältnis von 100% identifiziert: *H. pluvialis* CCAC Stämme 0055, 2072, 3305, 3319 und SAG 34-1n. Zusätzlich wurde gezeigt, dass eine Kombination aus Phosphatmangel und Salzstress (0.8% NaCl) die Astaxanthinproduktion effizient steigern kann: eine finale Astaxanthinkonzentration von $51 \mu\text{g mL}^{-1}$ auf absoluter Ebene und $204 \text{ pg Zelle}^{-1}$ auf zellulärer Ebene konnten erzielt werden. Grundsätzlich konnte die finale Astaxanthinkonzentration bei einer Salzkonzentration von 0.3% und 0.5% deutlich gesteigert werden. Ob eine weitere Steigerung der Astaxanthinproduktion zwischen einer Salzkonzentration von 0.3% bis 0.5% möglich ist, müsste in zukünftigen Analysen untersucht werden. Im Versuchsansatz zur Optimierung eines *H. pluvialis* Stammes durch EMS Mutagenese konnten keine Mutanten generiert werden, die in ihrem Wachstum oder in ihrer Astaxanthinproduktion im positive Sinne übermäßig verändert waren. Zukünftig könnten physikalische und chemische Mutagenesen kombiniert werden, um den Erfolg zu steigern. Die phylogenetischen Analysen ergaben, dass *H. pluvialis* eine monophyletische Gruppe ist und dass die physiologischen Differenzen möglicherweise auf verschiedene Ökotypen zurück zu führen sind.

Insgesamt erwies sich das Screenen von *H. pluvialis* Stämmen für effizientes Wachstum und effiziente Astaxanthinproduktion im Mikromaßstab als attraktive, zeit- und platzsparende Alternative zu den üblicherweise eingesetzten Methoden.



Abstract

The ketocarotenoid astaxanthin is naturally synthesized by some algae, plants, fungi and bacteria. However, the freshwater chlorophyte *Haematococcus pluvialis* exhibits the highest capacity to accumulate astaxanthin in nature with up to 4% of the dry weight. Natural astaxanthin from *H. pluvialis* is commercially applied as nutraceuticals for human health and predominantly, as a colouring agent for aquaculture. Due to high production costs for natural astaxanthin from *H. pluvialis*, the commercial astaxanthin market is currently dominated by the synthetic analogue. Since the demand for natural astaxanthin is steadily increasing, attempts for improving *H. pluvialis* mass culture systems are ongoing, especially on technical level in order to assure lower production costs and thus, to elevate the competitiveness of natural astaxanthin on the carotenoid market.

This PhD project focuses on improving *H. pluvialis* productivity on a biological level by selection and genetic manipulation of an efficient *H. pluvialis* strain. For this, 26 strains from geographically diverse regions were screened on a microscale level. Best growing strains were either subjected to different stress factors for astaxanthin production or manipulated by EMS mutagenesis for improving both, growth and astaxanthin production. Furthermore, phylogenetic analyses were performed.

Using the microscale approach for efficient growth, five strains were successfully detected with a maximal $AUC_{\text{exp}} / AUC_{\text{total}}$ ratio of 100%: *H. pluvialis* CCAC strains 0055, 2072, 3305, 3319 and SAG 34-1n. Additionally, the microscale approach successfully facilitated the detection of stress conditions for efficient astaxanthin production in *H. pluvialis* CCAC 3305: the combination of phosphorus-deficiency and salt stress (0.3% NaCl) yielded in a final astaxanthin concentration of $51 \mu\text{g mL}^{-1}$ in

total and 204 pg cell⁻¹ on a cellular level. In general, final concentration of total astaxanthin in full and nutrient deficient medium was increased when combined with 0.3 and 0.5%. Future analyses of salt concentrations ranging from 0.3 to 0.5% might reveal even more efficient kinetics of astaxanthin production. Furthermore, the strain improvement approach via EMS mutagenesis did not generate any hyper-growing or hyper-astaxanthin accumulating mutants suggesting coupling of physical and chemical mutagens for future molecular breeding approaches. Finally, phylogenetic analyses revealed that *H. pluvialis* is a monophyletic group comprising physiological differences possibly caused by different ecotypes.

Overall, microscale screening of *H. pluvialis* strains for efficient growth and astaxanthin production constitutes an attractive, time- and space-saving alternative to other generally applied methods.

Contents

Zusammenfassung	3
Abstract.....	5
Contents.....	7
List of abbreviations	9
List of units and symbols.....	13
List of tables	15
List of figures	16
1 Introduction	19
1.1 Carotenoids in nature	19
1.2 Astaxanthin as a commercial carotenoid.....	20
1.3 Natural astaxanthin from <i>Haematococcus pluvialis</i>	22
1.4 Attempts for <i>H. pluvialis</i> strain improvement by mutagenesis	25
1.5 Aims of this study	27
2 Material and methods	28
2.1 Cultivation and maintenance of microalgal strains	28
2.1.1 Microalgal strains.....	28
2.1.2 Culture medium	30
2.1.3 Cultivation conditions.....	31
2.1.4 Establishment of axenic cultures	31
2.1.5 Maintenance of axenic cultures	32
2.2 Physiological analysis.....	33
2.2.1 Analysis of growth kinetics for 26 <i>H. pluvialis</i> strains	33
2.2.2 Determination of temperature optima for selected <i>H. pluvialis</i> strains ...	35
2.2.3 Induction and quantification of astaxanthin in <i>H. pluvialis</i> CCAC 3305 ..	37
2.3 Molecular analysis	38
2.3.1 Isolation of genomic DNA.....	38
2.3.2 DNA quality control.....	39
2.3.3 Genome size estimation of 26 <i>H. pluvialis</i> strains	40
2.3.4 DNA sequencing and phylogenetic analyses of 26 <i>H. pluvialis</i> strains ..	41

2.4 Strain improvement approach	44
2.4.1 EMS mutagenesis of <i>H. pluvialis</i> CCAC 0125.....	44
2.4.2 Screening and verification of putative EMS mutants	46
2.4.3 Growth of suspended and immobilized EMS mutants.....	47
2.5 Data analysis	49
3 Results	50
3.1 Growth kinetics of <i>H. pluvialis</i> strains	50
3.2 Astaxanthin production in <i>H. pluvialis</i> CCAC 3305.....	55
3.3 Genome size of various <i>H. pluvialis</i> strains	62
3.4 Phylogenetic analysis of <i>H. pluvialis</i> strains	63
3.5 EMS mutagenesis of <i>H. pluvialis</i> CCAC 0125.....	66
4 Discussion	73
4.1 Efficient microscale screening of <i>H. pluvialis</i> concerning growth	73
4.2 Efficient microscale induction of astaxanthin in <i>H. pluvialis</i>	75
4.3 Genome size of <i>H. pluvialis</i>	77
4.4 Phylogeny of <i>H. pluvialis</i>	78
4.5 Putative EMS mutants of <i>H. pluvialis</i>	81
5 Conclusion and outlook	86
6 References.....	87
7 Appendix.....	100
7.1 Chemical index	100
7.2 Micrographs of <i>H. pluvialis</i> CCAC 0125	102
7.3 Set-up of microscale experiments	103
7.4 Supplementary data for phylogenetic analyses.....	107
7.4.1 IUPAC nucleotide ambiguity code	107
7.4.2 Supplementary data for <i>rbcl</i>	108
7.4.3 Supplementary data for ITS 2.....	109
7.5 Supplementary information on EMS mutants	110
7.5.1 Photographs and stereomicrographs of plates.....	110
7.5.2 Supplementary data for mutant verification	112
Acknowledgements	115
Erklärung	117
Lebenslauf	118

List of abbreviations

A	Adenine
Acetate	Glacial acetic acid
ACOI	Coimbra Collection of Algae, Portugal
Approx.	Approximately
AUC	Area under curve
AUC _{exp}	Area under exponential curve
AUC _{non-exp}	Area under non-exponential curve
AUC _{total}	Area under total curve
BG-11	Blue-green (culture medium) No. 11
BKT	Beta-carotene-ketolase
BSM	Bacterial standard medium
C	Cytosine
CBC(s)	Compensatory base change(s)
CCAC	Culture Collection of Algae at the University of Cologne, Germany
CCAP	Culture Collection of Algae and Protozoa, UK
CCCryo	Culture Collection of Cryophilic Algae
cfu	Colony forming units
CO ₂	Carbon dioxide
Col	Colony
CTAB	Cetyltrimethylammonium bromide
dc	Daughter colony
DMSO	Dimethyl sulfoxide
DNA	Deoxyribonucleic acid
dNTPs	Deoxyribonucleoside triphosphate
DPA	Diphenylamine

DW	Dry weight
E	Mutant(s) generated with EMS
EDTA	Ethylenediaminetetraacetic acid
e.g.	For example (Latin phrase: <i>exempli gratia</i>)
EMS	Ethyl methanesulfonate
et al.	And others (Latin phrase: <i>et alii</i>)
EtBr	Ethidium bromide
FACS	Fluorescence-activated cell sorting
G	Guanine
gDNA	Genomic DNA
GTR	Generalized Time Reversible
HEPES	4-(2-hydroxyethyl)-1-piperazineethanesulfonic acid
HSP70A	Heat-shock protein 70A
i	Index
ID	Identity
i.e.	That is (Latin phrase: <i>id est</i>)
IQR	Interquartile range
ITS2	Internal transcriber spacer 2
IUPAC	International Union of Pure and Applied Chemistry
LED	Light-emitting diode
LI	Light intensity
LSU	Large subunit
mc	Mother colony
ML	Maximum likelihood
MNNG	N-methyl-N-nitro-N-nitrosoguanidine
n	Number of replicates
n.a.	No details available
NIES	Microbial Culture Collection at the National Institute for Environmental Studies, Japan
No.	Number (Latin word: <i>numero</i>)
nt	Nucleotides
O ₂	Oxygen
OD	Optical density
PBR(s)	Photobioreactor(s)
PCM(s)	Polycarbonate membrane(s)

PCR	Polymerase chain reaction
PDS	Phytoene desaturase
PFD	Photon flux density
PMMA	Polymethyl methacrylate
PP	Polypropylene
PS	Polystyrene
PSBR(s)	Porous substrate bioreactor(s)
PSY	Phytoene synthase
PTOX	Plastid terminal oxidase
PVC	Polyvinyl chloride
PVP	Polyvinylpyrrolidone
rbcl	RuBisCo LSU
RBCS2	RuBisCo SSU
RCF	Relative centrifugal force
RuBisCo	Ribulose-1,5-bisphosphate carboxylase/ oxygenase
rDNA	Ribosomal DNA
RNA	Ribonucleic acid
rRNA	Ribosomal RNA
RAxML	Randomized Accelerated Maximum Likelihood
ROS	Reactive oxygen species
RT	Room temperature
RuBisCO	Ribulose-1,5-bisphosphate carboxylase/ oxygenase
SAG	Sammlung von Algenkulturen Göttingen, Germany
SD	Standard deviation
SDS	Sodium dodecyl sulfate
SE	Standard error
SSU	Small subunit
T	Thymine
TAE	Tris-Acetate-EDTA
Taq	<i>Thermus aquaticus</i>
TE	Tris-EDTA
TL	Twin-layer
Tris	Tris (hydroxymethyl) aminomethane
U	Uracil
UV	Ultraviolet

v.	Version
vs.	against, turned (Latin word: <i>versus</i>)
v/v	Volume per volume
WT	Wild type
w/v	Weight per volume

List of units and symbols

Units occurring in this thesis are listed in Table 1.

Table 1 List of units sorted by corresponding parameters in alphabetical order

Parameter	Name of unit	Symbol of unit
Electric unit	Ampere	A
	Volt	V
	Watt	W
Length	Meter	m
Mass	Gram	g
Molecular unit	Base pair	bp
	Molar [mol L^{-1}]	M
	Mole	mol
	Normality	N
	Svedberg	S
RCF	Gravitational force	<i>g</i>
Temperature	Degree Celsius	°C
Time	Day(s)	d
	Hour(s)	h
	Minute(s)	min
	Second(s)	s
Volume	Liter	L

Prefixes of units are listed in Table 2.

Table 2 List of prefixes sorted by increasing decimal sub-/ multiples of units

Sub-/ Multiple of unit	Name of prefix	Symbol of prefix
<i>Submultiple</i>		
10^{-12}	Pico	p
10^{-9}	Nano	n
10^{-6}	Micro	μ
10^{-3}	Milli	m
10^{-2}	Centi	c
<i>Multiple</i>		
10^3	Kilo	k
10^6	Mega	M
10^9	Giga	G

Mathematical and greek symbols occurring in this thesis are listed in Table 3.

Table 3 List of symbols alphabetically sorted by their meanings

Symbol	Meaning
β	Beta
R^2	Coefficient of determination
\emptyset	Diameter
$\gamma; \Gamma$	Gamma
∞	Infinity
I	Iota
%	Percent
Σ	Summation

List of tables

Table 1 List of units sorted by corresponding parameters in alphabetical order.....	13
Table 2 List of prefixes sorted by increasing decimal sub-/ multiples of units.....	14
Table 3 List of symbols alphabetically sorted by their meanings	14
Table 4 <i>Haematococcus pluvialis</i> strains	29
Table 5 Composition of modified BG-11 culture medium.....	30
Table 6 Composition of BSM and Sabouraud agar.....	31
Table 7 Composition of buffers required for CTAB-DNA extraction.....	38
Table 8 Composition of TAE buffer	40
Table 9 List of forward and reverse PCR primers and their 5' to 3' sequences.	41
Table 10 PCR program 'BM45cyc' for the amplification of <i>rbcL</i>	42
Table 11 PCR program 'BM55cyc' for the amplification of rDNA sequences	42
Table 12 Sequencing primers	43
Table 13 Chemical index.....	100
Table 14 IUPAC nucleotide ambiguity code.....	107

List of figures

Figure 1 Biosynthetic pathway of carotenoids in microalgae	21
Figure 2 Biosynthetic pathway of astaxanthin in <i>Haematococcus pluvialis</i>	24
Figure 3 Example of AUC determinations for growth analyses.....	34
Figure 4 Linear increase of temperature using the temperature gradient device.....	36
Figure 5 Astaxanthin calibration curve	38
Figure 6 Schematic visualization of applied primer combinations.....	42
Figure 7 Survival rates of <i>H. pluvialis</i> CCAC 0125 exposed to EMS	45
Figure 8 Example for verification of EMS mutants based on colony size	46
Figure 9 Schematic illustration of laboratory-scale TL PSBR	48
Figure 10 Growth kinetics of 26 <i>H. pluvialis</i> strains at 23°C and 50 $\mu\text{mol m}^{-2} \text{s}^{-1}$	51
Figure 11 Growth curves of <i>H. pluvialis</i> CCCryo 096-99 and SAG 44.96 from two independent experiments.....	52
Figure 12 Calculated growth parameters for 24 <i>H. pluvialis</i> strains.....	53
Figure 13 Cell densities of six selected <i>H. pluvialis</i> strains at ten different temperatures and 50 $\mu\text{mol photons m}^{-2} \text{s}^{-1}$	54
Figure 14 Temperature optimum of six selected <i>H. pluvialis</i> strains grown at ten different temperatures and 50 $\mu\text{mol photons m}^{-2} \text{s}^{-1}$	55
Figure 15 Comparison and correction of growth curves of <i>H. pluvialis</i> CCAC 3305 from independent experiments at 23°C and 50 $\mu\text{mol photons m}^{-2} \text{s}^{-1}$	57
Figure 16 Development of cell growth, absolute and cellular astaxanthin content of <i>H. pluvialis</i> CCAC 3305 grown at 23°C and 50 $\mu\text{mol photons m}^{-2} \text{s}^{-1}$ under optimal and stress conditions	58

Figure 17 Comparison of two independent salt stress experiments concerning cell growth, absolute and cellular astaxanthin content of <i>H. pluvialis</i> CCAC 3305 grown at 23°C and 50 $\mu\text{mol photons m}^{-2} \text{s}^{-1}$	59
Figure 18 Correction of two independent salt stress experiments concerning cell growth, absolute and cellular astaxanthin content of <i>H. pluvialis</i> CCAC 3305 grown at 23°C and 50 $\mu\text{mol photons m}^{-2} \text{s}^{-1}$	60
Figure 19 Development of cell growth, absolute and cellular astaxanthin content of <i>H. pluvialis</i> CCAC 3305 grown at 23°C and 50 $\mu\text{mol photons m}^{-2} \text{s}^{-1}$ under salt stress conditions	61
Figure 20 Genome size of 26 <i>H. pluvialis</i> strains	63
Figure 21 Phylogenetic tree from combined ML analyses of <i>rbcL</i> gene and rDNA sequences (5.8S, ITS2 and partial 28S)	64
Figure 22 Consensus secondary structure model of ITS2 in <i>H. pluvialis</i>	65
Figure 23 Number of achieved cfu for WT and EMS treated samples of <i>H. pluvialis</i> CCAC 0125	66
Figure 24 Development of colony size of WT and EMS treated samples at two different light intensities	67
Figure 25 Stereomicroscopical verification of WT colonies based on colony diameter	68
Figure 26 Stereomicroscopical verification of EMS mutants based on colony diameter	69
Figure 27 Growth curves of <i>H. pluvialis</i> CCAC 0125 WT and five EMS mutants grown at 23°C and 50 $\mu\text{mol photons m}^{-2} \text{s}^{-1}$	70
Figure 28 Calculated growth parameters for <i>H. pluvialis</i> CCAC 0125 WT and five EMS mutants	71
Figure 29 Biomass and astaxanthin kinetics of immobilized <i>H. pluvialis</i> CCAC 0125 WT and EMS mutant E1-16 col-4 using TL-PBSR	71
Figure 30 Comparison of <i>H. pluvialis</i> CCAC 0528 and SAG 34-1I with corresponding subisolates CCAC 1023 and SAG 34-1I (2), respectively	80
Figure 31 Comparison of biomass and astaxanthin kinetics of immobilized <i>H. pluvialis</i> CCAC 0125 WT _{K-Ref} taken from Kiperstok (2016) with EMS mutant E1-16 col-4	84
Figure 32 Micrographs of <i>H. pluvialis</i> CCAC 0125	102
Figure 33 Set-up of microscale experiments	103
Figure 34 Prototype of the temperature gradient device	103

Figure 35 Final temperature gradient device	104
Figure 36 Growth kinetics of CCAC 0055, CCAC 2072 and CCAC 3305 at ten different temperature conditions (11.8 to 31.8°C) and 50 $\mu\text{mol photons m}^{-2} \text{s}^{-1}$	105
Figure 37 Growth kinetics of CCAC 3319, SAG 34-1n and SAG 44.96 at ten different temperature conditions (11.8 to 31.8°C) and 50 $\mu\text{mol photons m}^{-2} \text{s}^{-1}$	106
Figure 38 Phylogenetic tree from ML analyses of <i>rbcL</i> gene.....	108
Figure 39 Phylogenetic tree from ML analyses of ITS2 rDNA sequences	109
Figure 40 Upside down incubation of agar plates	110
Figure 41 Exemplary stereomicrographs of WT and selected mutants	111
Figure 42 Non-reproducible EMS mutants based on stereomicroscopical analysis of colony diameter	112

1

Introduction

The highly diverse, polyphyletic group of pro- and eukaryotic algae contribute about 50% of global photosynthetic activity and constitute a considerable importance for scientific and commercial issues (Cardozo et al., 2007; Chacon-Lee & Gonzalez-Marino, 2010). One factor that displays the diversity of these organisms is their capability to populate various habitats with geographically diverse origin. The occurrence of algae is not limited to aqueous environments comprising freshwater, marine and brackish water. Terrestrial, epiphytic and epilithic appearance is also common, i.e. algae growing on soil, plants and stones, respectively. Along with a photosynthetic mode of life, heterotrophic, mixotrophic, symbiotic (e.g. lichens, endosymbionts) and parasitic life forms are known (Lee, 2008). Algae harbor diverse bioactive compounds as a consequence of adapting their metabolic machinery to respective environments or rather to environmental stresses (e.g. high or low temperature, drought, salinity or exposition to UV irradiance). Metabolites like polysaccharides, fatty acids or carotenoids are of great biotechnological interest since they can be applied as health food, feed additives or pharmaceuticals (Olaizola, 2003; Cardozo et al., 2007; Guedes et al., 2011).

1.1 Carotenoids in nature

Photosynthetic organisms, some bacteria and fungi are capable to synthesize carotenoids de novo, whereas vertebrates lack this ability and obtain carotenoids from their diet. Carotenoids constitute a group of lipid-soluble pigments comprising carotenes and xanthophylls. Carotenes consist of hydrocarbon chains with either free or cyclized ends (ionone rings). Xanthophylls are derivatives of carotenes with

oxygen containing functional groups substituted to the ionone rings. In microalgae, carotenoids are synthesized via the non-mevalonate pathway (Figure 1): isoprenoid molecules (C₅) are converted enzymatically to tetraterpenoid structures (C₄₀ polyene backbone). Carotenoids of photosynthetic organisms function as accessory pigments in light harvesting complexes of photosystems. Upon exposition to excess light, they serve as non-photochemical quenchers or scavengers of reactive oxygen species (ROS) or free radicals. Primary carotenoids serve as functional components of the photosynthetic apparatus and are localized in the thylakoid membrane, whereas secondary carotenoids serve as stress response molecules and rather occur in lipid vesicles in the plastid stroma or in the cytosol (Cardozo et al., 2007; Chandi & Gill, 2011; Guedes et al., 2011). Except for some microalgae, carotenoids are synthesized and accumulated within the plastids. However, some secondary xanthophylls like astaxanthin accumulate in the cytosol presuming a cytosolic site of carotenoid biosynthesis or an export mechanism from plastid to cytoplasm (Grünewald et al., 2001; Guerin et al., 2003; Lemoine & Schoefs, 2010; Guedes et al., 2011).

1.2 Astaxanthin as a commercial carotenoid

The worldwide market value for commercial carotenoids accounts for approximately 1.5 billion US\$ (reference year: 2014) with an estimated growth rate of 3.9% per year (BCC Research, 2015). Carotenoids are applied for food, cosmetic and pharmaceutical industries as colorants, antioxidants or anti-carcinogenic and anti-inflammatory compounds. For instance, β -carotene is valuable for human nutrition due to its pro-vitamin A activity. However, the high-value ketocarotenoid astaxanthin exhibits more than ten times higher antioxidant activity than β -carotene and other carotenoids (e.g. zeaxanthin or lutein). Astaxanthin is applied as health food, pharmaceuticals or feed additives, e.g. in aquaculture for the coloration of fins, skin and flesh of salmon or trout in order to increase the acceptance for the seafood market (Cardozo et al., 2007; Chandi & Gill, 2011; Guedes et al., 2011).

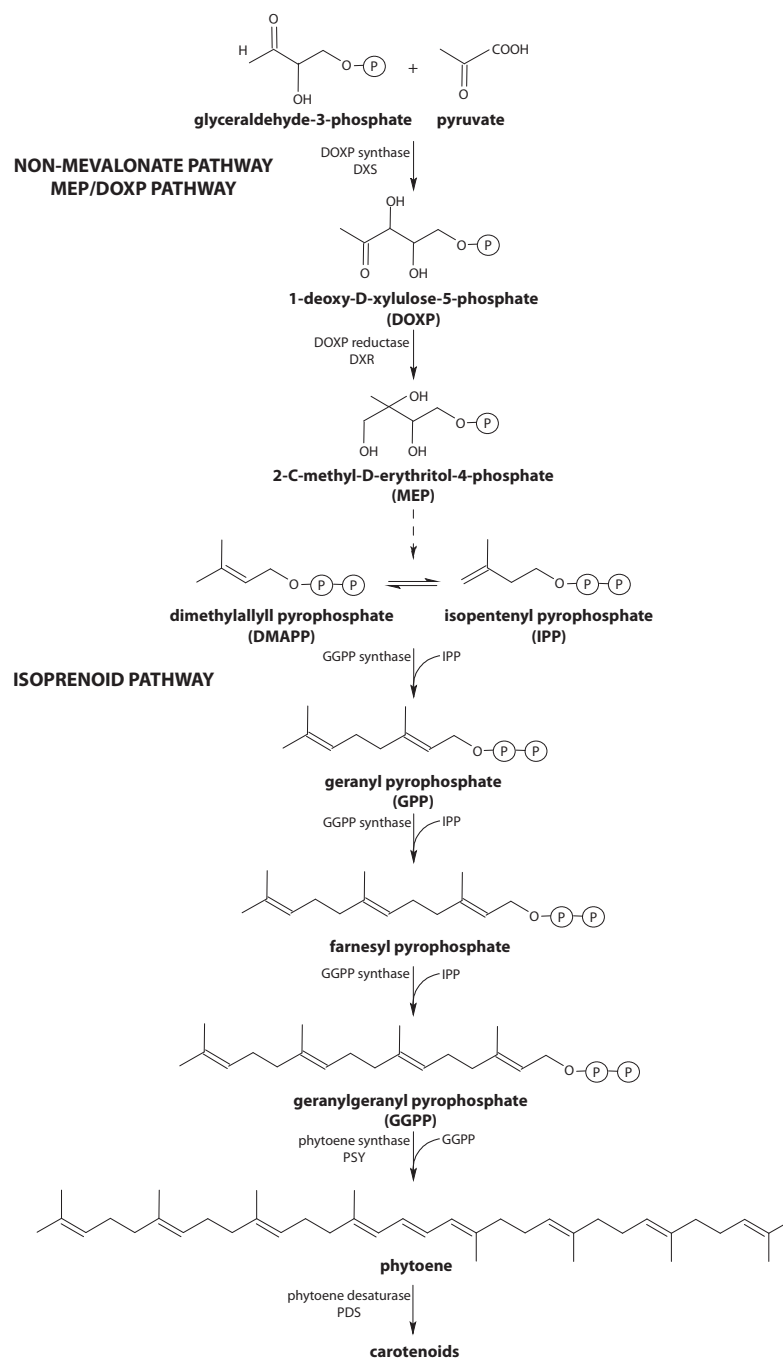


Figure 1 Biosynthetic pathway of carotenoids in microalgae. Pathway and involved enzymes were adapted from literature (Goodwin, 1961; Britton, 1976; Steinbrenner & Linden, 2001; Huang et al., 2006; Lohr, 2011) and structural formula were generated with the freeware ChemSketch (ACD/Labs, 2013).

The market value for astaxanthin accounts for approximately 447 million US\$ (reference year: 2014) and is expected to increase to more than 1.1 billion US\$ by the year 2020 (Industry Experts, 2015). In nature, astaxanthin is synthesized by some algae, plants, fungi and bacteria (Goodwin, 1961). In contrast to the commercial production of astaxanthin from natural sources, production costs for the synthetic analogue are low. The selling price of synthetic and natural astaxanthin

accounts for 1000 and 3000 \$ kg⁻¹, respectively. Consequently, more than 95% of commercially available astaxanthin derive from synthetic production by chemical synthesis. However, market demand for natural astaxanthin is increasing since chemical synthesis derives from petrochemicals and leads to the production of a mixture of stereoisomers (3R,3R', 3S,3S' and 3R,3S' enantiomers) with lower bioactivity than the natural analogue (3S,3S' conformation). Furthermore, optimization of natural astaxanthin production is progressing and thus future decrease of production costs is promising (Ausich, 1997; Lorenz & Cysewski, 2000; Guerin et al., 2003; Aflalo et al., 2007; Del Campo et al., 2007; Lemoine & Schoefs, 2010; Guedes et al., 2011)

1.3 Natural astaxanthin from *Haematococcus pluvialis*

The freshwater green alga *Haematococcus pluvialis* (Chlorophyceae) exhibits, with up to 4% by dry weight, the highest capacity to accumulate astaxanthin in nature. Astaxanthin (3,3'-dihydroxy-4,4'-diketo- β -carotene) is a derivative of β -carotene (Figure 2) and is accumulated upon stress conditions, e.g. nutrient deficiency, salt stress, high light intensities (Boussiba, 2000; Li et al., 2008; Lemoine & Schoefs, 2010).

The life cycle of *H. pluvialis* comprises different cell types based on environmental growth conditions. Under favorable conditions, *H. pluvialis* cells occur as ellipsoidal to spherical biflagellates with a cup-shaped chloroplast bearing multiple pyrenoids. The protoplast of flagellates is connected to the cell wall by numerous cytoplasmic strands. Under suboptimal conditions, cells shed their flagella and transform to coccoid palmella cells with a protoplast attached to the cell wall. In the vegetative stage, biflagellates and palmella cells can produce two to eight daughter cells by asexual reproduction. If adverse growth conditions are persistent, cells transform into enlarged aplanospores (or akinetes) (Elliott, 1934; Droop, 1953; Droop, 1954; Droop, 1955; Pocock, 1960). Akinetes are surrounded by a thick cellulose wall containing sporopollenin-like substances (algaenan). On the one hand, akinete formation is accompanied by cessation of mitotic cell division, decrease in photosynthetic and metabolic activity and on the other hand, by an increase in carbohydrate, lipid and astaxanthin content. Astaxanthin is accumulated in cytosolic lipid bodies, first around

the nucleus, then throughout the whole cytosol. The carotenoid fraction of akinetes contains up to 98% astaxanthin. Due to stability reasons, most of the astaxanthin molecules are esterified to fatty acids. The astaxanthin pool of akinetes consists of 70% monoesters, 25% diesters and 5% free astaxanthin. Storage of carbon and energy by astaxanthin accumulation facilitates *H. pluvialis* to survive unfavorable conditions. If akinetes are exposed back to optimal growth conditions, vegetative cell cycle is initiated by producing new zoospores (Boussiba, 2000; Hagen et al., 2002; Guerin et al., 2003; Damiani et al., 2006; Kang & Sim, 2008; Guedes et al., 2011).

Sexual reproduction is rarely reported for *H. pluvialis*. Extreme unfavourable growth conditions (e.g. starvation, desiccation or freezing), followed by optimal conditions seem to initiate gametogenesis. In this case, akinetes can release of up to 64 isogametes (Pocock, 1960; Lee & Ding, 1994; Triki et al., 1997; Pröschold, 1998).

For the commercial production of natural astaxanthin in large-scale facilities, *H. pluvialis* is first cultivated in enclosed photobioreactors under favorable growth conditions (green stage). Afterwards, the green biomass is transferred to open ponds where cells are exposed to stress conditions, e.g. high light intensities, in order to induce astaxanthin accumulation (red stage). The final commercial product contains up to 2% (w/w) astaxanthin of dry biomass after downstream processing, i.e. harvesting, drying and disruption of akinetes for pigment bioavailability. To date, this two-stage strategy is the most applied approach for natural astaxanthin production. However, mass cultivation of *H. pluvialis* for astaxanthin production still harbours a lot of difficulties, e.g. low productivity, high production costs or fungal contamination. Hence, future improvements on both, technical and biological level are of great biotechnological interest. (Ausich, 1997; Boussiba, 2000; Guerin et al., 2003; Aflalo et al., 2007; Del Campo et al., 2007; Li et al., 2008; Lemoine & Schoefs, 2010; Guedes et al., 2011; Kiperstok et al., 2016; Kiperstok, 2016).

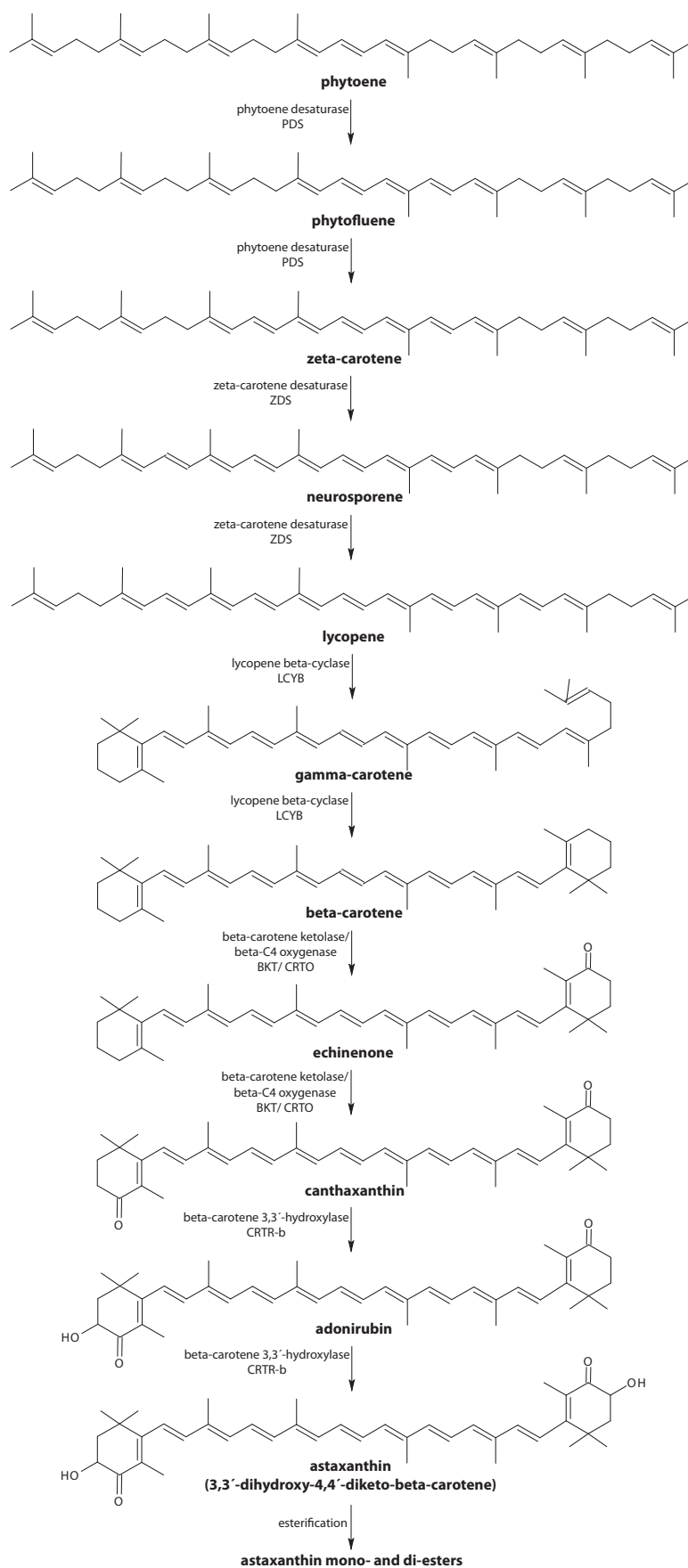


Figure 2 Biosynthetic pathway of astaxanthin in *Haematococcus pluvialis*. Pathway and involved enzymes were adapted from literature (Goodwin, 1961; Britton, 1976; Steinbrenner & Linden, 2001; Huang et al., 2006; Lohr, 2011) and structural formula were generated with the freeware ChemSketch (ACD/Labs, 2013).

1.4 Attempts for *H. pluvialis* strain improvement by mutagenesis

Genetic strain improvement of biotechnologically relevant species is a hot topic in biological sciences. Mutants can be either generated by site-directed mutagenesis or randomly by using physical (e.g. ionizing or ultraviolet radiation) or chemical (e.g. DNA alkylating agents) mutagens (Kodym & Afza, 2003).

Transformation of microalgae facilitates the increase of desired products by metabolic engineering. Microparticle bombardment is a common method for transformation using DNA-coated gold or tungsten particles to introduce exogenous DNA into the nuclear, chloroplast and mitochondrial genome. Transformation efficiencies can be increased using the glass bead method or electroporation, but in contrast to the biolistic method these two alternatives require protoplasts, thin-walled cells or mutants with reduced cell wall. In addition to the choice of transformation technique, other parameters like suitable promoters, biased codon usage, selectable marker genes and expression vectors have an impact on transformation efficiency (Pulz & Gross, 2004; Gong et al., 2011). Application of endogenous promoters enhances the expression of introduced genes probably by counteracting epigenetic gene silencing (Specht et al., 2010).

The green alga *Chlamydomonas reinhardtii* is one of the most intensively investigated microalgal species for stable genetic manipulations of the nuclear, chloroplast and mitochondrial genome. This is due to the fact that the entire genome sequences and metabolic pathways of *C. reinhardtii* are known (Pulz & Gross, 2004; Gong et al., 2011). However, the genome sequence of *H. pluvialis* is not annotated yet. Thus, transformation reports for *H. pluvialis* are comparatively rather rare.

Phytoene synthase (PSY), phytoene desaturase (PDS) and β -carotene-ketolase 1 to 3 (BKT1-3) constitute key regulatory enzymes in the pathway of astaxanthin biosynthesis (Figure 1; Figure 2). Hence, mutations or overexpression of the corresponding genes (*psy*, *pds*, *bkt1-3*) can increase the capacity for astaxanthin accumulation (Lemoine & Schoefs, 2010). Indeed, nuclear transformation of *C. reinhardtii* with *psy* isolated from *Chlorella zofingiensis* (Cordero et al., 2011) and *Dunaliella salina* (Couso et al., 2011) under the control of endogenous promoters

RBCS2 and HSP70A revealed that overexpression of *psy* resulted in about 2-fold elevated carotenoid levels when compared to the wild type (WT) strain. Similarly, astaxanthin content in *H. pluvialis* could be increased 2 to 3-fold using *bkt* and *pds* for transformation (Steinbrenner & Sandmann, 2006; Wang et al., 2012; Sharon-Gojman et al., 2015; Kathiresan et al., 2015)

Potential selectable markers were established for *H. pluvialis* by transformation. Antibiotic genes were transferred by *Agrobacterium*-mediated transformation into *H. pluvialis* conferring hygromycin resistance as a possible, future selectable marker (Kathiresan et al., 2009). Steinbrenner & Sandmann (2006) developed a transformation protocol for *H. pluvialis* where site-directed mutagenesis was utilized for changing the leucine codon of endogenous *pds* to an arginine codon. Introduction of modified *pds* by biolistic bombardment led to elevated accumulation of astaxanthin under stress conditions. At the same time, expression of mutated *pds* conferred norflurazon resistance. Norflurazon is a herbicide that interferes with PDS in a direct manner by competing with the cofactor (probably PTOX) for the binding site and thus, interrupts the biosynthetic pathway of astaxanthin. Consequently, modified *pds* can be used to increase astaxanthin levels, but also function as a selectable marker (Steinbrenner & Sandmann, 2006; Li et al., 2010).

However, random mutagenesis is the most widespread method for generating *H. pluvialis* mutants. Major advantages comprise the high efficiency for mutations, the generation of a large pool of mutants and particularly, the status 'non-transgenic' since no exogenous DNA is introduced into the organism. Ethyl methanesulfonate (EMS) and N-methyl-N-nitro-N-nitrosoguanidine (MNNG) are the most applied chemical mutagens for this purpose (Tjahjono et al., 1994b; Chumpolkulwong et al., 1997; Tripathi et al., 2001; Chen et al., 2003; Hu et al., 2008; Hong et al., 2012; Gomez et al., 2013). Increase of astaxanthin accumulation is the main desired target of random mutagenesis in *H. pluvialis*, but additional random improvements (e.g. concerning growth) make this approach even more favorable. For instance, Hu et al. (2008) generated a MNNG mutant (MT 2877) that exhibited the same patterns of growth and pigment composition in the vegetative stage like the WT strain. But under stress conditions the mutant accumulated astaxanthin twice as much as the WT and at the same time photosynthetic activity and survival during stress exposition was considerably higher.

1.5 Aims of this study

Improvement of growth and astaxanthin production in *Haematococcus pluvialis* is a highly topical subject in microalgal biotechnology. In addition to multiple factors, selection of appropriate strains is one crucial issue influencing the outcome of scientific approaches. Considering the high number of *H. pluvialis* strains that is available in several culture collections, only a little number of strains is subjected in biotechnological research. Since classical strain selection can be time-consuming, a fast screening method for multiple samples is required.

The aim of this PhD research project was to screen various *H. pluvialis* strains with different geographical origins for their biotechnological potential. A microscale screening method was implemented to facilitate both, simultaneous cultivation of different strains and induction of astaxanthin accumulation with several stress factors. Furthermore, strains were analysed on phylogenetical level based on the *rbcL* and nuclear-encoded ribosomal operon in order to test if there was any correlation of achieved data and the geographic diversity of strains. Finally, one selected strain was randomly mutagenized with ethyl methanesulfonate (EMS) as an approach for strain optimization. Generated mutants were screened for elevated growth and astaxanthin accumulation.

2

Material and methods

All chemicals that were used in this study during the performance of experiments are listed in the appendix (Table 13).

2.1 Cultivation and maintenance of microalgal strains

2.1.1 Microalgal strains

Within this PhD research project, 26 *Haematococcus pluvialis* strains with different geographical origins were analyzed (Table 4). Most of the strains were kindly provided by the Culture Collection of Algae at the University of Cologne, Germany (CCAC). Remaining strains were purchased from different culture collections: Coimbra Collection of Algae, Portugal (ACOI); Culture Collection of Algae and Protozoa, UK (CCAP); Microbial Culture Collection at the National Institute for Environmental Studies, Japan (NIES); Sammlung von Algenkulturen Göttingen, Germany (SAG) and Culture Collection of Cryophilic Algae, Germany (CCCryo).

Furthermore, a reference organism was required for molecular analyses. Since the genome of *Chlamydomonas reinhardtii* is completely sequenced (nucleus, mitochondrion, chloroplast), three strains from the SAG were chosen for this purpose: SAG 11-32a (- mating type), SAG 11-32b (+ mating type) and SAG 11-32aM (variant selected by U. G. Schlösser in 1963 from 11-32a). All three *Chlamydomonas* strains originated from Massachusetts, USA and were isolated from soil of a potato field near Amherst by G.M. Smith in 1945.

Table 4 *Haematococcus pluvialis* strains

Strain ID	Isolator	Origin
ACOI - 276	M. F. Santos (1987)	Portugal, Serra da Estrela. Pond near Lagoa Comprida.
CCAC 0055	Powalowski (1990)	Germany, Lohmar near Cologne. Reservoir for rain water.
CCAC 0125	Naumann (2004)	Germany, Asbach-Oberplag / Westerwald.
CCAC 0129	B. Melkonian (2004)	Germany, Lohmar (near Cologne).
CCAC 0526	*n.a.	*n.a.
CCAC 0528	*n.a.	*n.a.
CCAC 0529	*n.a.	*n.a.
CCAC 0868	Sineshchekov	Russia, Moscow. Biological Institute of the State University.
CCAC 0869	Sineshchekov	Russia, Moscow. Biological Institute of the State University.
CCAC 1023	*n.a.	FACS-subisolate of CCAC 0528 (1993)
CCAC 2072	Podola (2000)	Germany, Cologne. Botany Department of the University of Cologne.
CCAC 3305	M. Melkonian (2010)	Germany, Cologne, Wahner Heide, Fuchskaule. Freshwater.
CCAC 3319	M. Melkonian (2010)	Switzerland, Rylle. Freshwater.
CCAC 3323	M. Melkonian (2010)	Switzerland, Rylle. Freshwater.
CCAP 34/13	Ott (1959)	USA, Ferrum, Virginia. Bird bath.
CCAP 34/14	Ott (1989)	USA, Cattonsville, Maryland. Cement urn.
CCCryo 096-99	T. Leya (1999)	Australia, Tilba-Tilba, NSW. Dried out concrete bird bath.
NIES-144	Ichimura (1964)	Japan, Sapporo Sapporo, Hokkaido.
SAG 34-1a	Pringsheim (before 1970)	Sweden, Aneboda.
SAG 34-1b	Mainx (probably 1931)	Former Czechoslovakia.
SAG 34-1f	Pringsheim (1932)	Norway, Spitzbergen. From dry crust on a stone.
SAG 34-1h	Droop (1951)	Finland, Tvärminne. Supralittoral rock pool.
SAG 34-1i	Zehnder (1953)	Switzerland, Zürich. Holy-water font on church yard Sihlfeld.
SAG 34-1i (2)	Zehnder (1953)	FACS-subisolate of SAG 34-1i (1993)
SAG 34-1n	Zehnder (1953)	Switzerland, Graubünden. Little "blood pond" near Samnun.
SAG 44.96	Schlösser (1969)	South Africa, Cape Town. Soil from Cape Flats "De Klip"; leg. M. A. Pocock, 1967.

*n.a. - no details available

2.1.2 Culture medium

Microalgae were cultivated in modified BG-11 medium (Table 5) based on the recipe from Stanier et al. (1971). Major modifications of the original recipe comprise the absence of the organic compound citrate (that would otherwise promote bacterial growth) and addition of the buffer HEPES (Good's buffer) with a buffering capacity of pH 6.8 - 8.2 (Good et al., 1966).

Components of BG-11 medium were dissolved in bidistilled water under continuous stirring. Stock solutions of main nutrients, trace elements, Fe-EDTA, vitamins and HEPES buffer were used for the preparation of BG-11 medium. The pH was adjusted to 7.3 - 7.4 with 1 M sodium hydroxide. BG-11 medium was sterilized immediately by autoclaving (Systec VX-150). Stock solutions and sterile culture media were stored at 4°C until use.

Table 5 Composition of modified BG-11 culture medium.

Component	Amount per liter stock solution	Final concentration in BG-11 medium
Main nutrients	<i>40 mL stock solution per liter BG-11 medium</i>	
NaNO ₃	37.500 g	17.65 mM
K ₂ HPO ₄ x 3 H ₂ O	1.000 g	0.23 mM
MgSO ₄ x 7 H ₂ O	1.875 g	0.30 mM
CaCl ₂ x 2 H ₂ O	1.620 g	0.44 mM
Na ₂ CO ₃	0.500 g	0.19 mM
Trace elements	<i>1 mL stock solution per liter BG-11 medium</i>	
H ₃ BO ₃	2.86 g	46.26 µM
MnCl ₂ x 4 H ₂ O	1.81 g	9.15 µM
ZnSO ₄ x 7 H ₂ O	0.22 g	0.77 µM
Na ₂ MoO ₄ x 2 H ₂ O	0.39 g	1.60 µM
CuSO ₄ x 5 H ₂ O	79.0 mg	0.32 µM
Co(NO ₃) ₂ x 6 H ₂ O	49.4 mg	0.17 µM
Fe-EDTA	<i>1 mL stock solution per liter BG-11 medium</i>	
EDTA (Titriplex II)	5.22 g	17.86 µM
FeSO ₄ x 7 H ₂ O	4.98 g	17.91 µM
KOH (1 N)	54 mL	54.00 µM
Vitamins	<i>1 mL stock solution per liter BG-11 medium</i>	
Cyanocobalamin (Vitamin B ₁₂)	0.2 mg	0.15 nM
Biotin (Vitamin B ₇)	1.0 mg	4.00 nM
Thiamine- HCl (Vitamin B ₁)	100.0 mg	0.30 µM
Niacinamide	0.1 mg	0.80 nM
Buffer	<i>1 mL stock solution per liter BG-11 medium</i>	
HEPES	238.31 g	1.00 mM

pH 7.3 - 7.4

If necessary, solid BG-11 was prepared by adding of 1 to 1.5 % agar to the culture medium prior to autoclaving. After sterilization, 20 to 25 mL were poured into petri dishes under sterile conditions using a clean bench (Kojair Biowizard Silver SL-130, Class II).

2.1.3 Cultivation conditions

All microalgal strains were maintained in climate chambers (Johnson Controls) with discontinuous light supply (14:10 hours light:dark cycle). Light was provided by fluorescent lamps (L36W/640i energy saver cool white & L58W/956 BioLux fluorescent lamps, Osram, Munich, Germany). Cultures grown at 16 or 23°C were exposed to PFD rates of 40 or 60 $\mu\text{mol photons m}^{-2} \text{s}^{-1}$, respectively. In the following, these conditions apply to 'growth at 16 or 23°C' (if not otherwise indicated). Light intensities were measured with a light meter (LI-250A, LI-COR).

2.1.4 Establishment of axenic cultures

Prior to the performance of major experiments, the sterility status of all microalgal cultures was tested. Presence of bacterial contaminations was monitored by cultivating strains in liquid or solid BG-11 medium supplemented with 1 to 50 % bacterial standard medium (BSM; Table 6). Fungal contaminations were monitored using fungal test plates containing 4.7% Sabouraud agar (Table 6).

Table 6 Composition of BSM and Sabouraud agar

Compound	Concentration [%]
BSM	
Peptone	0.8
Glucose	0.1
Beef extract	0.1
Yeast extract	0.1
Sabouraud agar	
Meat and casein peptone	1.0
Glucose	2.0
Agar	1.7

In order to prevent possible effects of bacteria on microalgal growth, all bacteria-containing cultures were made axenic via the 'atomized cell spray technique' (Pringsheim, 1946; Andersen & Kawachi, 2005) under sterile conditions. Approximately 10 mL of dense *H. pluvialis* suspension cultures were washed twice with BG-11 medium. A sterile glass capillary tube was placed into the suspension. Compressed air was conducted through a sterile filter to the upper tip of the glass capillary tube. As a consequence, suspension was forced upwards through the glass capillary tube to the outside forming a particulate matter. Solid BG-11 plates supplemented with 1% BSM and 1% agar were exposed to that suspension aerosol so that cells were scattered on the agar surface. Plates were incubated at 16°C until colonies were visible macroscopically. Bacteria-free colonies could be distinguished from contaminated ones by shape and color of the colony rim. Bacteria-contaminated colonies showed an irregular and whitish rim whereas bacteria-free ones were clearly round and green. Bacteria-free colonies were transferred into liquid BG-11 medium and cultivated under the same conditions as before. In total, 17 of 26 *H. pluvialis* strains were made axenic using this procedure. Remaining 9 strains were already free of contaminants.

Sterility of axenic cultures was tested regularly (twice a year). To test bacterial contaminations, microalgal suspensions were cultivated in liquid BG-11 medium containing 0, 1, 10 and 50% BSM. If bacteria were present, suspensions showed a whitish to yellowish turbidity. To test fungal contaminations, algal suspensions were grown on solid fungal test plates. However, fungi were never observed within algal cultures during this project.

2.1.5 Maintenance of axenic cultures

Axenic cultures were maintained both in a solid and liquid state at 16°C. Cultures on agar slants served as back-up material. Suspension cultures were grown in 100 mL Erlenmeyer flasks containing 50 mL BG-11 medium. Cells from agar slants and suspension cultures were subcultivated regularly every 6 months and 4 weeks, respectively.

Prior to the main experiments, fresh cultures were grown at 23°C. If large quantities of algal material were required, suspensions were grown in aerated 1 to 5 L Erlenmeyer flasks with half volume of BG-11 medium. Aeration was conducted with compressed air and 0.5% CO₂ at a flow rate of 0.5 mL min⁻¹. Cultures were refreshed with new BG-11 medium two to three days before use. Finally, the physiological status of microalgae was checked by light microscopy (Olympus CX41 including DP20 camera) and only vegetative cells from the logarithmic phase were exposed to experiments.

2.2 Physiological analysis

2.2.1 Analysis of growth kinetics for 26 *H. pluvialis* strains

Microscale growth experiments were conducted at 23°C and $50.54 \pm 1.38 \mu\text{mol photons m}^{-2} \text{ s}^{-1}$ in 96-well polystyrene (PS) plates (flat bottom, BD Falcon™) containing samples of suspension cultures. To avoid evaporation of sample volumes, multititer plates were placed into two humid chambers. These chambers were placed into a custom-made cultivation box with the possibility of adjustable LED illumination from the bottom (see appendix, Figure 33). Each humid chamber basically consisted of a transparent glass box with a capacity of 20 L (20 cm x 20 cm x 25 cm) and a removable lid. Except for the bottom, glass boxes were wrapped with aluminium foil, so that samples were later illuminated with LED light exclusively from the bottom. A relative humidity of 94.3% was established by pouring distilled water into glass boxes until a water level with approximately 5 cm of height was reached and by loading the lid with 1 kg weight (2x 500 mL flasks filled with water). For the placement of multititer plates, a transparent rack of approximately 6 cm height was placed into each humid chamber. Each rack offered space for three multititer plates without any contact to the water level. Thus, six multititer plates loaded with samples could be set up in two humid chambers simultaneously.

Microalgal samples were prepared by diluting suspension cultures to a cell density of $2.5 \times 10^4 \text{ cells mL}^{-1}$. 200 μL of diluted samples were applied in four replicates á 2x2 into two different multititer plates at different positions (concerning wells and humid

chambers) to exclude any positional artefacts. The outermost wells were filled with sterile water á 250 µL well⁻¹ to intensify the effect of humidity. Optical density (OD) and cell number of samples was monitored for six days. OD was measured spectrophotometrically at 750 nm with a multiplate reader (Tecan Infinite M200 including i-control software). For cell counts, 200 µL of samples were mixed with an equal volume of 2.5% glutaraldehyde to fix motile cells. Cell density was determined microscopically by counting at least 250 cells sample⁻¹ with a hemocytometer (Neubauer improved bright-line).

Exponential growth phases of plotted results were identified by curve fitting. Specific growth rates (μ) and doubling times were (t_d) calculated for each strain with the following exponential growth equation:

$$N = N_0 \cdot e^{(\mu \cdot t_i)}$$

$$\Leftrightarrow \mu = \frac{\ln N - \ln N_0}{t - t_0} = \frac{\ln 2}{t_d} = \frac{0.693}{t_d}$$

$$\Leftrightarrow t_d = \frac{\ln 2}{\mu} = \frac{0.693}{\mu}$$

with N and N_0 representing the number of cells at time point i (t_i) and zero, respectively. Since length of exponential phases was variable among the strains, the parameters μ and t_d alone were misleading with respect to growth efficiency. Thus, area under curve (AUC) calculations were included into analyses (Figure 3). The ratio of the area under exponential (AUC_{exp}) to the total (AUC_{total}) growth curve revealed best growing strains.

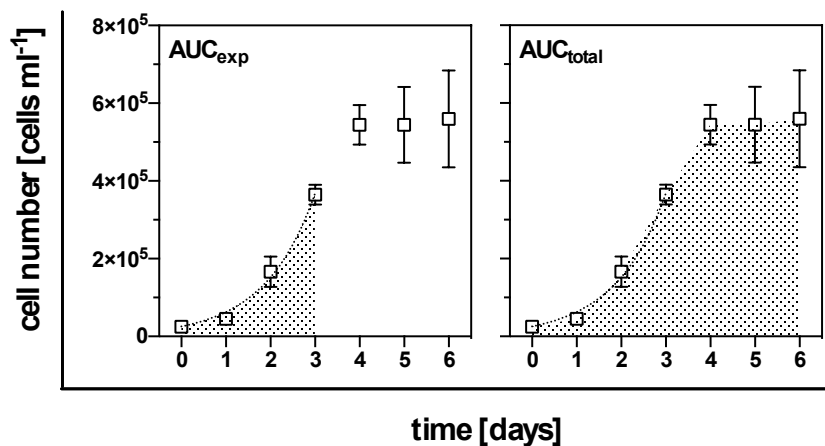


Figure 3 Example of AUC determinations for growth analyses. Growth efficiency of strains was determined with the ratio of AUC_{exp} and AUC_{total} . The illustrated growth curve was selected randomly from results.

2.2.2 Determination of temperature optima for selected *H. pluvialis* strains

To analyze if good growing strains would even grow better when cultivated at a different temperature, individual temperature optima of six selected *H. pluvialis* strains was determined (CCAC strains 0055, 2072, 3305, 3319 and SAG strains 34-1n, 44.96). A set-up was established facilitating growth of strains in a 96-well format along a temperature gradient. The technical realization of the temperature gradient module was kindly performed by the internal workshop of the Cologne Biocenter (University of Cologne, Germany).

Basically, a metal plate (13 cm x 11 cm) with direct contact to the bottom of a 96-well PS plate was simultaneously cooled down and heated up from opposite sides so that a temperature gradient was formed along the metal plate. The transfer of temperature to the metal plate was realized by circulating cool and warm water from two thermostats (Thermo Haake, Circulator D10, model K10) underneath each side of the metal plate. To exclude heat dissipation and the influence of ambient temperature, the metal plate and pipes from thermostats were covered with thermo-insulating material (see appendix, Figure 34).

During pretests, a 96-well plate was filled with 200 μL water well⁻¹ and placed onto the temperature gradient device. Since intensive condensation occurred at the lid of the multitier plate, a hollow thermo-lid was produced by the internal workshop. Warm water was conducted through the thermo-lid by a third thermostat. Placing the thermo-lid onto the multititer lid prevented condensation. For later illumination of samples from the top, a light sheet of 96 LED lamps (OSRAM Opto Semiconductors, OSRON SX ECE, LUW CN7M) matching the regular pattern of the 96-well plate with adjustable light intensities was produced by the fine mechanical workshop of the Institute of Physics I (University of Cologne, Germany). A black perforated board (with the number of perforations corresponding to number of wells and LEDs) was placed between LED sheet and thermo-lid to avoid scattering of light. Furthermore, the temperature gradient module was placed in a humid chamber with 96.2% relative humidity to prevent evaporation of samples (see appendix, Figure 35).

Set-up and settings were optimized until a stable and linear gradient was established. Temperature for cool and warm water was set to -4°C and 40°C , respectively. The third thermostat was set to 35.5°C resulting in a temperature of 30.5°C on the thermo-lid surface. Temperature of water within each well of multititer plate was measured. A gradient ranging from 9.8°C to 34.0°C from left to right column of multititer plate was established. Temperature increased within rows linearly from one column to the next with 2.2°C (Figure 4).

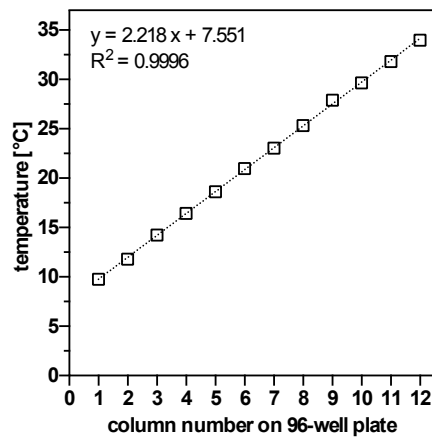


Figure 4 Linear increase of temperature using the temperature gradient device. Temperature increased linearly from column one to twelve of a 96-well plate filled with $200\ \mu\text{L}$ water per well. *Mean \pm SD; n = 8 (wells of each column)*.

Since only one loaded 96-well plate could be placed on the temperature gradient, analysis of selected *H. pluvialis* strains was arranged in a series, i.e. strains could not be analyzed simultaneously. To determine the temperature optimum of each strain, respective suspension culture was diluted to initial cell density of 2.5×10^4 cells mL^{-1} . Diluted sample was transferred á $200\ \mu\text{L well}^{-1}$ into the multititer plate with the outermost wells loaded with $250\ \mu\text{L sterile water well}^{-1}$. Thus, samples were later exposed to ten different temperatures ranging from $11.8 \pm 0.3\ ^{\circ}\text{C}$ to $31.8 \pm 0.1\ ^{\circ}\text{C}$. Samples were illuminated with $50.30 \pm 2.19\ \mu\text{mol photons m}^{-2}\ \text{s}^{-1}$ of LED light. Growth was monitored for four to six days with three time points of sampling. A duplicate of samples was removed at each time point to determine cell density via cell counts (compare section 2.2.1). The determined cell number was plotted against applied temperatures to reveal the temperature optimum.

2.2.3 Induction and quantification of astaxanthin in *H. pluvialis* CCAC 3305

The work described in this section was performed by Andreas Franzen and Frederik Koepsell under the guidance of Zehra Çebi.

Microscale astaxanthin induction experiments were carried at 23°C and 50.54 ± 1.38 $\mu\text{mol photons m}^{-2} \text{s}^{-1}$ in 96-well PS plates containing samples of suspension cultures of *H. pluvialis* CCAC 3305. Experimental set-up and loading of multititer plates were performed according to section 2.2.1. Samples were diluted to an initial cell density of 1.5×10^5 to 3×10^5 cells mL^{-1} in full, nitrogen- and phosphorus-deficient BG-11 medium supplemented with different salt concentration ranging from 0 to 0.8% sodium chloride (NaCl). The experiment was conducted for eleven days. Growth was monitored by cell counts (compare section 2.2.1).

Astaxanthin was extracted and quantified according to the method of Li et al. (2012) with minor modifications concerning handling of microscale samples and incubation times. Samples were transferred into a 96-well polypropylene (PP) plate (V-bottom, 4titude®). Cells were harvested by centrifugation at $800 \times g$ for five minutes (Heraeus Multifuge 3SR+, Thermo Scientific). Pellets of samples were mixed with 200 μL dimethyl sulfoxide (DMSO). Prior to incubation of samples for 10 minutes at 70°C in a water bath, PP plates were first sealed with an adhesive polyester film (VWR) and then fixed with styrofoam pieces by metal clamps to allow floating on the water surface. After incubation at 70°C, samples were centrifuged for 5 minutes at $3,000 \times g$. Extraction was repeated until the pellet was colourless. Supernatants were collected and mixed well before spectrophotometrical analysis. 200 μL of each sample was transferred in triplicates into a 96-well PS plate. Absorbances were measured in a plate reader (Tecan, Infinite M200) at 530 nm.

To facilitate astaxanthin quantification of samples, a synthetic astaxanthin standard was serially diluted in DMSO. Four replicates of each dilution were transferred into 96-well PS plate and absorbances were measured at 530 nm. Absorbances were plotted against respective concentrations of astaxanthin standard (Figure 5). The equation for linear regression was used to quantify the astaxanthin concentration in samples.

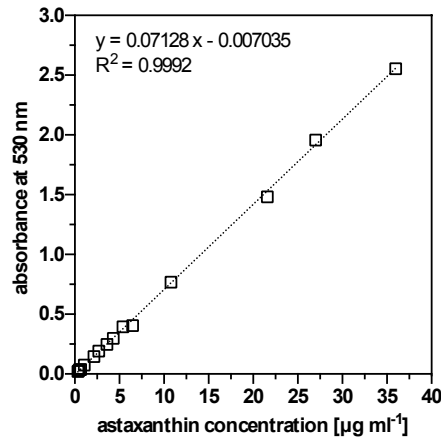


Figure 5 Astaxanthin calibration curve. Dotted line depicts the linear increase of astaxanthin concentration with spectrophotometrically measured absorbances at 530 nm. *Mean \pm SD; n = 4.*

2.3 Molecular analysis

To test if there was genetic diversity among subjected *H. pluvialis* strains, analyses on molecular levels were conducted. Desired genes and sequences were isolated, amplified and sequenced for phylogenetic approaches.

2.3.1 Isolation of genomic DNA

Genomic DNA was isolated via the CTAB method modified from the protocol of Rogers & Bendich (1985). Composition of required buffers are listed in Table 7.

Table 7 Composition of buffers required for CTAB-DNA extraction

Compound	Concentration
TE buffer	
Tris-HCl (pH8)	0.010 M
Na ₂ EDTA x 2 H ₂ O	0.001 M
CTAB buffer	
NaCl	1.400 M
Tris-HCl (pH8)	0.100 M
Na ₂ EDTA x 2 H ₂ O	0.025 M
CTAB	2% (w/v)

Predominantly flagellated cells were harvested from 4 to 8 mL of dense microalgal cultures by centrifugation (500 x g, 5 min). Cell pellets (approx. 0.2 mL) were shock frozen in liquid nitrogen. Sterile glass beads were added to frozen pellets. 180 μL TE

buffer, 140 μL 5% SDS and 5 μL proteinase K (10 mg mL^{-1}) were added to the samples, mixed by vortexing and incubated at 60°C with agitation (20 min). After this mechanical, chemical and thermal rupture of cells, samples were exposed to RNA digestion and DNA extraction by adding 100 μL 5M NaCl, 5 μL RNase A (10 mg mL^{-1}) and 1 mL of preheated (60°C) CTAB buffer. Samples were mixed by vortexing and incubated at 60°C with agitation (10 min). Cell debris was separated from DNA extracts by centrifugation (12,000 $\times g$, 5 min). Each supernatant was mixed with an equal volume of a chloroform-isoamyl alcohol solution (24:1). Samples were vortexed and incubated at room temperature (RT) for 10 minutes. Phases were separated by centrifugation (12,000 $\times g$, 15 min). The upper phase containing DNA was mixed with 2/3 volume of precooled (-20°C) isopropyl alcohol by vortexing. DNA was precipitated at -20°C for at least one hour. After centrifugation (17,000 $\times g$, 15 min, 4°C), the supernatant was removed and the DNA pellet was washed twice with 1 mL of precooled (-20°C) 80% ethanol (17,000 $\times g$, 5 min, 4°C). Each DNA pellet was air dried at RT and finally, dissolved in 50 - 200 μL TE buffer. DNA samples were stored at -20°C until use.

2.3.2 DNA quality control

DNA purity was analysed spectrophotometrically (Nanodrop 2000, Thermo Scientific) by inspection of measured spectra. Pure DNA is characterized by an absorbance maximum at a wavelength of 260 nm. Detectable absorbances at 230 or 280 nm are an indication for contaminations like proteins and carbohydrates or ethanol and phenolic compounds, respectively. These contaminations may result from chemicals used during the DNA extraction procedure or even from the subjected biological material itself. DNA quality was considered as pure if ratio of absorbances from 260:280 nm and from 260:230 nm resulted in values of approximately 1.8 and 2.0, respectively. Within this study, extracted DNA was free of mentioned contaminations.

Although DNA is more stable than other intracellular molecules (e.g. RNA) in an extracellular environment, DNA degradation during extraction or other handling procedures is possible. Spectrophotometrical analysis of DNA is a good tool to determine the purity of DNA samples, but it gives no evidence for DNA stability, since degraded DNA might still have the capability to absorb at 230 nm. Degradation status

of DNA samples could be easily detected via agarose gel electrophoresis. Aliquots of DNA samples (2 - 3 μL) were mixed with 2 μL of 5x Green GoTaqTM loading dye and applied on an agarose gel (1% in TAE buffer, Table 8) supplemented with 0.00002% of the DNA intercalating agent ethidium bromide (EtBr). As a DNA size marker, 2 μL of 1 kbp DNA ladder was also loaded on the agarose gel. Electrophoretical DNA migration was conducted with 120 V and 30 mA (Biometra Standard Power Pack P25) for 20 - 40 minutes. Due to the fluorescent properties of EtBr, DNA could be visualized when exposed to UV light (Intas Gel Imager including Intas GDS software). Intact genomic DNA poorly migrates on the agarose gel under these conditions. However, migration of degraded DNA or short DNA fragments is clearly visible due to lower molecular mass. Within this study, no degraded DNA was detected.

Table 8 Composition of TAE buffer

Compound	Concentration [mM]
Tris	40
Glacial acetic acid	20
Na ₂ EDTA x 2 H ₂ O	1

2.3.3 Genome size estimation of 26 *H. pluvialis* strains

Since to date the genome of *H. pluvialis* is not annotated and its size is unknown, the genome size was estimated for all subjected strains. Prior to DNA extraction via the CTAB method, cell density was determined using a hemocytometer (Neubauer improved bright-line). After DNA extraction, DNA concentration was measured spectrophotometrically (Nanodrop 2000, ThermoScientific). DNA content per cell was calculated and converted to Gbp units; according to Kapraun (2007) 1 pg DNA equals 978 Mbp.

To evaluate the accuracy of this method, *Chlamydomonas reinhardtii* was applied as a reference organism. *C. reinhardtii* SAG 11-32a, SAG 11-32b and SAG 11-32aM were treated analogously to estimate the genome size.

2.3.4 DNA sequencing and phylogenetic analyses of 26 *H. pluvialis* strains

The work described in this section was predominantly performed by Irina Maiber under the guidance of Zehra Çebi. Sequences were kindly corrected and aligned by Dr. Nicole Sausen.

Plastid-encoded *rbcL* gene and nuclear-encoded ribosomal DNA sequences (rDNA) were used as targets for the sequencing approach. Desired sequences were amplified via the polymerase chain reaction (PCR) method (Saiki et al., 1988). Prior to PCR reactions, DNA samples were diluted to a concentration of 15 ng μL^{-1} . PCR was conducted in 25 - 50 μL reaction volumes containing nuclease-free water, 1x DreamTaq buffer, 0.2 mM dNTPs, 0.1 μM forward and reverse primer (Table 9; Figure 6) 0.025 units μL^{-1} DreamTaq DNA polymerase and 0.5 - 2 μL of diluted DNA template.

Table 9 List of forward (F) and reverse (R) PCR primers and their 5' to 3' sequences. Primers were used for amplification of *rbcL* gene and rDNA sequences.

Primer	Sequence
<i>rbcL</i> primers (kindly generated by Dr. B. Marin)	
<i>rbcL</i> _1a (F)	ATGKYWCCACAAACWGARAC
<i>rbcL</i> _1b (F)	TGCTGGNTTYAAAGCNGGKG
<i>rbcL</i> _3 (R)	TCTTTCCAWACTTCACAHGCWGCWG
<i>rDNA</i> primers (Marin et al., 2003; Marin, 2012)	
336 (F)	GACCGATAGCGAACAAGTA
1380 (F)	GCGTTGAWTACGTCCCTGCC
1495 (R)	CCAYGTCCAAYTGCTGTTACRTGG
B22 (R)	CTTCCCTCAYRGTA CTGTTGTYGC
EAF3 (F)	TCGACAATCTGGTTGATCCTGCCAG
ITS03 (F)	CGATGAAGAACGYAGCGA
ITS055 (R)	CTCCTTGGTCCGTGTTTCAAGACGGG

PCR was conducted in a thermocycler (Primus 96 Plus, MWG Biotech). Depending on the annealing temperature of applied primers, two different PCR programs, 'BM45cyc' (Table 10) and 'BM55cyc' (Table 11), were used to amplify *rbcL* and rDNA sequences, respectively.

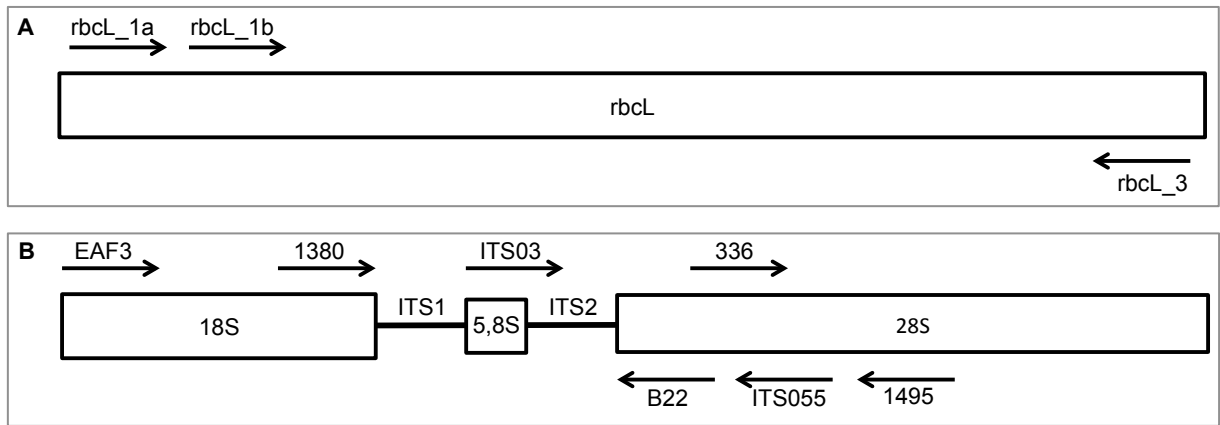


Figure 6 Schematic visualization of applied primer combinations. Primers were targeting **[A]** the *rbcL* gene (1428 nt) and **[B]** rDNA sequences (Marin, 2012): 18S (1800 nt), ITS1, 5.8S (160 nt), ITS2 and 28S (3300 nt). *nt* - nucleotides

Table 10 PCR program 'BM45cyc' for the amplification of *rbcL*

PCR step	Temperature [°C]	Time [min]
Initial denaturation	95	3.00
30 cycles:		
Denaturation	95	0.45
Annealing	45	1.00
Elongation	72	3.00
Final elongation	68	5.00
Final condition	15	∞

Table 11 PCR program 'BM55cyc' for the amplification of rDNA sequences

PCR step	Temperature [°C]	Time [min]
Initial denaturation	95	3.00
30 cycles:		
Denaturation	95	0.45
Annealing	55	1.00
Elongation	72	3.00
Final elongation	72	5.00
Final condition	8	∞

Amplicons were verified by DNA fragment size via agarose gel electrophoresis. Prior to sequencing, PCR products were purified. For this, DNA of PCR samples was precipitated with the same volume of precooled (-20°C) isopropyl alcohol over night. After centrifugation (17,000 x *g*, 15 min, 4°C), the supernatant was carefully discarded. The DNA pellet was washed twice with 1 mL of precooled (-20°C) 80% ethanol (17,000 x *g*, 15 min, 4°C), air-dried and dissolved in 25 µL nuclease-free water. DNA content was quantified spectrophotometrically. Purified PCR samples were diluted to a concentration of 12 ng µL⁻¹. 13.5 µL of diluted samples were mixed

with 1.5 µL of desired primers for sequencing reactions (Table 12). Mixed samples were transferred into a 96-well sequencing plate and finally, sequenced according to the Sanger method in an ABI sequencer by Eurofins Genomics.

Table 12 Sequencing primers. Primers used for sequencing are marked with "x". Primers were targeting the *rbcL* gene and rDNA sequences (5.8S, ITS2 and partial 28S).

strain	rbcL_1b	rbcL_3	ITS03	B22	ITS055	1495	336
ACOI - 276	x	x	x	x			
CCAC 0055	x	x	x	x	x		
CCAC 0125	x	x	x	x	x	x	x
CCAC 0129	x	x	x	x	x		
CCAC 0526	x	x	x	x	x		
CCAC 0528	x	x	x	x			
CCAC 0529	x	x	x	x	x		
CCAC 0868	x	x	x	x			
CCAC 0869	x	x	x	x	x		
CCAC 1023	x	x	x	x	x		
CCAC 2072	x	x	x	x	x	x	x
CCAC 3305	x	x	x	x	x		
CCAC 3319	x	x	x	x			
CCAC 3323	x	x	x	x	x		
CCAP 34/13	x	x	x	x	x		
CCAP 34/14	x	x	x	x	x	x	x
CCCryo 096-99	x	x	x	x	x	x	x
NIES-144	x	x	x	x	x	x	x
SAG 34-1a	x	x	x	x	x	x	x
SAG 34-1b	x	x	x	x	x		
SAG 34-1f	x	x	x	x	x	x	x
SAG 34-1h	x	x	x	x	x	x	x
SAG 34-1l	x	x	x	x	x		
SAG 34-1l (2)	x	x	x	x	x		
SAG 34-1n	x	x	x	x	x		
SAG 44.96	x	x	x	x	x		

Sequences were assembled and manually corrected with the AlignIR™ software (v.2.0.48, LI-COR) using the IUPAC nucleotide ambiguity code (see appendix, Table 14). If two base signals were detected at the same position of the sequence, the clearly dominant peak was referred as the actual one. But if peaks of bases were overlapping or not clearly distinct, the corresponding position was marked with respective ambiguity. After sequence correction, the consensus sequence was exported to the alignment editor SeaView (v.4.4). Corresponding sequences of other and identical *H. pluvialis* strains available on NCBI (National Center for Biotechnology Information) were included into the alignment aiming an increase in

resolution of phylogenetic results by maximum taxon sampling. The data sets for rbcL, 5.8S, ITS2 and 28S were analyzed both, separately and jointly. Tree topologies were analyzed by maximum likelihood (ML) and calculated with Randomized Accelerated Maximum Likelihood (RAxML v.7.3.2, PThreads) on the supercomputer CHEOPS (Cologne High Efficiency Operating Plattform for Science) of the RRZK (Regionales Rechenzentrum der Universität zu Köln). GTR+I+ Γ (Generalized Time Reversible) was used as a model of DNA evolution. Furthermore, the best one of 100 trees was chosen for tree topology. 1,000 ML-bootstraps were calculated with RAxML for each gene separately to support the robustness of tree topologies. Trees were edited with SeaView and Adobe Illustrator CS4. Furthermore, the secondary structure of ITS2 was constructed based on the model for Chaetophorales, Chaetopeltidales, Oedogoniales and Sphaeropleales described by Caisová et al. (2013). After the identification of spacer regions, the secondary structure for helices one to four of ITS2 were calculated with the program Mfold. Helices of all analyzed *H. pluvialis* strains were homologized to reconstruct a consensus secondary structure of ITS2. The numbering and labeling system for ITS2 nucleotides and basepairs was adopted from Caisová et al. (2011).

2.4 Strain improvement approach

2.4.1 EMS mutagenesis of *H. pluvialis* CCAC 0125

Ethyl methanesulfonate (EMS) is an guanine alkylating agent that is often used for random mutagenesis (Rhaese & Boetker, 1973; Klug et al., 2011;). Although the mutation rate of EMS cannot be predicted, choosing a lethal dose of 50% for mutagenesis can minimize multiple mutations. Unique mutations per genome can be aimed from a statistical point of view when the number of cells exposed to EMS corresponds to the genome size (Flynn et al., 2002).

Based on this information, *H. pluvialis* CCAC 0125 was mutagenized with EMS according to Flynn et al. (2002). First, survival rates were determined. For this, cells from the mid-logarithmic phase were harvested (800 x g, 5 min) and concentrated to density of 3.7×10^9 cells corresponding the genome size of 3.7 Gbp. Cells were

treated with a final concentration of 46 mM EMS for 0 to 45 minutes. Incubation was performed in the dark with gentle agitation. After incubation, samples were washed twice with an equal volume of 10% sodium thiosulfate (EMS inactivating solution) and once with BG-11 medium. Samples were resuspended in BG-11 medium and incubated in the dark at 16°C over night. A dilution series of cells was spread on 1.5% agar plates (200 to 800 cells plate⁻¹). Five to seven plates were prepared per condition and incubated upside down for two weeks at 23°C with $24.88 \pm 6.02 \mu\text{mol photons m}^{-2} \text{s}^{-1}$ (LI₂₅) of LED light in custom-made cultivation box (Figure 40). The number of colony forming units (cfu) was determined stereomicroscopically (Olympus SZX16 including DP71 camera and cell[^]f Imaging software). Survival rates (Figure 7) were calculated based on the achieved number of cfu and initially applied number of cells. Values were corrected with the ones of non-treated cells (0 min EMS).

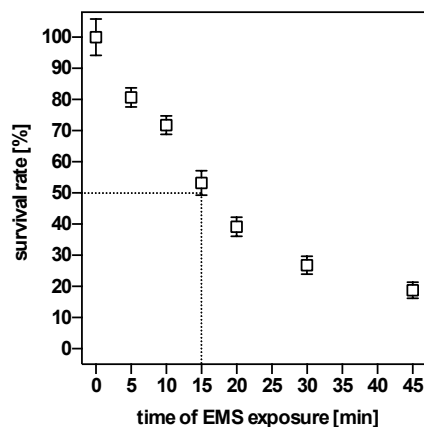


Figure 7 Survival rates of *H. pluvialis* CCAC 0125 exposed to EMS for 0 to 45 minutes. Dotted line depicts the exposition time (15 min) leading to 50% survival. Mean \pm SD; $n = 5$ to 7 plates.

For the main mutagenesis experiment, triplicates of samples were treated with EMS analogously to the method above, except for the EMS exposition time, number of plated cells, final number of plates and incubation time. Triplicate of samples were treated with EMS for 0 and 15 minutes and designated as WT1-WT3 and E1-E3, respectively. Eight and 32 agar plates with 200 cells plate⁻¹ were prepared for each replicate of WT_i and E_i, respectively. Samples were incubated for three weeks at 23°C and LI₂₅. All plates (Σ 120 plates) were documented by stereomicroscopic photography. The number of single colonies was counted and the number of colonies in merged clusters was estimated, so that the total number of cfu could be calculated. Furthermore, each colony (col) was designated with an ID (Sample_i + Plate_{No.} + col-No.) using a labeling grid (PetriStickerTM) with 100 squares (0.36 cm² square⁻¹).

Finally, colonies were exposed to light stress with $91.34 \pm 24.98 \mu\text{mol photons m}^{-2} \text{s}^{-1}$ (LI_{90}) for further eleven days. Plates were analyzed analogously as described above.

2.4.2 Screening and verification of putative EMS mutants

Mutants were screened in two steps based on elevated colony size and/ or pigmentation after exposition to LI_{25} and after LI_{90} . Colony diameter (\emptyset) of 1372 WT and 2272 mutants colonies were measured with the freeware ImageJ. Red pigmentation caused by astaxanthin accumulation was evaluated visually. 360 putative mutant colonies were selected this way. To verify the results, five WT colonies and 118 of selected E1 colonies were picked, grown in liquid BG-11 medium, replated on agar plates and analyzed again based on colony size. 8306 daughter colonies (dc) of 118 mother colonies (mc) were analyzed. Since several mutant dc derived from a unique mc, t-test analysis for statistics could not be performed (see bar charts, Figure 8). However, data sets could be analyzed based on the distribution of values using box plots. The “box” of the plot represents the interquartile range (IQR) comprising 50% of measured values. If \emptyset_{mc} correlated to these midspread values of \emptyset_{dc} , dc were considered as reproducible (see box plots, Figure 8). Otherwise, achieved data and thus the mutation event in general could not be verified.

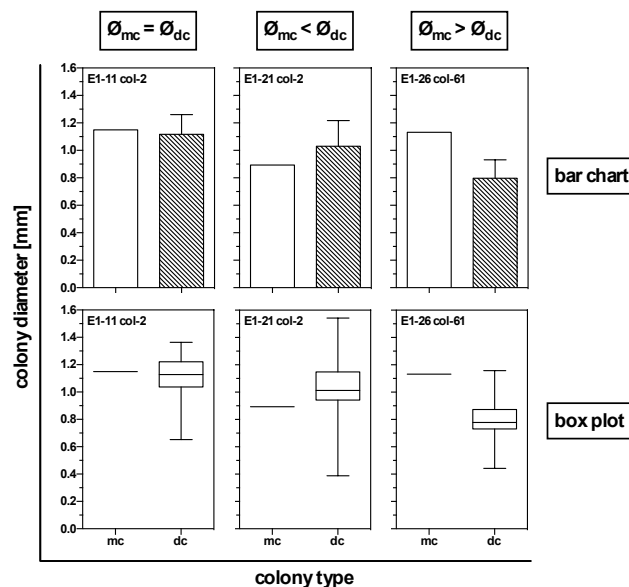


Figure 8 Example for verification of EMS mutants based on colony size. “ $\emptyset_{\text{mc}} = \emptyset_{\text{dc}}$ ” indicates that diameter of mother colonies (\emptyset_{mc}) correlated with midspread values of daughter colonies (\emptyset_{dc}), i.e. previous data were reproducible and mutation could be verified. Otherwise, data were not reproducible (“ $\emptyset_{\text{mc}} < \emptyset_{\text{dc}}$ ” and “ $\emptyset_{\text{mc}} > \emptyset_{\text{dc}}$ ”).

2.4.3 Growth of suspended and immobilized EMS mutants

The work described in this section was performed by Daniyal Ahmad under the guidance of Zehra Çebi.

To improve cultivation patterns for biotechnological approaches, *H. pluvialis* is usually applied in suspension cultures and with an upcoming trend in an immobilized state. For this, both cultivation modes were tested for *H. pluvialis* CCAC 0125 and derivative EMS mutants. For suspension cultures of WT and five verified mutants (E1-11 col-2, E1-16 col-4, E1-16 col-29; E1-17 col-9 and E1-17 col-4), microscale growth experiments were set up and performed according to section 2.2.1.

Growth and astaxanthin production of immobilized WT and one selected mutant (E1-16 col-4) were analyzed using the twin-layer (TL) system and a two-step approach according to Kiperstok (2016). The TL system was established in the Melkonian laboratory (Cologne Biocenter, University of Cologne, Germany) for microalgal applications, first in the sense of long-term biosensors (Podola & Melkonian, 2003) and later as a high-throughput cultivation technique in a 96-well format (Nowack et al., 2005). This type of cultivation facilitates the separation of immobilized microalgae from the bulk of the culture medium. However diffusion of nutrients from the medium through the source and substrate layer to immobilized algae will not be hindered. Immobilized microalgae are capable to use light, CO₂ and O₂ from the ambient atmosphere. Over the past years, the TL system was further improved to tubular, solid-state photobioreactors (PBR), a novel type of porous substrate bioreactors (PSBR). Laboratory scale TL-PSBR (Figure 9) used in this study are based on previous descriptions (Shi et al., 2007; Naumann et al., 2013; Benstein et al., 2014; Schultze et al., 2015).

The hard case of PSBR basically consisted of transparent PMMA (polymethyl methacrylate) tubes (50 cm length, ø 12 cm) mounted on a PVC (polyvinyl chloride) pedestal with cavities for 1 L media bottles. Glass fiber slices of 50 cm x 10 cm size (80 g m⁻²; Isola AS, Eidanger, Norway) were fixed in PVC caps fitting PMMA tubes and vertically arranged in PMMA tubes and served as macroporous source layers. Media, placed in the PVC pedestal, circulated through PVC (Rauclair, Germany) and pump connector tubes (Spetec, Erding, Germany) by using peristaltic pumps. Media

was applied to the source layer from the top at a flow rate of 3 mL min^{-1} . Gravity-driven media flowed through the source layer back to the media reservoir and was recycled until exchange with fresh medium every two to three days. Evaporated water was compensated with the addition of water when required. PMMA tubes were aerated with a mixture of compressed air and 5% CO_2 (v/v) at a flow rate of 1 L min^{-1} .

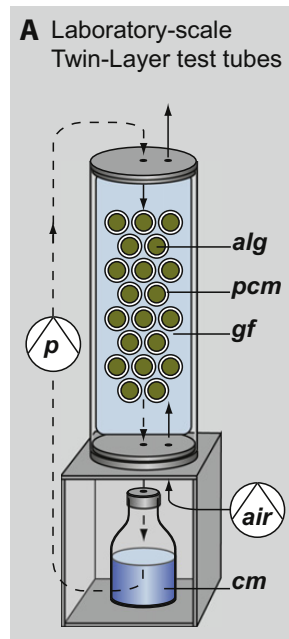


Figure 9 Schematic illustration of laboratory-scale TL PSBR taken from Schultze et al. (2015). *air* – air and CO_2 supply, *alg* – immobilized microalgae, *cm* – culture medium, *gf* – glass fiber slice, *p* – peristaltic pump, *pcm* – polycarbonate membrane.

The biological part of PSBRs comprised *H. pluvialis* cells immobilized on PCM (polycarbonate membranes, PC40, $0.4 \mu\text{m}$ pore size, $\varnothing 25 \text{ mm}$, Whatman, Dassel, Germany) as microporous substrate layers. For this, cells from the logarithmic phase were harvested by centrifugation (500 g , 10 min). PCM were placed on gel blotting paper (GB002; Schleicher & Schuell, Dassel, Germany) upon cellulose tissues. Harvested cells were filtrated on PCM by gravimetical flow using a PVC template with six cavities of 18 mm diameter and resulting in a circular inoculation area of 2.5447 cm^2 . Initial biomass density was adjusted to a dry weight (DW) of 5 g m^{-2} . Prepared filters were arranged on pre-wetted glass fiber slices in PMMA tubes by self-adhesion. For biomass production, immobilized cells were exposed PFD rates of $90 \mu\text{mol photons m}^{-2} \text{ s}^{-1}$. Subsequently, samples were illuminated with $1,000 \mu\text{mol photons m}^{-2} \text{ s}^{-1}$ to induce astaxanthin production. Illumination was conducted with a light/ dark cycle of 14/ 10 hours with natural light and sodium discharge lamps (SON-T AGRO 400W, Philips, Hamburg, Germany). Measured humidity in the PSBR tubes

was more than 85 %. PSBR were set up in a rooftop greenhouse (Cologne Biocenter, University of Cologne, Germany) at 25 ± 3 °C.

Every two to three days, triplicates of filters were harvested. Biomass trespassing the initial inoculation area was scraped off carefully from PCM. Samples were freeze-dried for at least two hours until constant weight. Total dry weight of lyophilized samples was determined using an analytical balance (Sartorius, Bovenden, Germany). To calculate the biomass [g m^{-2}], weight of samples was calculated by subtracting each PCM weight (4.44 ± 0.01 mg) from the total weight and by dividing the calculated sample weight with the initial inoculation area. Samples were stored at -20°C until astaxanthin extraction. One to two mg freeze-dried samples were used for astaxanthin extraction. Extraction was carried out in 2 mL Eppendorf tubes according to the method described in section 2.2.3. Total astaxanthin [g m^{-2}] and astaxanthin content [% DW] were calculated. Finally, results for WT and mutants were compared.

2.5 Data analysis

Data were assembled and arranged with Microsoft Excel for Mac 2011 (v.14.5.9). GraphPad Prism (v.6.0) was used for both, creation of graphs and analysis of data. For statistics, data were first analyzed for normal distribution using the Kolmogorov-Smirnov test. If normal distribution was present, data were compared using parametric t-test or one-/ two-way ANOVA. Post-hoc analyses were performed with multiple comparison tests like Bonferroni correction or Tukey's range test. If data were not normally distributed, non-parametric tests like Mann-Whitney U or Kruskal-Wallis were applied. Significant differences could be verified if p values were ≤ 0.05 .

3

Results

3.1 Growth kinetics of *H. pluvialis* strains

Growth kinetics of 26 *H. pluvialis* strains was analyzed in a short-time microscale approach. Achieved growth curves display a typical course of batch cultures (Figure 10). Over a time period of six days, strains were either partially (at least three days) or completely in the exponential phase so that growth rates could be determined for all strains (Figure 12 A). During the experiment, different growth patterns were observed (Figure 10). Twelve strains reached the stationary phase on day four (CCAC strains 0526, 0528, 0868, 0869, 1023; NIES-144, SAG 34-1b, SAG 34-1l, SAG 34-1l(2)) or day five (CCAC 0529, SAG 34-1a; SAG 34-1h). A decline phase could be observed between the days four to six for five strains (CCAC 0125, CCAC 0129, CCAP 34/13, CCAP 34/14, CCCryo 096-99). Remaining nine strains exhibited exclusively exponential growth for six days (CCAC strains 0055, 2072, 3305, 3319; SAG 34-1n) or for four to five days (ACOI-276, CCAC 3323, SAG 34-1f, SAG 44.96). Overall, the initial density of 2.5×10^4 cells mL^{-1} increased to a maximum cell density of 1.1×10^6 cells mL^{-1} in three strains (CCAC 3305, CCAC 3319, SAG 34-1n). Two strains exhibited the lowest cell densities of 1.6 and 1.7×10^5 cells mL^{-1} (ACOI-276 and SAG 34-1f, respectively); thus, both strains were excluded from further analyses.

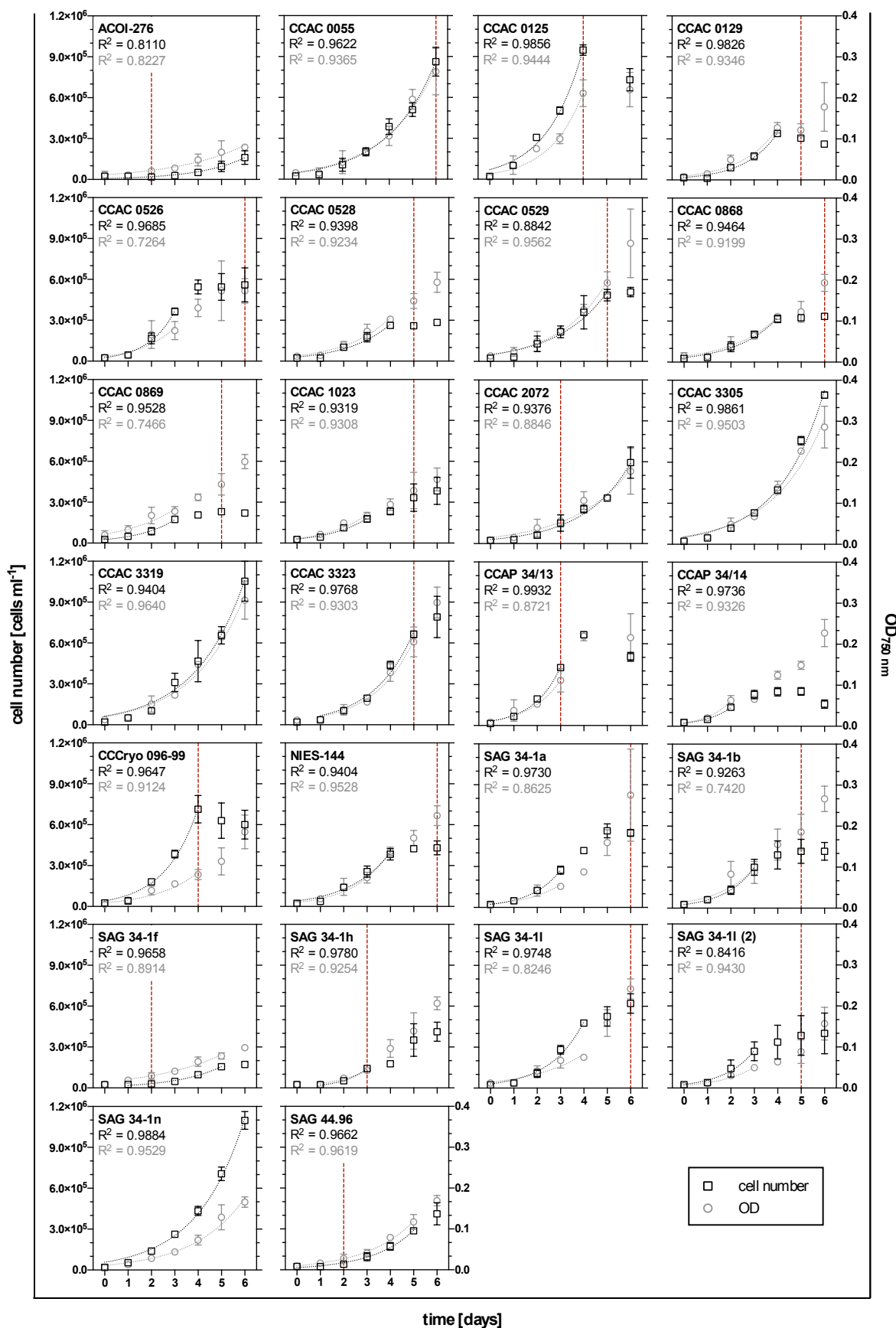


Figure 10 Growth kinetics of 26 *H. pluvialis* strains at 23°C and 50 $\mu\text{mol photons m}^{-2} \text{s}^{-1}$. Development of growth (left y axis) and OD_{750nm} (right y axis) was monitored over six days. Exponential phase of both parameters is represented by black and grey dotted curves with corresponding R² values. Vertical red, dashed line depicts the first appearance of astaxanthin accumulation. Mean \pm SD; n = 4.

In addition to growth, OD was measured at 750 nm for all 26 *H. pluvialis* strains to test if there was an obvious correlation with cell densities (Figure 10). OD correlated with cell densities predominantly during the exponential phase except for seven strains (CCAC 0125, CCAC 0526, CCCryo 096-99, SAG 34-1a, SAG 34-1l, SAG 34-1l(2), SAG 34-1n). Beyond the exponential phase, there was no distinct correlation pattern between cell density and OD; either correlation persisted (e.g. CCAC 1023) or the course of OD deviated from growth curve of cells. In some cases the deviation might be explained by the possible increase of cell size during the stationary/ decline phase (e.g. CCAP 34/14) or with the observation of astaxanthin accumulation (e.g. CCAC 0528, CCAC 0869, SAG 34-1b). However, astaxanthin accumulation alone seems not be the reason for different trends of OD and growth curves (e.g. CCAC 2072, SAG 44.96). Overall, OD measurements could not be readily applied as an alternative method for cell counts since several discrepancies were existent.

To test the reproducibility of the applied microscale method, monitoring of growth was repeated for two selected strains (CCCryo 096-99 and SAG 44.96) in an independent experiment. Since there were no significant differences between data sets, reproducibility could be verified for the screening approach (Figure 11).

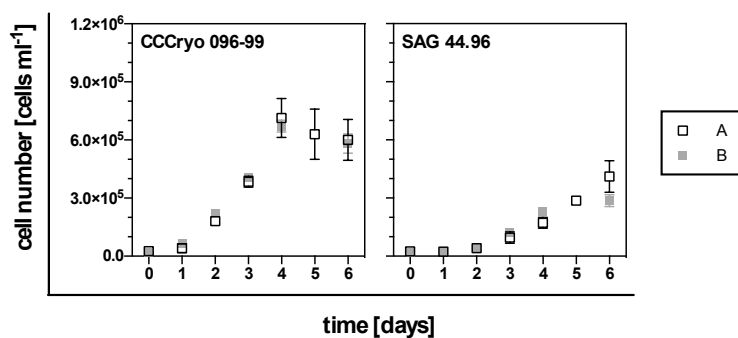


Figure 11 Growth curves of *H. pluvialis* CCCryo 096-99 and SAG 44.96 from two independent experiments. Data sets A and B showed no significant differences. *Mean* \pm *SD*; *n* = 4.

To screen for the best growing strains, it was insufficient to focus solely on specific growth rates or doubling times (Figure 12 A and B), because length of the exponential phase and growth patterns in general were quite variable amongst the strains. For instance, CCAC 3305 exhibited the lowest specific growth rate of 0.452 day⁻¹ and thus, the highest doubling time of 1.538 days. Conversely, SAG 34-1h had the highest growth rate of 1.071 day⁻¹ with the lowest doubling time of 0.715 days.

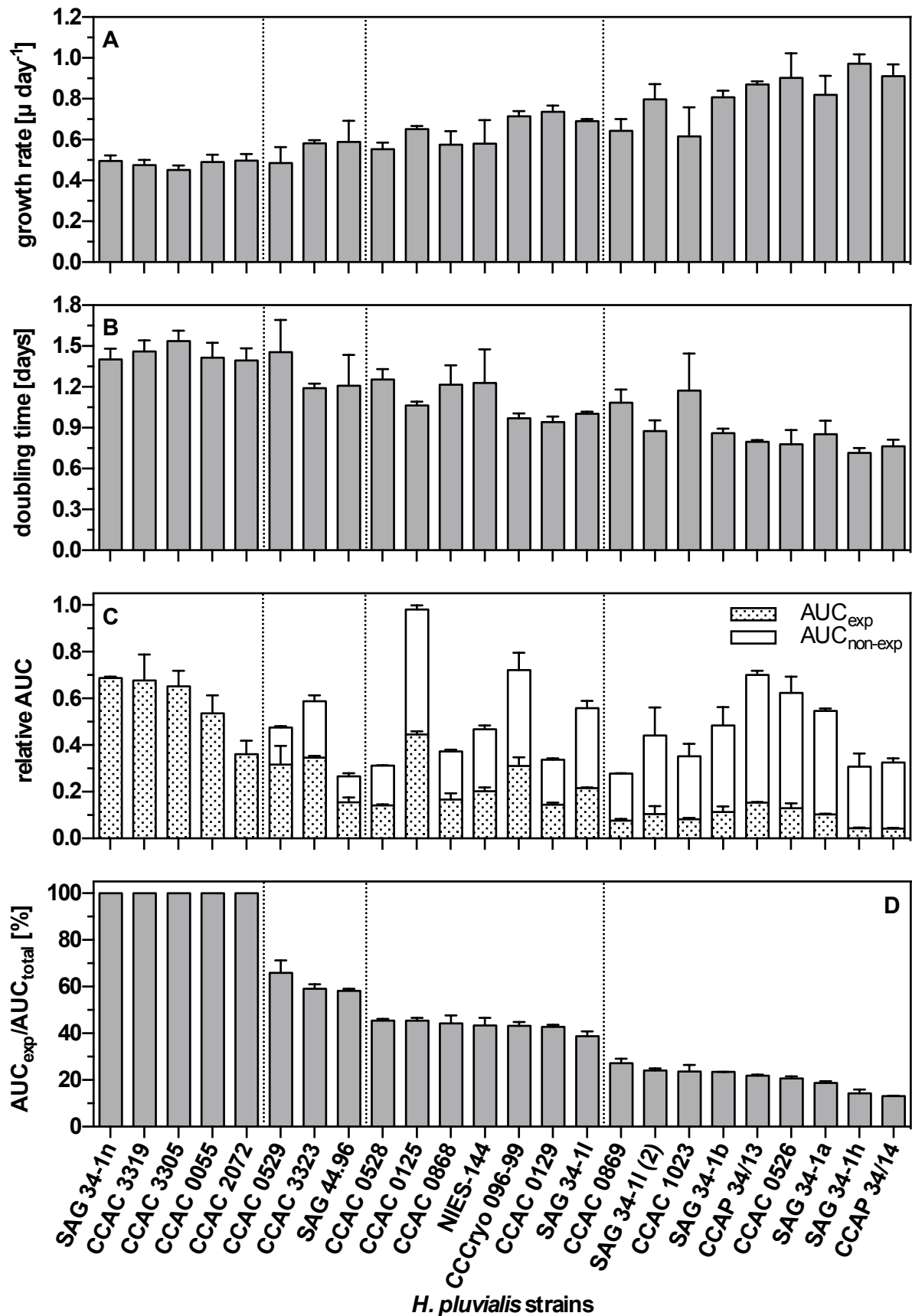


Figure 12 Calculated growth parameters for 24 *H. pluvialis* strains. Specific growth rate μ **[A]** and doubling time **[B]** were calculated from each exponential phase. Growth efficiency was evaluated using AUC_{total} **[C]** and the ratio of AUC_{exp} to AUC_{total} **[D]**. Results are sorted with decreasing growth efficiency and divided into four groups by vertical dotted lines. Mean \pm SD; $n = 4$.

However, growth curves clearly show that CCAC 3305 was much better growing than SAG 34-1h (Figure 10). Consequently specific growth rates were not the parameter of choice for screening strains. To solve this contradiction, the area under the exponential (AUC_{exp}) and non-exponential ($AUC_{\text{non-exp}}$) growth curves was calculated (Figure 12 C). Finally, the ratio of AUC_{exp} to the total AUC (AUC_{total}) revealed best growing strains (Figure 12 D). Strains were divided into four groups based on their growth efficiency. The four groups constitute five, three, seven and nine strains with a $AUC_{\text{exp}} / AUC_{\text{total}}$ ratio of 100, approximately 60, 40 and up to 20%, respectively.

To analyze if a different cultivation temperature would increase growth efficiency, individual temperature optima of six selected *H. pluvialis* strains was determined. For this, the five best growing strains with a $AUC_{\text{exp}} / AUC_{\text{total}}$ ratio of 100% (CCAC strains 0055, 2072, 3305, 3319 and SAG 34-1n) and one additional strain with a lower $AUC_{\text{exp}} / AUC_{\text{total}}$ ratio of approximately 60% (SAG 44.96) were grown along a temperature gradient ranging from 11.8 ± 0.3 °C to 31.8 ± 0.1 °C (see appendix, Figure 36, Figure 37). Plotting the cell density against respective temperatures revealed the Gaussian distribution of achieved data with the peak value representing the temperature optimum of each strain (Figure 13).

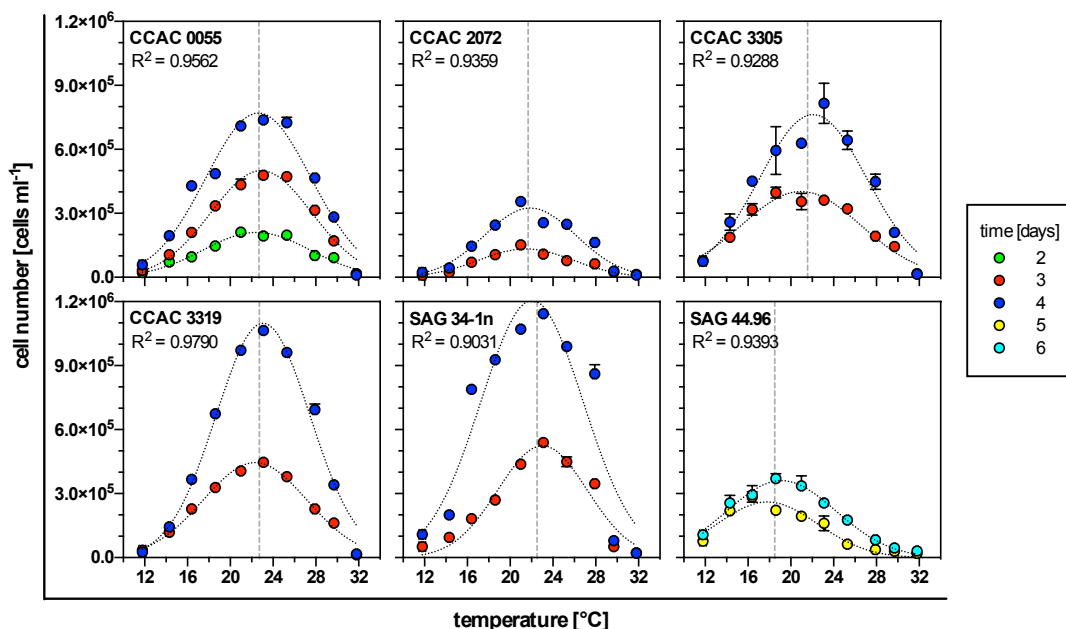


Figure 13 Cell densities of six selected *H. pluvialis* strains at ten different temperatures and 50 $\mu\text{mol photons m}^{-2} \text{s}^{-1}$. *H. pluvialis* strains were grown for four to six days along a linear temperature gradient with a range of 11.8 to 31.8°C. The average temperature optimum of each strain from different time points is depicted by vertical grey dashed lines. Each dotted curve highlights the Gaussian distribution of achieved data. $Mean \pm SE$; $n = 2$.

The effect of favorable temperature on growth was detectable for most of the selected strains from the second day of cultivation. However, in SAG 44.96 temperature effect was detected three days later, starting on the fifth day. Applied conditions seemed to be stressful for SAG 44.96 since akinete formation occurred between 18 and 32°C (see appendix, Figure 37). Thus, comparison of SAG 44.96 with the remaining ones should be considered critically. The determined temperature optimum of $18,47 \pm 0,93$ °C for SAG 44.96 was significantly lower than the average temperature optimum of $22,26 \pm 0,66$ °C of remaining strains (Figure 14). In an additional experiment, CCAC 3305 was subjected to the same conditions except for the light intensity; increasing the light intensity from 50 to 100 $\mu\text{mol m}^{-2} \text{s}^{-1}$ had no effect on the temperature optimum, only growth was boosted (data not shown).

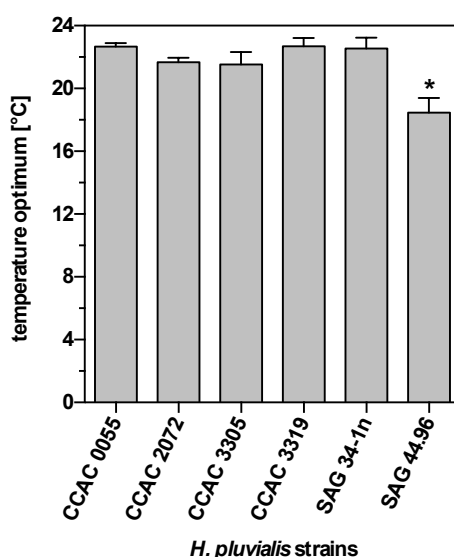


Figure 14 Temperature optimum of six selected *H. pluvialis* strains grown at ten different temperatures and 50 $\mu\text{mol photons m}^{-2} \text{s}^{-1}$. Temperature optima achieved at the last two time points of each replicate were fused into one data set per strain. *Mean \pm SD; n = 4.*

3.2 Astaxanthin production in *H. pluvialis* CCAC 3305

Since growth experiments revealed the best growing strains in a microscale set-up (compare section 3.1), *H. pluvialis* CCAC 3305 was selected for microscale astaxanthin induction experiments. *H. pluvialis* CCAC 3305 was grown in full, nitrogen- and phosphorus-deficient BG-11 medium supplemented with different salt concentrations ranging from 0 to 0.8% sodium chloride (NaCl). Effect of nutrient deficiency and salt stress on growth and astaxanthin content was analyzed.

At first, growth of CCAC 3305 in full BG-11 medium without any salt supplementation (data set AF) was compared to the data set (ZÇ) from section 3.1 (compare Figure 10) to evaluate the reproducibility of both results (Figure 15). The trends of exponential phases were similar, but time-shifted due to different initial cell densities ($N_{0,AF}$ and $N_{0,ZÇ}$). Specific growth rates μ_{AF} and $\mu_{ZÇ}$ were slightly different with 0.457 and 0.513 day⁻¹. The equations for respective exponential phases were as follows:

$$N = N_0 \cdot e^{(\mu \cdot t)}$$

$$N_{AF} = 263510 \cdot e^{(0.457 \cdot t)}; R^2 = 0.9771$$

$$N_{ZÇ} = 51871 \cdot e^{(0.513 \cdot t)}; R^2 = 0.9861$$

Since cells from the logarithmic phase were applied for both experiments, the time shift could be calculated as follows:

$$N_{0,AF} = N_{0,ZÇ} \cdot e^{(\mu_{ZÇ} \cdot t)}$$

$$\Leftrightarrow t = \frac{\ln N_{0,AF} - \ln N_{0,ZÇ}}{\mu_{ZÇ}} = 2.98$$

Accordingly, data set AF was corrected by shifting the data for three days ($AF_{shifted}$). Data correction resulted in four overlapping data points of data set ZÇ and $AF_{shifted}$ between day three and six. Since there were no significant differences between overlapping data points, data sets ZÇ and $AF_{shifted}$ were merged into a single data set generating the following equation for exponential growth in *H. pluvialis* CCAC 3305:

$$N = N_{0,merged} \cdot e^{(\mu_{merged} \cdot t)}$$

$$N = 57991 \cdot e^{(0.494 \cdot t)}; R^2 = 0.9837$$

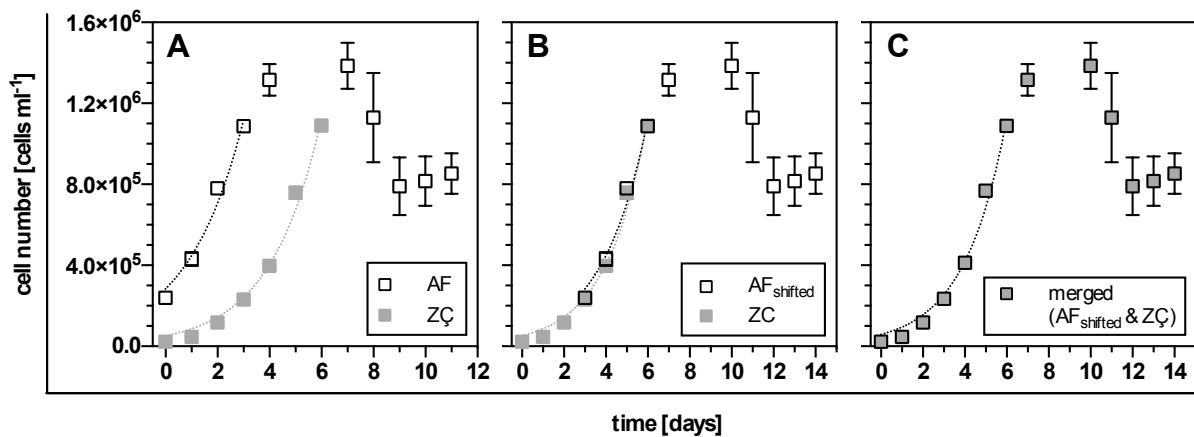


Figure 15 Comparison and correction of growth curves of *H. pluvialis* CCAC 3305 from independent experiments at 23°C and 50 $\mu\text{mol photons m}^{-2} \text{s}^{-1}$. **[A]** Data sets ZÇ and AF with different initial cell densities were compared. **[B]** Results were corrected by shifting data according to exponential growth equation. **[C]** Since overlapping data points from corrected results were not significantly different, data sets were merged. *Mean \pm SD; $n = 3$ (AF) or $n = 4$ (ZÇ).*

The effect of nutrient deficiency (-P, -N) and salt stress on growth and astaxanthin kinetics was analyzed (Figure 16). Nutrient deficiency had no significant effect on growth until day two when compared to full BG-11 medium. From day three to eight nutrient deficiency led to lower cell densities than in full medium. From day eight to ten cell densities were similar, since growth curve in full medium showed a decline phase from day seven to eight. Application of 0.1 and 0.2 % NaCl had a decreasing effect on cells grown in full and -P medium. However, cell densities in -N medium were similar to the ones without salt stress. Salt concentrations of 0.3 to 0.5% NaCl effected cells grown in full, -P and -N medium drastically and in the same way: first initial cell densities declined until day two, then slightly increased and stabilized at the following days. In all conditions, astaxanthin accumulation started at day three to four. Final astaxanthin was highest for cells grown in -P medium supplemented with 0.3% NaCl: total astaxanthin accounted for 51 $\mu\text{g mL}^{-1}$ with an astaxanthin content of 204 pg cell^{-1} . In general, final total astaxanthin concentration in full, -P and -N medium was increased when combined with 0.3 to 0.5%.

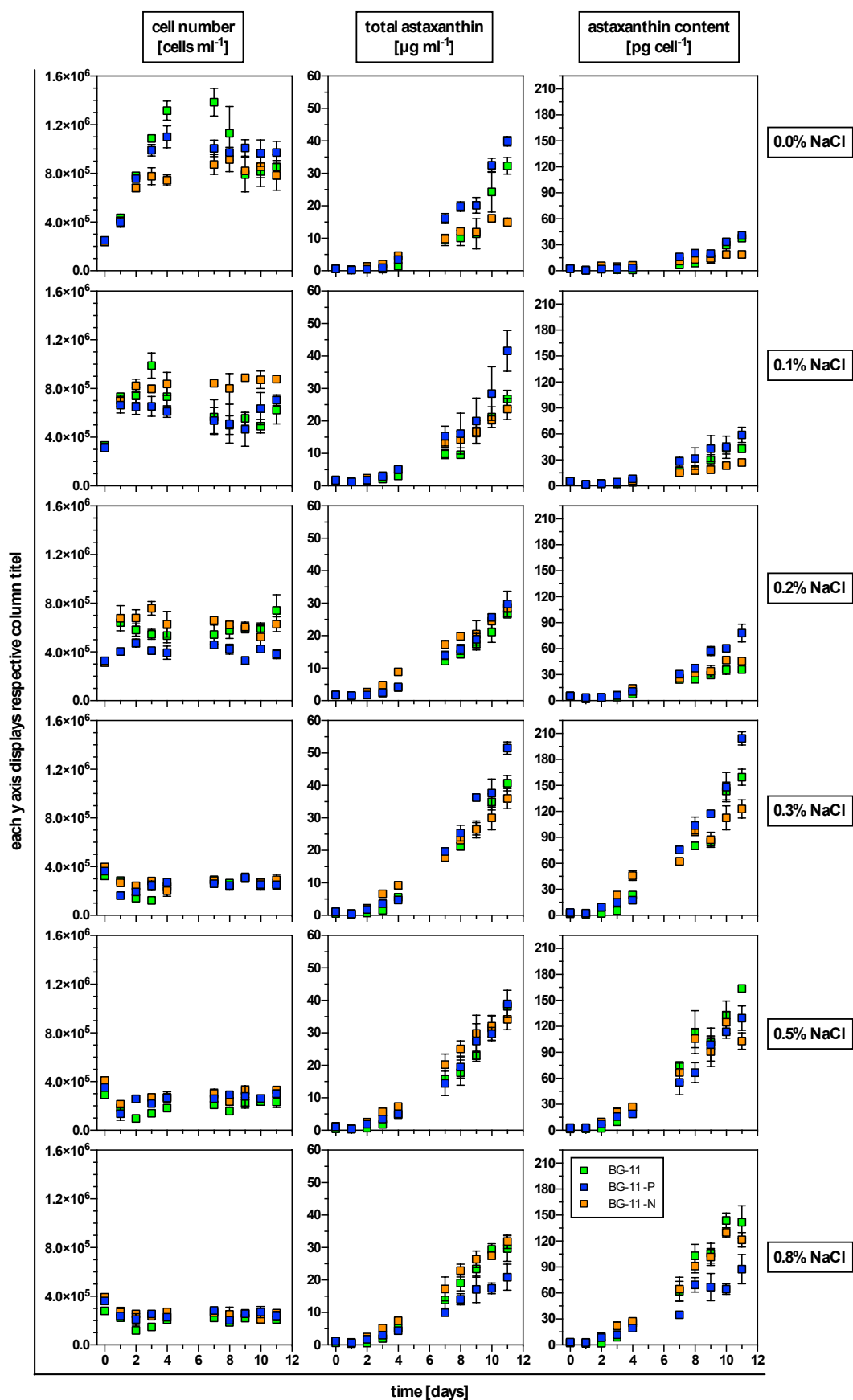


Figure 16 Development of cell growth, absolute and cellular astaxanthin content of *H. pluvialis* CCAC 3305 grown at 23°C and 50 µmol photons m⁻² s⁻¹ under optimal and stress conditions. Samples were grown in full, nitrogen deficient (-N) and phosphorus deficient (-P) BG-11 medium supplied with six different salt concentrations ranging from 0 to 0.8% NaCl. Mean ± SD; n = 3.

Since there was a gap of information between 0.3 and 0.5% NaCl supplementation with respect to astaxanthin kinetics (data set AF), the experiment was repeated with higher resolution of salt concentrations in full BG-11 medium (data set FK). At first, results for data sets AF and FK were compared with respect to growth in in BG-11 medium supplemented with 0.3 and 0.5% NaCl (Figure 17). The trends for growth and astaxanthin accumulation were similar. However, data set AF generally yielded in higher values than FK since the initially applied cell density was higher, too.

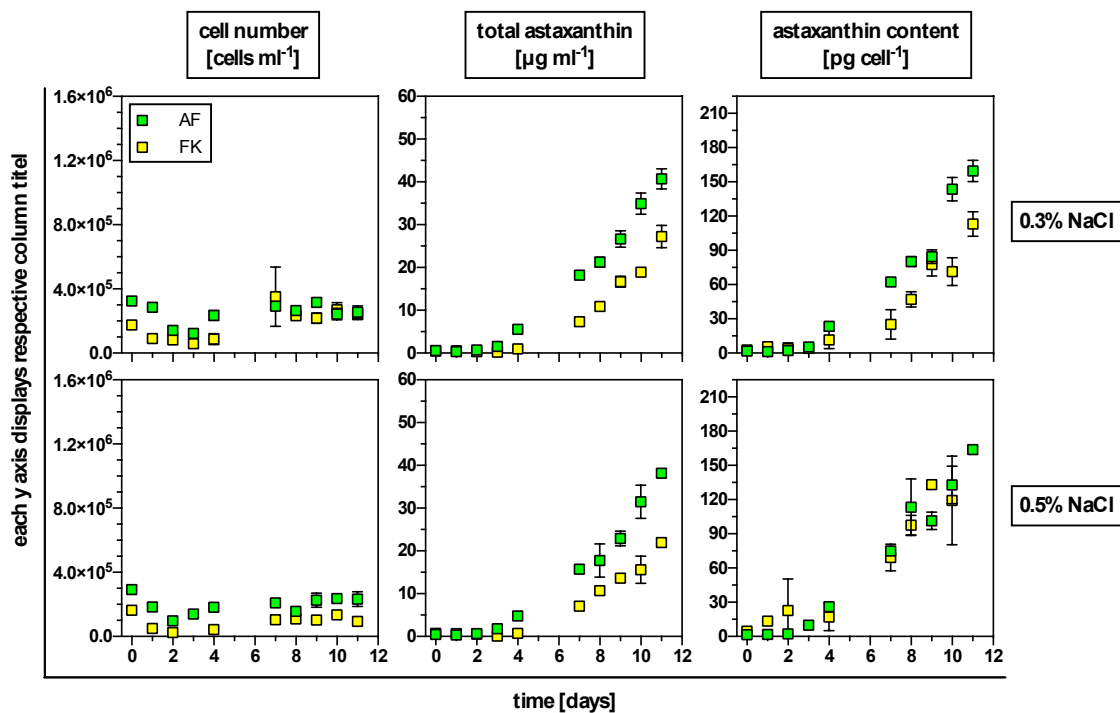


Figure 17 Comparison of two independent salt stress experiments concerning cell growth, absolute and cellular astaxanthin content of *H. pluvialis* CCAC 3305 grown at 23°C and 50 $\mu\text{mol photons m}^{-2} \text{s}^{-1}$. Samples were grown in full BG-11 medium supplied with 0.3 and 0.5% NaCl. Data sets AF and FK were achieved from independent experiments. *Mean* \pm *SD*; *n* = 3.

To make the data sets more comparable, data set AF was shifted for 1.2 days ($\text{AF}_{\text{shifted}}$) according to exponential growth equation as already described in this section (Figure 18). Statistical analyses between data sets could not be performed since time shift value was not integer. In contrast to salt free medium where this shifting strategy led to perfectly matching results concerning cell densities, data correction had to be handled with critical care since the presence of stress conditions, especially until day four, limited the comparability of results.

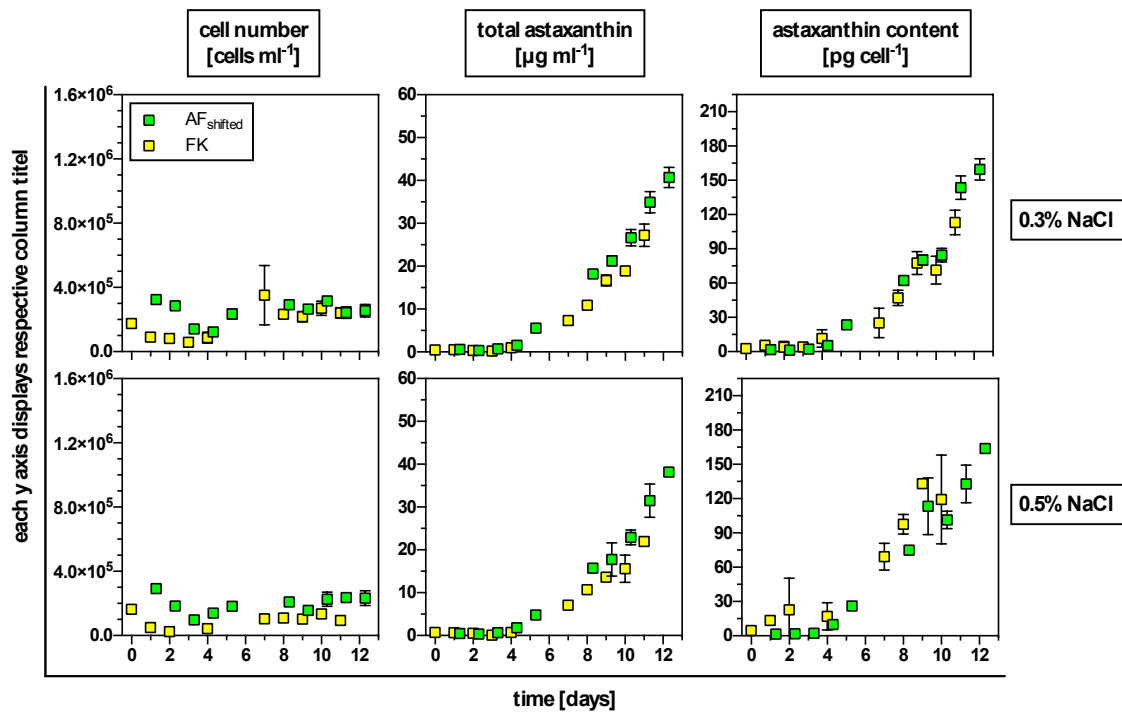


Figure 18 Correction of two independent salt stress experiments concerning cell growth, absolute and cellular astaxanthin content of *H. pluvialis* CCAC 3305 grown at 23°C and 50 μmol photons m⁻² s⁻¹. Samples were grown in full BG-11 medium supplied with 0.3 and 0.5% NaCl. Data sets AF and FK were corrected due to different initial cell densities. For this AF data set was shifted for 1.2 days according to the exponential growth equation. Mean ± SD; n = 3.

The complete data set FK was analyzed; data set AF_{shifted} was included at coincident salt concentrations (Figure 19). Similar to previous results, initial cell densities first declined until day two to three, then slightly increased and stabilized at the following days. Until day eight, there were no significant differences for data set FK between the applied salt concentrations with respect to total astaxanthin concentration. Significant differences were evident on day nine for 0.30 vs. 0.50% and 0.35 vs. 0.40 to 0.50% NaCl. On day ten and eleven, significant differences were evident for 0.25 vs. 0.35/ 0.50%, 0.30 vs. 0.50%, 0.35 vs. 0.40 to 0.50% and 0.50% vs. 0.40 to 0.45%. Cellular astaxanthin concentrations were not significantly different until day six. On day seven and eight, 0.45 vs. 0.25/ 0.30% and 0.50 vs. 0.25 to 0.35% were significantly different. On day nine, significant differences could be detected for 0.25 vs. 0.35 to 0.50%, 0.30 vs. 0.40 to 0.50% and 0.45 vs. 0.35/ 0.40%. On day ten, cellular astaxanthin differed significantly for 0.25/ 0.30% vs. 0.45/ 0.50%. On the final day, most significant differences were evident for 0.25% vs. all other salt concentrations, 0.40 vs. 0.30/ 0.35%, 0.45 vs. 0.30 to 0.40% and finally, 0.50 vs. 0.30 to 0.40%.

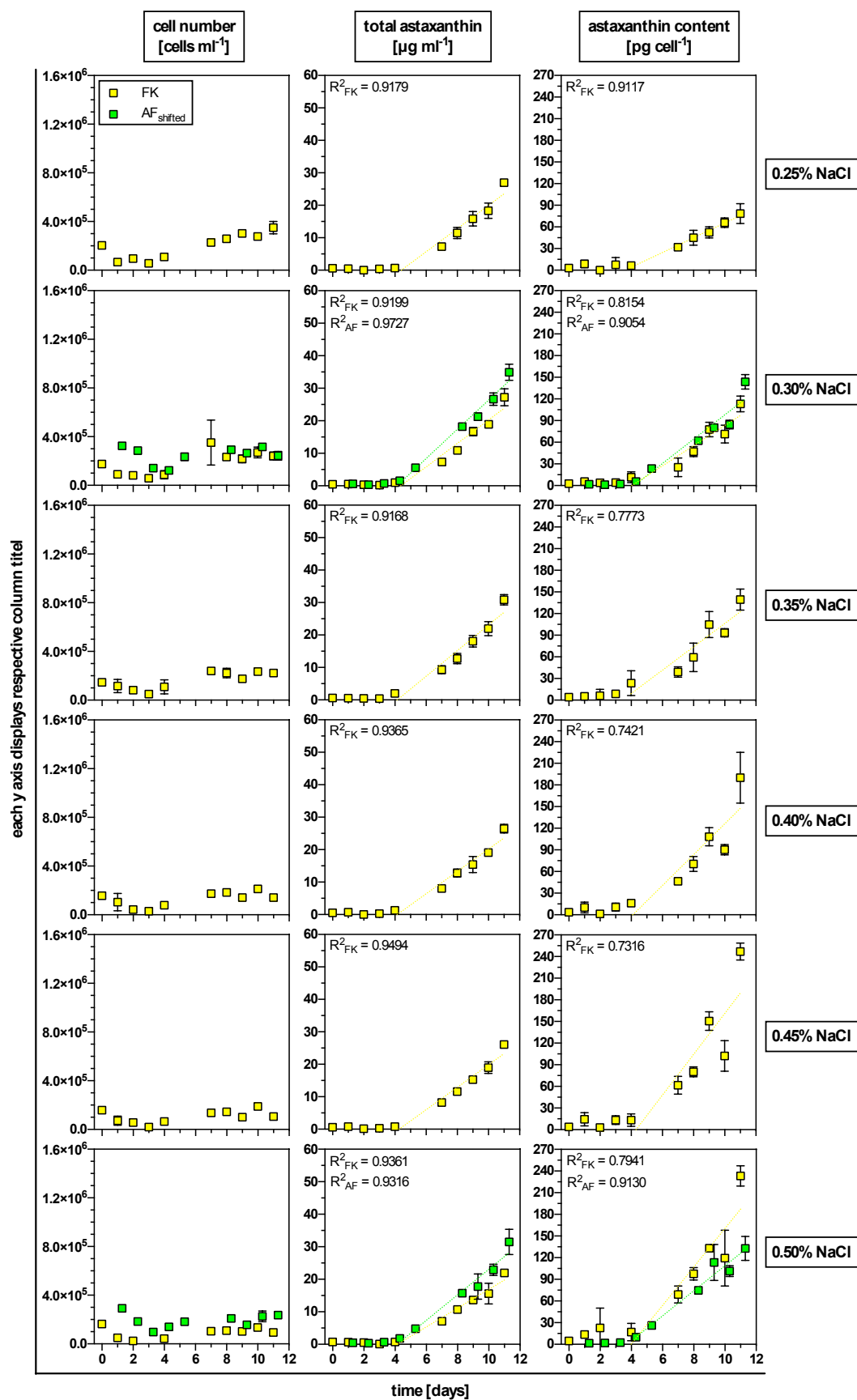


Figure 19 Development of cell growth, absolute and cellular astaxanthin content of *H. pluvialis* CCAC 3305 grown at 23°C and 50 $\mu\text{mol photons m}^{-2} \text{s}^{-1}$ under salt stress conditions. Cells were grown in full BG-11 medium supplied with six different salt concentrations ranging from 0.3 to 0.5% NaCl. Mean \pm SD; $n = 3$.

Overall, accumulation rate of total astaxanthin from data set FK was best at 0.35% NaCl condition with a rate $4.0 \mu\text{g mL}^{-1} \text{ day}^{-1}$; final astaxanthin concentration accounted for $30 \mu\text{g mL}^{-1}$. However, accumulation rate of $4.5 \mu\text{g mL}^{-1} \text{ day}^{-1}$ and final astaxanthin concentration of $35 \mu\text{g mL}^{-1}$ was higher at 0.30% NaCl for data set AF_{shifted}. The highest final cellular astaxanthin content of 247 pg cell^{-1} was detected at 0.45% NaCl. However, the gap of information between 0.3% and 0.5% NaCl could not be robustly enlightened with respect to astaxanthin kinetics since data sets FK and AF/ AF_{shifted} could not be tested for significant differences.

3.3 Genome size of various *H. pluvialis* strains

Since to date the genome of *H. pluvialis* is not annotated and its size is unknown, the genome size was estimated for all subjected strains (Figure 20). DNA from a determined number of cells was extracted and cellular DNA content was converted to Gbp units according to Kapraun (2007). To evaluate the accuracy of this method, *Chlamydomonas reinhardtii* was applied as a reference organism. The genome size of *C. reinhardtii* accounts for approximately 120 Mbp (Merchant et al., 2007). Here, the genome size of *C. reinhardtii* was estimated to be $98.4 \pm 8.2 \text{ Mbp}$ (data not shown), i.e. the result was close to the literature value, but 20 Mbp lower.

Estimated genome sizes for *H. pluvialis* strains ranged from $2.6 \pm 0.6 \text{ Gbp}$ to $7.8 \pm 0.4 \text{ Gbp}$ with SAG 34-11(2) and CCAC 0055 possessing the minimum and maximum value, respectively. One half of tested strains had a genome size of up to four Gbp while the other half possessed a genome size more than four to approximately eight Gbp. In comparison to *C. reinhardtii*, genome size of *H. pluvialis* was 26- to 80-fold higher.

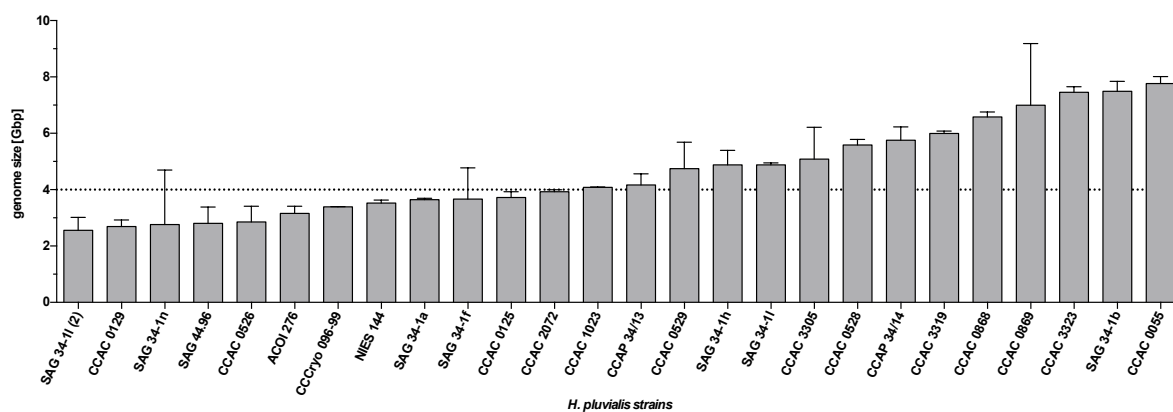


Figure 20 Genome size of 26 *H. pluvialis* strains. Data were sorted with increasing genome size [Gbp]. Mean \pm SE; $n = 2$.

3.4 Phylogenetic analysis of *H. pluvialis* strains

Since the variety of subjected *H. pluvialis* strains, originating from different geographical regions, were similar in morphology, but showed different physiological properties, it was interesting to test if there was any genetic diversity among the strains and any correlation to achieved data. Therefore, strains were analyzed on a phylogenetic level based on *rbcL* gene and rDNA sequences (5.8S, ITS2 and partial 28S).

Phylogenetic tree from combined analyses basically revealed that *H. pluvialis* was monophyletic (Figure 21). Buchheim et al. (2013) categorized *H. pluvialis* into five lineages (A to E). In this study, a distinct separation of lineage A and E was not supported. Instead, ACOI-276 and SAG 34-1h designated as lineage E by Buchheim et al. (2013), were grouped into lineage A within this study. Most of analyzed taxa were grouped into lineage A. Lineage B constituted five foreign taxa based on ITS2 sequences only. Lineage C comprised four taxa including SAG 34-1f. Lineage D comprised only one taxon: SAG 44.96.

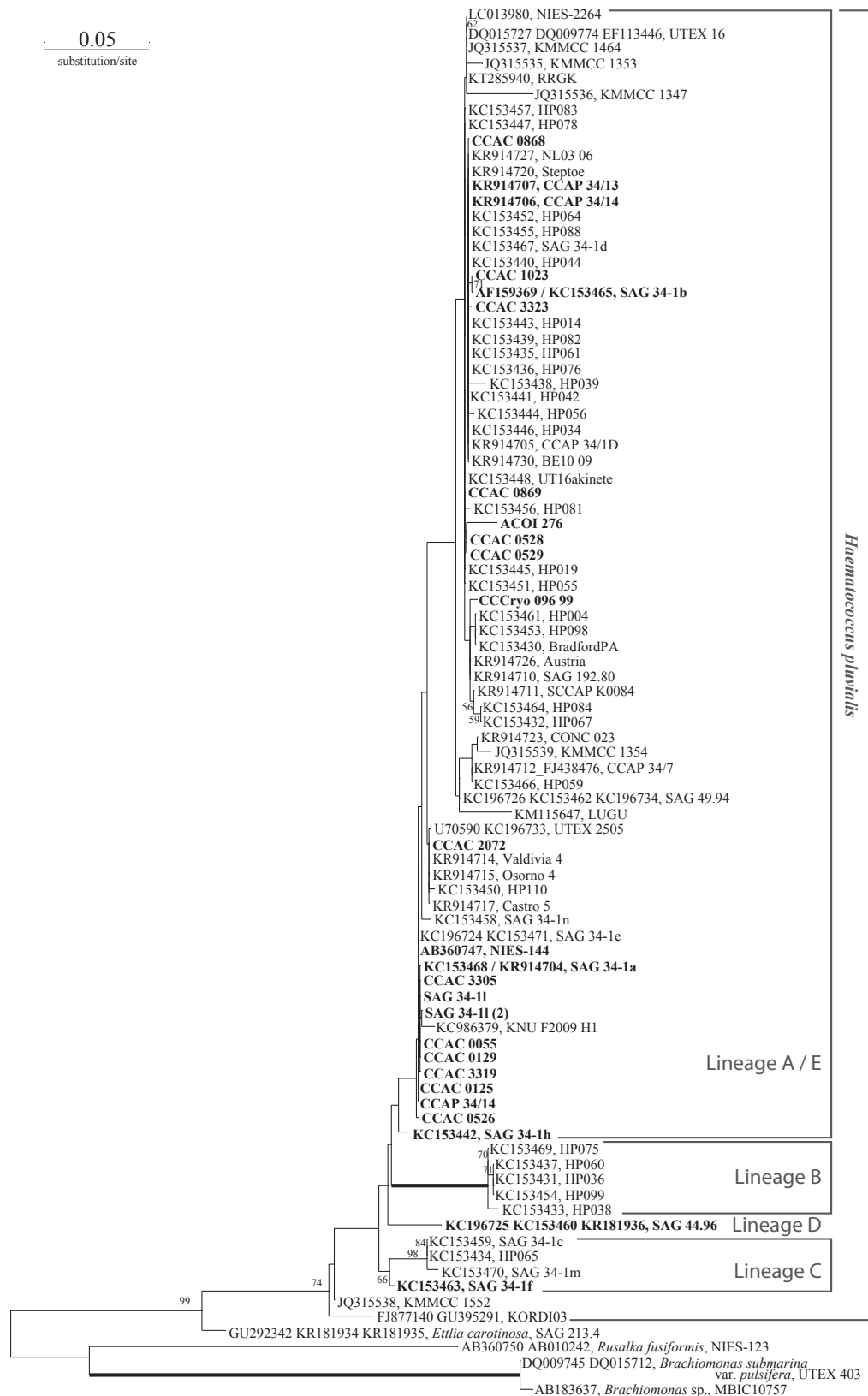


Figure 21 Phylogenetic tree from combined ML analyses of *rbcl* gene and rDNA sequences (5.8S, ITS2 and partial 28S). GTR+I+ Γ was used as an evolution model. Values at the branches represent ML-bootstrap from 1,000 pseudo-replicates. Maximum support is indicated by thick branches. Tree comprises 90 taxa including four outgroups. Bold highlighted taxa represent strains subjected in this study. Lineage categories were adapted from Buchheim et al. (2013). Scale bar = 0.05 nucleotide substitutions site⁻¹.

Consensus secondary structure of ITS2 was reconstructed based on the model for Chaetophorales, Chaetopeltidales, Oedogoniales and Sphaeropleales described by Caisová et al. (2013). ITS2 sequences of *H. pluvialis* strains were highly conservative with only a few variable positions (Figure 22). Variable positions were predominantly close or within loops. Spacer regions were predominantly conservative; only one position between helix two and three, and one position between helix three and four were slightly variable. Variations affected the level of nucleotide conservation and/ or the length of sequence. Variability due to nucleotide insertions was identified just for SAG 44.96.

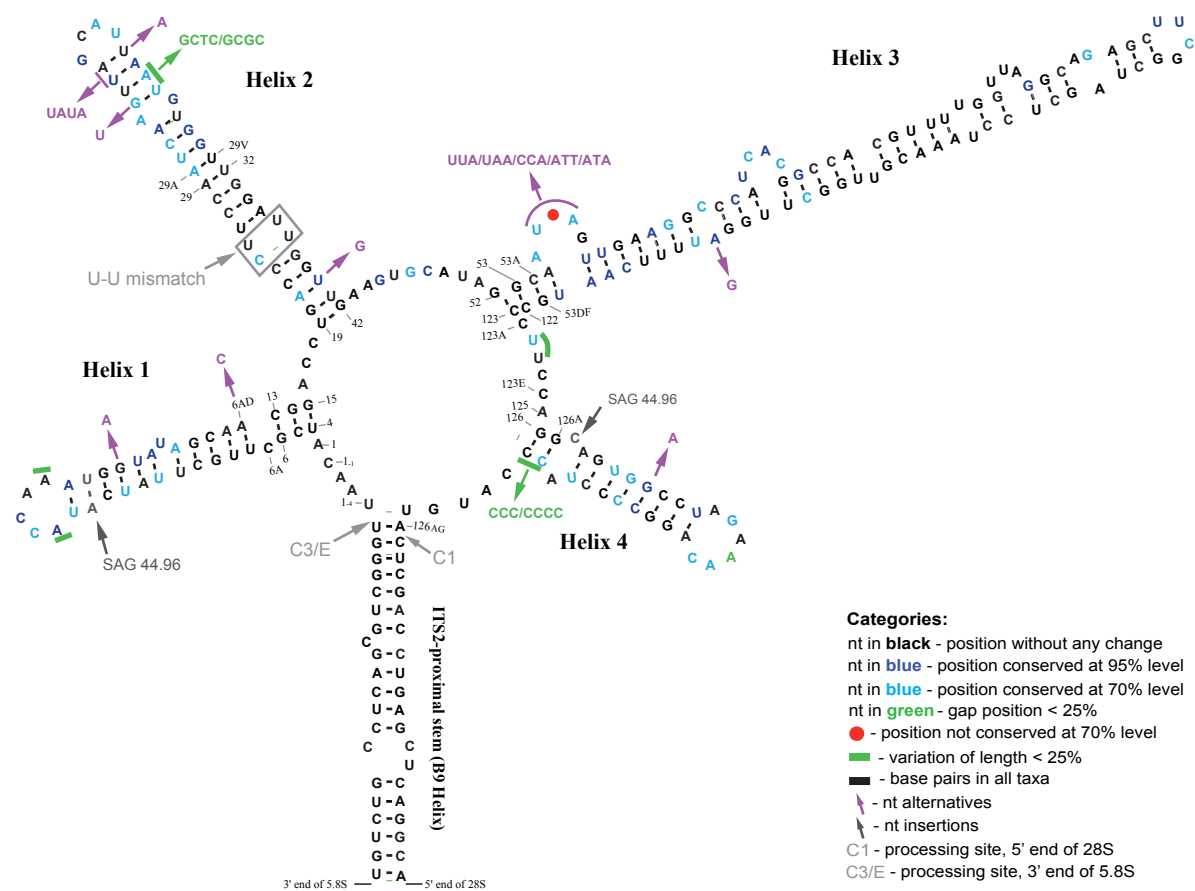


Figure 22 Consensus secondary structure model of ITS2 in *H. pluvialis*. ITS2 sequences of 72 taxa were homologized for reconstruction of secondary structure. Categories were adopted from Caisová et al. (2011). *nt* - nucleotides.

3.5 EMS mutagenesis of *H. pluvialis* CCAC 0125

Ethyl methanesulfonate (EMS) is an guanine alkylating agent that is often used for random mutagenesis (Rhaese & Boetker, 1973; Klug et al., 2011;). Although the mutation rate of EMS cannot be predicted, choosing a lethal dose of 50% for mutagenesis can minimize multiple mutations. Unique mutations per genome can be aimed from a statistical point of view when the number of cells exposed to EMS corresponds to the genome size (Flynn et al., 2002). Based on this information, one *H. pluvialis* strain was selected and mutagenized with EMS according to Flynn et al. (2002). Since mutant screening was conducted on solid BG-11 medium, a strain capable for efficient growth and astaxanthin accumulation in an immobilized state was chosen. According to Kiperstok (2016), *H. pluvialis* CCAC 0125 fulfilled these requirements and was consequently chosen for the EMS mutagenesis approach.

Wild type (WT_i) and EMS treated (E_i) samples were plated on several agar plates and consecutively cultivated at 24.28 ± 6.02 (LI₂₅) and 91.34 ± 24.98 (LI₉₀) $\mu\text{mol photons m}^{-2} \text{s}^{-1}$ for three weeks and eleven days, respectively. The number of single colony forming units (cfu) was counted and the number of colonies merged clusters was estimated, so that the total number of cfu could be calculated (Figure 23). About one half of detected cfu was merged in colony clusters in WT and EMS treated samples. Survival rates of EMS samples accounted for $38.77 \pm 2.59\%$ instead of 50%.

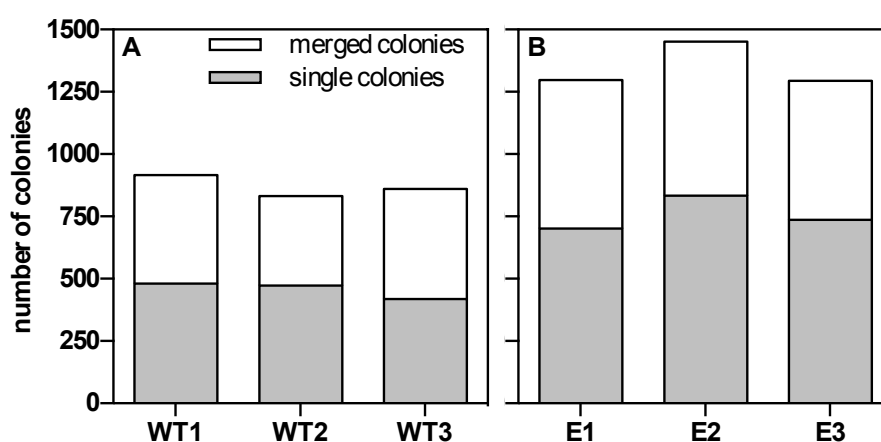


Figure 23 Number of achieved cfu for WT and EMS treated samples of *H. pluvialis* CCAC 0125. Samples WT1-WT3 [A] and E1-E3 [B] were analyzed by stereomicroscopy.

Colony diameter (\emptyset) of 1372 WT and 2272 mutant colonies was measured (Figure 24) and pigmentation of cfu caused by astaxanthin accumulation was evaluated visually (see appendix, Figure 41). After exposition to LI_{25} and LI_{90} , colony diameter of WT and EMS samples increased 48 and 43% from 0.71 ± 0.20 to 1.05 ± 0.28 mm and 1.00 ± 0.28 to 1.43 ± 0.36 mm, respectively. Minimal and maximal values of WT were 0.23 and 1.46 mm at LI_{25} and 0.34 and 2.04 mm at LI_{90} , respectively. Minimal and maximal values of EMS samples accounted for 0.04 and 2.14 mm at LI_{25} and 0.15 and 2.92 mm at LI_{90} , respectively. Generally, variations in colony size were significantly different between WT and EMS samples, and between the two applied light intensities.

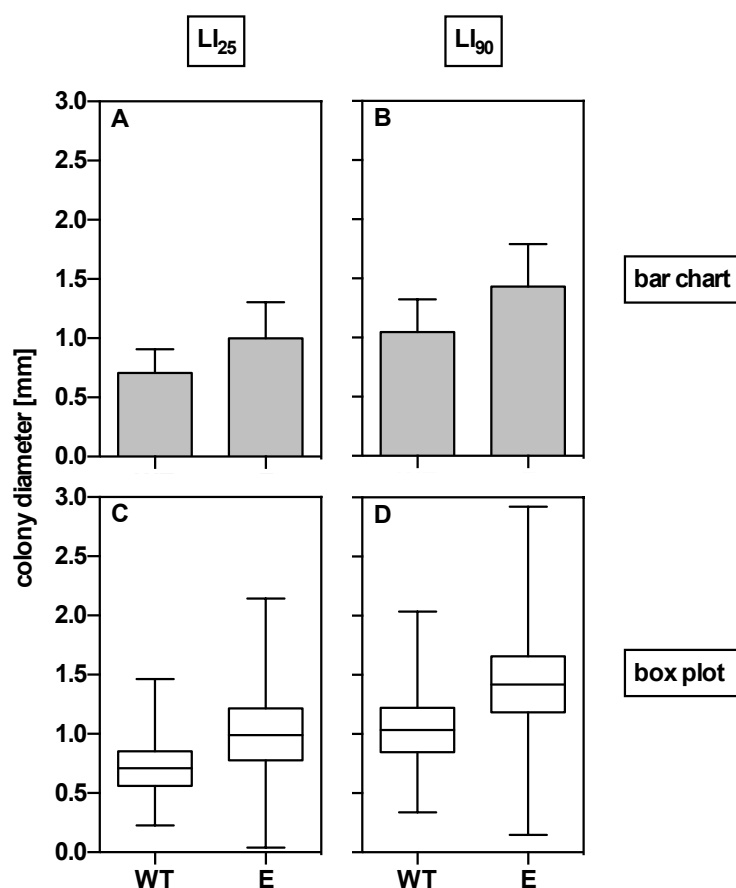


Figure 24 Development of colony size of WT and EMS treated samples at two different light intensities. Samples (WT and E) were first grown at 23°C and $25 \mu\text{mol photons m}^{-2} \text{s}^{-1}$ (LI_{25}) for three weeks [A and C]. Samples were grown for further eleven days at $90 \mu\text{mol photons m}^{-2} \text{s}^{-1}$ (LI_{90}) [B and D]. Mean \pm SD are illustrated in bar graphs [A and B]. Corresponding box plots visualize detected minima and maxima of data sets and the range of midspread values [C and D]. $n_{WT} = 1372$; $n_E = 2272$.

360 putative mutant colonies were selected from 2272 single cfu based on colony size and/ or pigmentation. To verify achieved results, 118 of selected mutant colonies were replated on solid medium and analyzed again with respect to colony size. As a control, five WT colonies were randomly selected from 1372 single cfu and treated the same way. In total, 375 WT and 8306 mutant colonies were analyzed after replating.

Colony sizes of replated WT daughter colonies were in accordance with colony sizes of respective five mother colonies. There was no significant difference for average colony size of replated WT and WT colonies from the previous experiment: mean \pm SD of WT colony diameter accounted for 0.71 ± 0.20 mm (Figure 25).

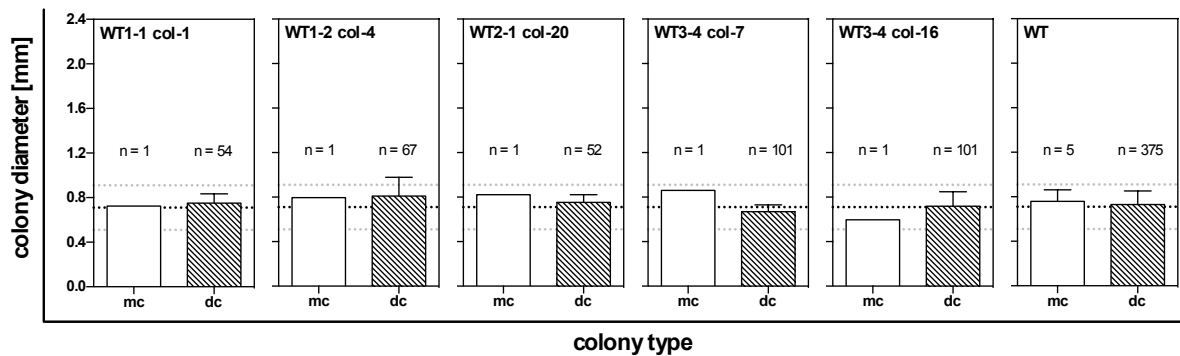


Figure 25 Stereomicroscopical verification of WT colonies based on colony diameter. Five randomly selected mother colonies (mc) and their replated daughter colonies (dc) were reproducible in colony size. Mean \pm SD of left five figures is represented in the right figure. Mean \pm SD of WT colony diameter from previous analyses is represented by horizontal black and grey dotted lines, respectively.

Colony sizes of 118 selected mutant colonies were predominantly not reproducible (see appendix Figure 42); 70 of 118 replated colonies (59%) were smaller in size and 20 of 118 colonies (17%) were bigger in colony size than respective mother colonies. Only 28 of 118 (24%) selected colonies were reproducible with respect to colony size (Figure 26). From the 28 verified mutant colonies, 17 mutant colonies were bigger, six were smaller and five were similar to the WT colony size.

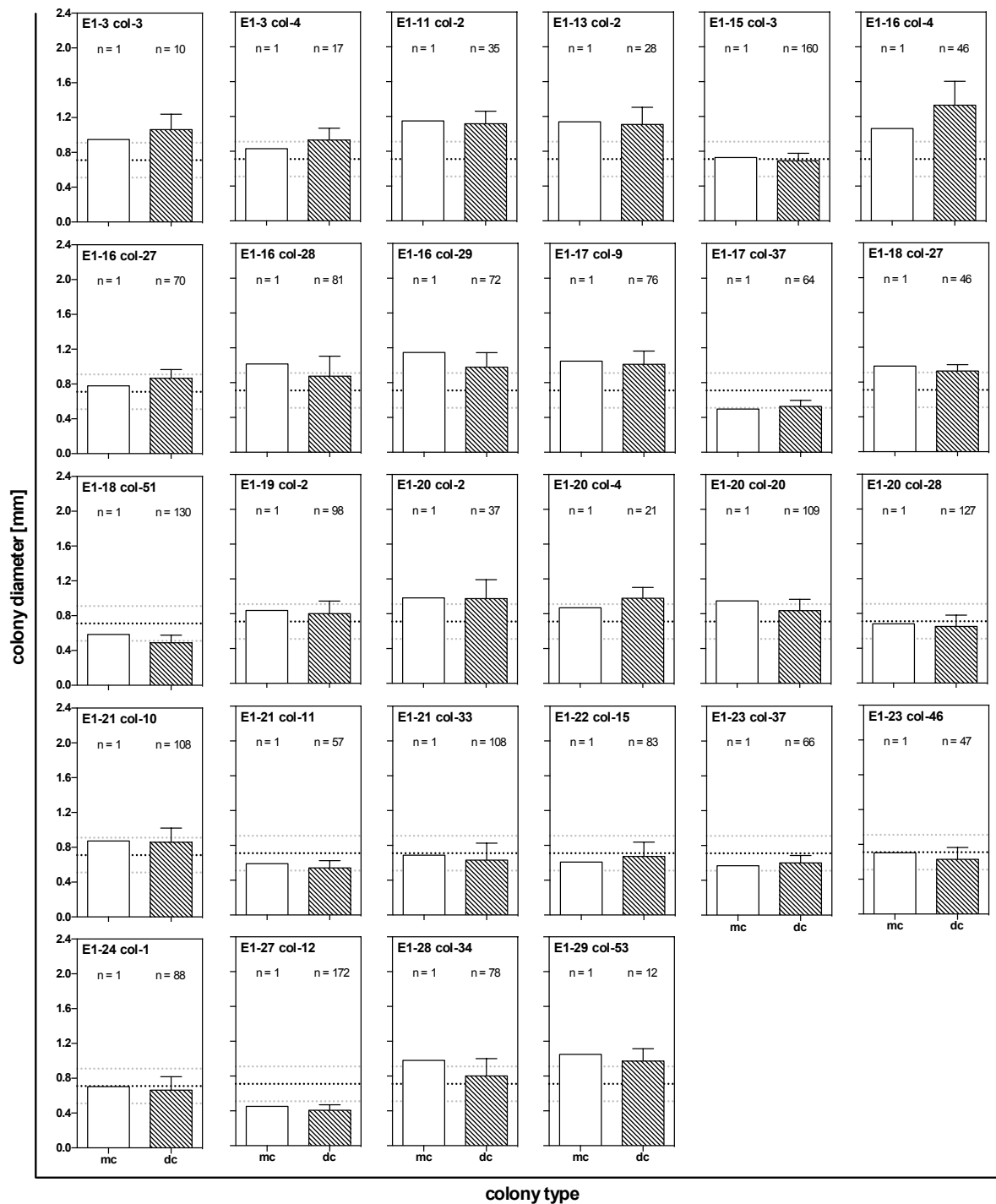


Figure 26 Stereomicroscopical verification of EMS mutants based on colony diameter. 28 mother colonies (mc) and their corresponding daughter colonies (dc) were reproducible in colony size. Horizontal dotted lines represent mean (black) \pm SD (grey) of WT colony diameter.

Five verified EMS mutants (E1-11 col-2, E1-16 col-4, E1-16 col-29; E1-17 col-9 and E1-17 col-4) were further analyzed with respect to their growth pattern in suspension. One WT colony was treated analogously. Growth of suspended WT colony was compared with the results achieved for the suspension culture of *H. pluvialis* CCAC 0125 (WT_{ZÇ-Ref}) from previous experiments (Figure 10). Furthermore, growth kinetics

of WT and EMS mutants were compared (Figure 27). Growth of WT and WT_{ZC-Ref} was exponential over the tested time period of four days, but cell densities were significantly different from day two to four. Exponential growth of all tested mutants was limited until day two. Growth pattern of mutant E1-11 col-2 was similar to WT, but with a significantly higher cell density on day three. Similarly, cell densities of E1-16 col-4 and E1-17 col-9 were conform with WT until day three; on day four both mutants showed significantly lower cell densities than WT. Mutants E1-16 col-29 and E1-17 col-37 showed significantly lower cell densities than WT on day two and four.

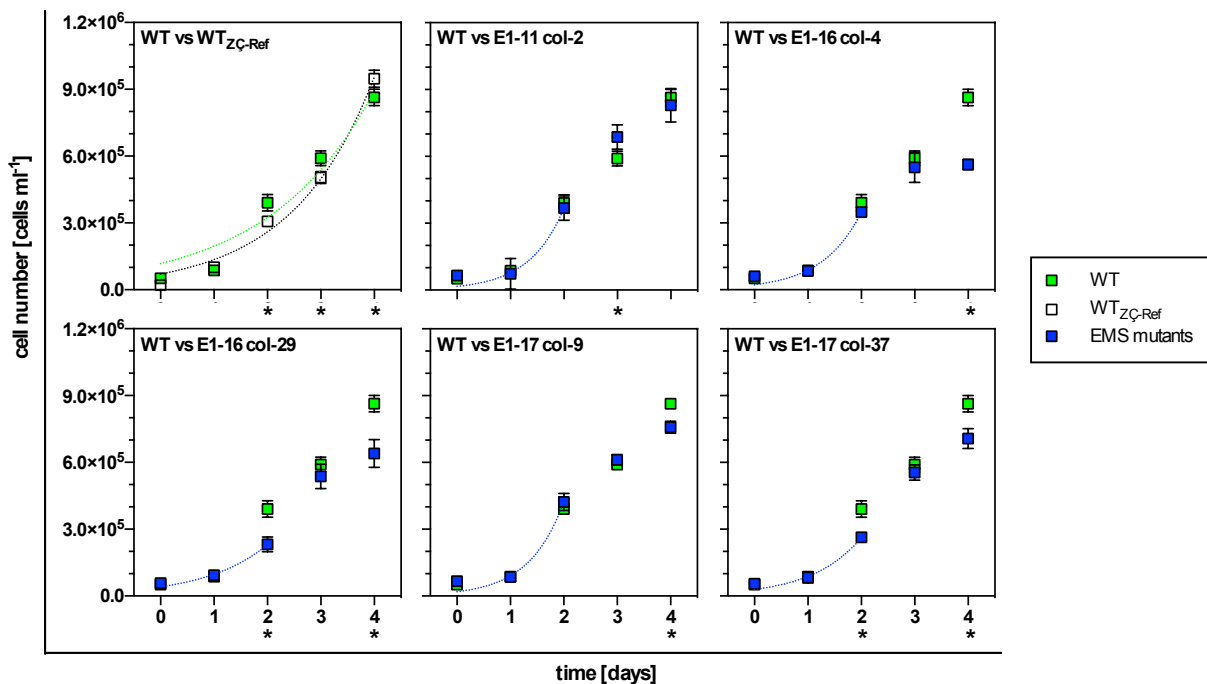


Figure 27 Growth curves of *H. pluvialis* CCAC 0125 WT and five EMS mutants grown at 23°C and 50 $\mu\text{mol photons m}^{-2} \text{s}^{-1}$. Dotted curves represent exponential phases. Significant differences are marked with an asterisk at corresponding time points. Mean \pm SD; $n = 4$.

Further growth parameters were calculated for WT and mutants (Figure 28). Specific growth rates of mutants ranged from 0.876 day^{-1} (E1-16 col-29) to 2.061 day^{-1} (E1-11 col-2) and were generally higher than specific growth rates of WT and WT_{ZC-Ref} (0.507 and 0.651 day^{-1} , respectively). Doubling times of mutants varied from 0.452 days (E1-17 col-9) to 0.819 days (E1-16 col-29) and were lower than WT and WT_{ZC-Ref} (1.368 and 1.065 days, respectively). AUC calculation showed that AUC_{exp}/AUC_{total} ratio was 100% for WT and WT_{ZC-Ref} and that growth efficiency of all mutants was significantly lower with a maximal AUC_{exp}/AUC_{total} ratio of 19%.

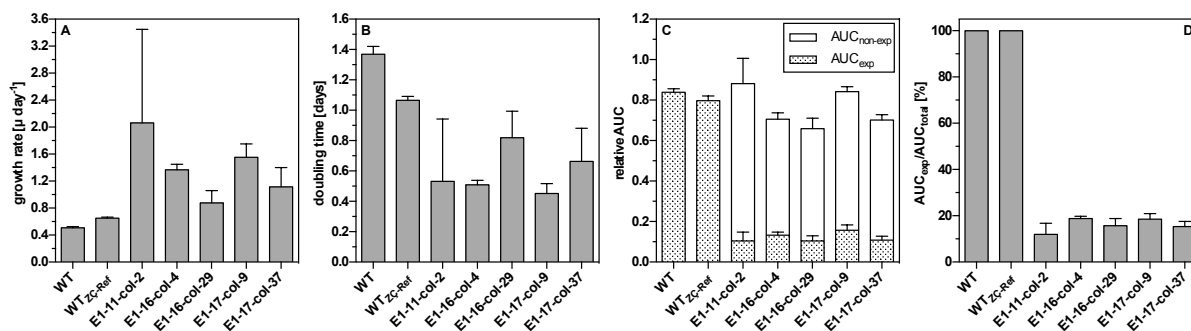


Figure 28 Calculated growth parameters for *H. pluvialis* CCAC 0125 WT and five EMS mutants. Specific growth rate μ **[A]** and doubling time **[B]** were calculated from each exponential phase of growth curves. Growth efficiency was evaluated using AUC_{total} **[C]** and the AUC_{exp} / AUC_{total} ratio **[D]**. Mean \pm SD; $n = 4$.

Furthermore, WT and E1-16 col-4 were analyzed for growth and astaxanthin production in an immobilized state using laboratory scale TL-PSBR. The experiment was conducted in two steps according to Kiperstok (2016): samples were first cultivated at $90 \mu\text{mol photons m}^{-2} \text{s}^{-1}$ for eight days and then exposed to $1,000 \mu\text{mol photons m}^{-2} \text{s}^{-1}$ for further eight. Development of biomass and astaxanthin accumulation was monitored (Figure 29).

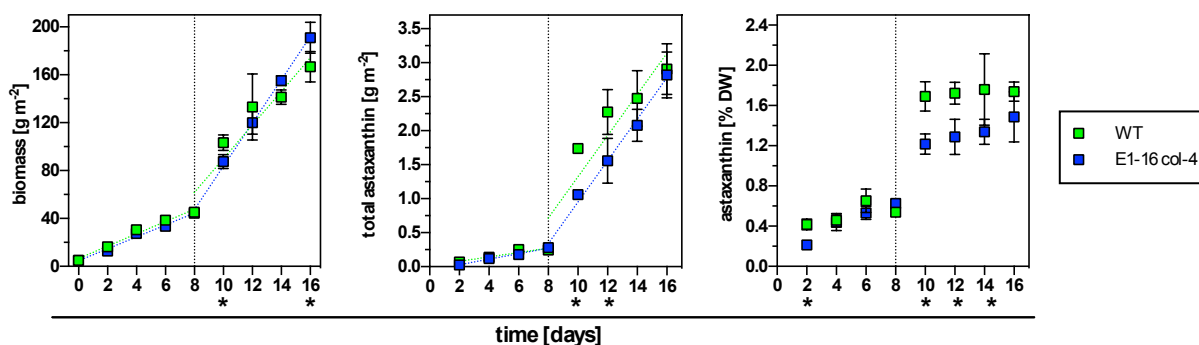


Figure 29 Biomass and astaxanthin kinetics of immobilized *H. pluvialis* CCAC 0125 WT and EMS mutant E1-16 col-4 using TL-PBSR. Samples were cultivated in a two-step approach according to Kiperstok (2016) using 90 and $1,000 \mu\text{mol photons m}^{-2} \text{s}^{-1}$ for the first and last eight days of cultivation, respectively. Time point of light switch is represented by vertical dotted line. **[A]** Biomass, **[B]** total astaxanthin and **[C]** astaxanthin content were analyzed. Productivities were calculated from linear regression indicated by colored dotted lines. Significant differences are marked with an asterisk at corresponding time points. Mean \pm SD; $n = 3$.

For the first eight days of cultivation, biomass and total astaxanthin of WT and mutant E1-16 col-4 were not significantly different with average productivities of 5 and $0.035 \text{ g m}^{-2} \text{ day}^{-1}$, respectively. Application of high light on day eight boosted both, biomass and astaxanthin production in WT and mutant. It has to be noted that WT samples were slightly dried out between day nine and ten; this clearly affected total astaxanthin for WT on day ten and twelve with significantly higher values than in the

mutant. However, total astaxanthin productivity had the same rate with $0.30 \text{ g m}^{-2} \text{ day}^{-1}$. Astaxanthin content increased between day eight to ten from approximately 0.55% to 1.7% in WT and to 1.2% in E1-16 col-4. Final astaxanthin content of approximately 1.6% was not significantly different between WT and mutant. Similarly, final total astaxanthin was not significantly different between WT and mutant with approximately 2.85 g m^{-2} . Final biomass of E1-16 col-4 was significantly higher than in WT with 191 and 166 g m^{-2} , respectively. Biomass productivity accounted for 14 and $18 \text{ g m}^{-2} \text{ day}^{-1}$ in the last eight days for WT and mutant, respectively. However, comparison of WT and E1-16 col-4 is critical due to partial drying-out of WT samples during the experiment.

Research on *Haematococcus pluvialis* is a highly topical subject in physiological, molecular and biotechnological analyses. Improving growth and astaxanthin accumulation is dependent on multiple factors comprising the choice of strains, type of growth medium (with or without organics), light source (natural vs. artificial fluorescent or LED light), light quality (PFD rates, low or high wavelengths), type of stress conditions for astaxanthin induction, and moreover, the type of cultivation system (suspension vs. immobilized cultures). Considering the number of combinable varieties of mentioned factors, it is no surprise that literature research on *H. pluvialis* by online inquiry gives an output of more than 10,000 results (status from 2016-10-05) with first descriptive publications dating back to the mid-19th century (Flotow, 1844). However, most of the literature has been published in the last two decades (9,500 of 10,000 results).

4.1 Efficient microscale screening of *H. pluvialis* concerning growth

Considering the high number of *H. pluvialis* strains available in several culture collections, only a small fraction is subjected in research. Since strain selection is one crucial factor for biotechnological applications, 26 geographically diverse *H. pluvialis* strains were analyzed in this study (Table 4).

Growth of *H. pluvialis* strains was monitored simultaneously in a short-time microscale set-up (Figure 10). The initial cell density of 2.5×10^4 cells ml⁻¹ increased within six days to a maximum cell density of 1.1×10^6 cells ml⁻¹ in 3 strains (CCAC 3305, CCAC 3319, SAG 34-1n). Specific growth rates varied from of 0.452 day⁻¹ to

1.071 day⁻¹ (Figure 12) which is quite realistic when compared to literature values. Fan et al. (1994) reported a specific growth rate of 1.296 day⁻¹ for a SAG strain grown with an initial cell density of 2.5×10^5 cells ml⁻¹ in BG-11 with 1.5% CO₂ aeration at 25°C and 130 μmol photons m⁻² s⁻¹ (fluorescent light); unfortunately it was not further specified which SAG strain in particular was used. In this study, a maximum growth rate of 1.071 day⁻¹ was determined for SAG 34-1h at a lower light intensity of 50 μmol photons m⁻² s⁻¹ and without any CO₂ supply. Katsuda et al. (2004) reported a specific growth rate of 0.552 day⁻¹ for NIES-144. Although cultivation conditions were clearly different (Kobayashi's basal medium, 20°C, 2.8 μmol photons m⁻² s⁻¹) in the approach of Katsuda et al. (2004), the specific growth rate of NIES-144 was in accordance with the growth rate of 0.581 ± 0.115 day⁻¹ determined in this study.

To screen for the best growing *H. pluvialis* strains, it was insufficient to focus solely on specific growth rates or doubling times, because length of the exponential phase and growth patterns in general were quite variable amongst the strains. Using AUC analyses (Figure 12) revealed five best growing strains with an AUC_{exp} / AUC_{total} ratio of 100% (CCAC strains 0055, 2072, 3305, 3319 and SAG 34-1n). Since growth can be optimized at a more favorable temperature, these five strains together with an additional strain (SAG 44.96) were grown along a temperature gradient ranging from 11.8 ± 0.3 °C to 31.8 ± 0.1 °C to determine each temperature optimum (Figure 13). Fan et al. (1994) reported that temperature optimum of a SAG strain (not further specified) was at 25 to 28°C. Except for SAG 44.96, the average temperature optimum of five selected strains was at 22.26 ± 0.66 °C in this study (Figure 14). This might be explained by their origin from temperate regions or by their adaptation to conditions in culture collections over the years of cultivation. The determined temperature optimum for the South African strain SAG 44.96 was at 18.47 ± 0.93 °C, but this result must be considered critically since applied conditions seemed to be stressful for this strain resulting in akinete formation (between 18 and 32°C).

Although the simultaneous screening of *H. pluvialis* strains in a 96-well format was successful, it has to be noted that few strains might not cope with this type of cultivation. Transferring cultures from glass vessels and a larger volume to a small size volume in a plastic environment might have an effect on growth. For instance, ACOI-276 and SAG 34-1n were not conspicuously different than remaining cultures

when maintained in 100 mL Erlenmeyer flasks. However, in microscale experiments both strains exhibited the worst outcome in growth (Figure 10); this was apparent for macroscopical inspection and for the lowest determined cell densities (1.6 and 1.7×10^5 cells ml^{-1}) after six days of growth. Adapting cultures to microscale cultivation in multititer plates prior to such experiments might solve this problem.

4.2 Efficient microscale induction of astaxanthin in *H. pluvialis*

Since growth experiments revealed the best growing strains in a microscale set-up (Figure 12), *H. pluvialis* CCAC 3305 was selected for microscale astaxanthin induction experiments. *H. pluvialis* CCAC 3305 was grown in full, nitrogen- and phosphorus-deficient BG-11 medium supplemented with different salt concentration ranging from 0 to 0.8% sodium chloride (NaCl). Effect of nutrient deficiency and salt stress on growth and astaxanthin content was analyzed. Furthermore, comparison of independent data sets (AF and ZÇ) from experiments with stress-free conditions, i.e. full BG-11 medium without any salt supplementation, was possible despite different applied initial cell densities. This was facilitated via time shift strategy based on the exponential growth equation. However, this strategy was not useful if stress conditions were applied.

Nutrient deficiency generally led to lower cell densities than in full medium (Figure 16). Application of 0.1 to 0.2 % NaCl had a decreasing effect on cells grown in full and phosphorus deficient medium. However, cell densities in nitrogen deficient medium were similar to the ones without any salt stress. This might be explained by the fact that cells grown in nitrogen-deficient medium supplemented with 0 to 0.2% NaCl accumulated astaxanthin in the vegetative stage, i.e. akinete formation was not observed (data not shown). This observation was accordance with reports from literature (Grünwald et al., 1997; Grünwald & Hagen, 2000; Hagen et al., 2000) where astaxanthin accumulation occurred in flagellates of *H. pluvialis* and was not coupled to akinete formation.

Application of salt concentrations ranging from 0.3 to 0.5% NaCl effected cells grown in full and nutrient deficient medium drastically showing the same pattern: decline of initial cell densities for two days, slight increase and stabilization of cell densities at a

low level. In all conditions, astaxanthin accumulation started at day three to four of cultivation. Final astaxanthin was highest for cells grown in phosphorus-deficient medium supplemented with 0.3% NaCl: total astaxanthin accounted for $51 \mu\text{g mL}^{-1}$ with an astaxanthin content of 204 pg cell^{-1} . In general, final concentration of total astaxanthin in full and nutrient deficient medium was increased when combined with 0.3 to 0.5%. In a further experiment, the range of salt concentration was applied in higher resolution to identify the best concentration for astaxanthin accumulation (Figure 19). Unfortunately, independent data sets (AF and FK) could not be compared on a statistical level, since initial cell densities were different and the time shift strategy for comparison was critical. However, the trends for growth and astaxanthin accumulation were similar in both data sets at coincident salt concentration of 0.3 and 0.5%, but the rates of astaxanthin accumulation were clearly different. The previous data sets (AF) generally yielded in higher values than in the repeated experiment (FK) since the initially applied cell density was higher as well. For instance, the best astaxanthin accumulation rate ($4.0 \mu\text{g mL}^{-1} \text{ day}^{-1}$) was observed for 0.35% salt stress in the repeated experiment whereas the previous experiment yielded in a higher rate ($4.5 \mu\text{g mL}^{-1} \text{ day}^{-1}$) at 0.30% NaCl. Consequently, it remained unclear whether a salt concentration between 0.3 and 0.5% would have boosted astaxanthin kinetics. Further experiments should be conducted in the future to clarify this issue, but with strict elaborateness concerning the application of identical initial cell densities.

In literature, 0.8% NaCl concentration is often used as a stress factor to induce astaxanthin production in *H. pluvialis* (Boussiba & Vonshak, 1991; Boussiba et al., 1999; Boussiba, 2000; Kang et al., 2006; Li et al., 2008). For instance, Boussiba and Vonshak (1991) cultivated a *H. pluvialis* SAG strain (not further specified) in nitrogen-deficient medium supplemented with 0.8% NaCl. Cultures were aerated with 1.5% CO_2 and grown at 28°C and $85 \mu\text{mol photons m}^{-2} \text{ s}^{-1}$; after eight days of cultivation $90 \text{ pg astaxanthin cell}^{-1}$ was achieved. This was comparable to the cellular astaxanthin content of 103 pg cell^{-1} achieved in this study with less operational efforts. Furthermore, more efficient results were achieved in this study when 0.3 to 0.5% NaCl was applied for salt stress.

4.3 Genome size of *H. pluvialis*

The genome size of all 26 *H. pluvialis* strains were calculated with a very simple method: DNA was extracted from a determined number of cells and cellular DNA was converted into Gbp units according to Kapraun (2007). Calculated genome sizes varied between 2.6 ± 0.6 Gbp (SAG 34-11(2)) and 7.8 ± 0.4 Gbp (CCAC 0055). To evaluate the validity of applied method, *Chlamydomonas reinhardtii* was used as a reference organism. *C. reinhardtii* is a unicellular chlorophyte with an entirely sequenced genome. The nuclear, chloroplastidial and mitochondrial genome size of *C. reinhardtii* accounts for approximately 120, 0.2 and 0.016 Mbp, respectively (Merchant et al., 2007). In this study, a genome size of 98.4 ± 8.2 Mbp was calculated for *C. reinhardtii* which is close to the actual size with approximately 20 Mbp of underestimation. In comparison to *C. reinhardtii*, genome size of *H. pluvialis* was 26- to 80-fold higher. The genome size of other algal group vary between 0.1 to 200 Mbp (Holm-Hansen, 1969; Veldhuis et al., 1997). Thus, genome size of *H. pluvialis* might appear extremely huge at first sight. It is striking that there is marginal information on genome size or DNA content in literature with respect to *H. pluvialis*. Tjahjono et al. (1994a) mentioned a DNA content of $11.3 \text{ pg cell}^{-1}$ for NIES-144 that was determined via a colorimetric diphenylamine method and normalized to diploid status. Green algae are usually haploid during their asexual life cycle, only for meiotic events two haploid cells fuse to form a diploid zygote (Lee, 2008). The DNA content mentioned by Tjahjono et al. (1994a) would consequently correspond to $5.65 \text{ pg cell}^{-1}$ in haploid cells which equals 5.5 Gbp. In this study, a genome size of 3.5 ± 0.1 Gbp was determined for NIES-144; the deviation from the literature value might be explained by the different methods applied.

The range of estimated genome sizes of *H. pluvialis* was not comparable with other unicellular chlorophytes. However, dinoflagellates possess larger genomes than other eukaryotes ranging from three Gbp (*Symbiodinium* spp.) to 245 Gbp (*Prorocentrum micans*) (Hou & Lin, 2009). Thus, genome size of *Symbiodinium* spp. was more likely comparable with the ones of *H. pluvialis*. It has to be noted that the method for genome size estimation applied in this study, not only includes nuclear, but also chloroplastial and mitochondrial DNA. Consequently, the large genome size might be explained by a high gene copy number or large fractions of non-coding DNA

repeats within the chloroplast. Although sexual reproduction was rarely observed in *H. pluvialis*, another scenario for explaining the large genome size might be a past fatal meiotic event leading to genome duplication or polyploidy. But these speculations need to be proved in future investigations. Especially, it should be clarified if the large genome size of *H. pluvialis* is caused by the chloroplastial and/ or by the nuclear DNA to gain more insight on a molecular level.

4.4 Phylogeny of *H. pluvialis*

Since the geographically diverse *H. pluvialis* strains subjected in this study were similar in morphology, but showed different physiological properties, phylogenetic analyses based on *rbcL* gene and rDNA sequences (5.8S, ITS2 and partial 28S) were conducted to reveal possible correlations of achieved data. The *rbcL* gene is located in the chloroplastial genome and encodes the large subunit of RuBisCo, a key enzyme for CO₂ fixation in the Calvin cycle. Thus, RuBisCo is essential for photoautotroph organisms. Since the *rbcL* gene is highly conservative, it is frequently used for barcoding (Lee, 2008).

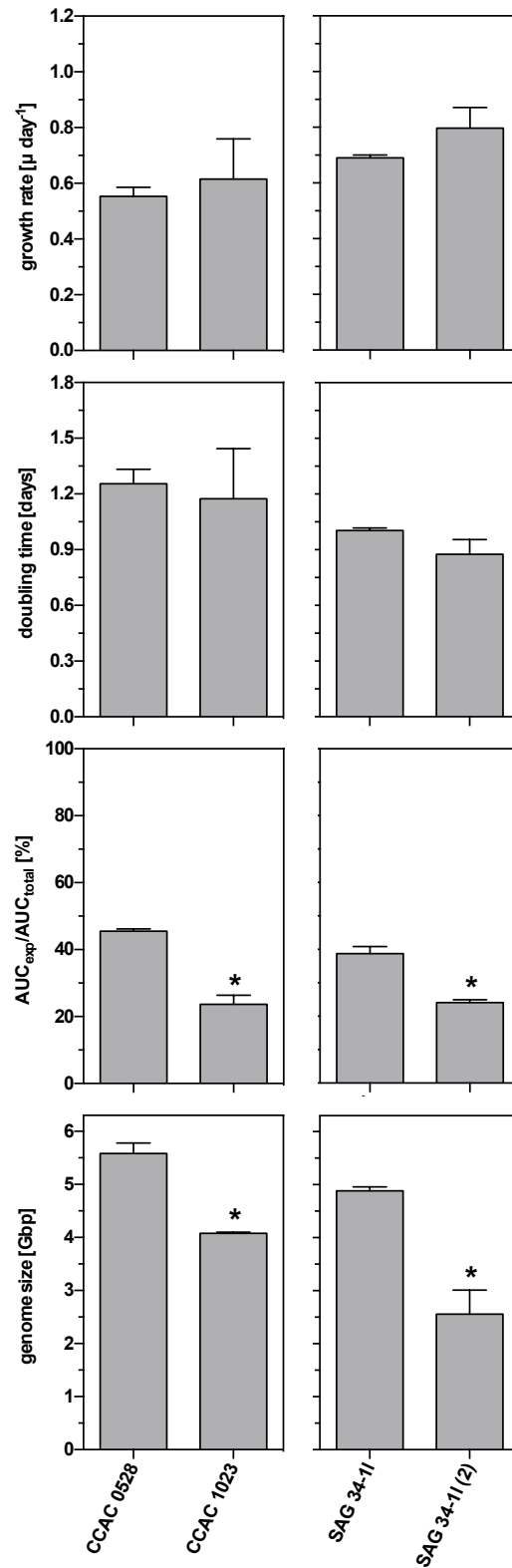
The rDNA sequence of ITS2 is located in the nuclear genome between 5.8S and 28S rRNA genes encoding the large subunits of ribosomes. Since ITS2 is a “fast evolving part” of the rRNA operon with high variability in sequence length, it is a useful tool to uncover genetic differences between closely related species (Caisová et al., 2011). Transcription of ITS2 rDNA into pre-rRNA is followed by folding processes into a secondary structure consisting of four helices connected by spacer regions. Spacer regions between helix one and two and between helix two and three are conservative. First base pairs in helix one and first eleven base pairs in helix two are conservative as well. Possible compensatory base changes (CBCs) within the ITS2 helices can be used to characterize and identify species (Caisová et al., 2013).

Phylogenetic trees from both, single gene analyses of *rbcL* (see appendix, Figure 38) and ITS2 (see appendix, Figure 39) and combined gene analyses of 5.8S, ITS2 and partial 28S (Figure 21) basically revealed that *H. pluvialis* was monophyletic. This result was in accordance with the results of Buchheim et al. (2013). Furthermore, Buchheim et al. (2013) categorized *H. pluvialis* into five lineages (A to E). In this

study, lineages A to E were verified in ITS2 analyses (Figure 39). However, a distinct separation of lineage A and E was not supported in combined gene analyses (Figure 21). Instead, ACOI-276 and SAG 34-1h designated as lineage E by Buchheim et al. (2013), were grouped into lineage A within this study suggesting a crossover of both lineages. *H. pluvialis* strains from this study were predominantly grouped into lineage A; SAG 34-1f and SAG 44.96 were grouped in lineage C and D, respectively.

The consensus secondary structure of ITS2 in *H. pluvialis* corresponded to the model described by Caisová et al. (2013) for Chaetophorales, Chaetopeltidales, Oedogoniales and Sphaeropleales. ITS2 sequences of *H. pluvialis* strains were highly conservative with only a few variable positions (Figure 22). Compensatory base changes (CBCs) were not detected for *H. pluvialis* strains within this study. However, Buchheim et al. (2013) reported one CBC for SAG 34-1m when SAG 34-1c and SAG 44.96 were excluded from analyses.

Overall, phylogenetic results of *H. pluvialis* strains showed no clear correlation to achieved data concerning growth parameters or genome sizes. Differences on a physiological level are probably caused by different ecotypes of *H. pluvialis*. This assumption is supported by peculiarities in alignments of *rbcL* and ITS2 sequences: double nucleotide signals at the third codon position were frequently detected for *rbcL* and unreadable sequence parts occurred in ITS2 due to variation in length. However, microevolutionary events leading to a genetic drift over time cannot be excluded, e.g. during subcultivation of strains. For instance, the analyzed 26 *H. pluvialis* strains included two strains, CCAC 0528 and SAG 34-1I, and their corresponding FACS-subisolates, CCAC 1023 and SAG 34-1I (2), respectively (Table 4). The two strains and respective subisolates were consistent with respect to specific growth rate and doubling time, but they differed significantly from each other with respect to AUC_{exp}/AUC_{total} ratio and genome size (Figure 30). This indicates that isolation of single cells from a culture harbors the risk of selecting random mutants and generating a subculture with an altered genotype.



H. pluvialis strains

Figure 30 Comparison of *H. pluvialis* CCAC 0528 and SAG 34-1I with corresponding subisolates CCAC 1023 and SAG 34-1I (2), respectively. Specific growth rate, doubling time, AUC_{exp}/AUC_{total} ratio and genome size of each strain were compared with data from respective subisolate. Asterisks represent significant differences.

4.5 Putative EMS mutants of *H. pluvialis*

Generation of *H. pluvialis* mutants by directed or random mutagenesis can lead to two to three-fold higher astaxanthin contents than in wild type (WT) strains (Tripathi et al., 2001; Steinbrenner & Sandmann, 2006; Hu et al., 2008; Wang et al., 2012; Sharon-Gojman et al., 2015; Kathiresan et al., 2015;). Modification of genes encoding key regulatory enzymes (PSY, PDS and BKT) of the carotenoid biosynthetic pathway is the main target of directed mutagenesis. Steinbrenner & Sandmann (2006) developed a transformation protocol for *H. pluvialis* where the leucine codon of endogenous *pds* was changed to an arginine codon by site-directed mutagenesis. Introduction of mutated *pds* by biolistic bombardment led to elevated accumulation of astaxanthin under stress conditions. At the same time, expression of modified *pds* conferred herbicide (norflurazon) resistance and thus, acted as a selectable marker. However, stable transformation of *H. pluvialis* were missing for a long time (Chen et al., 2003; Steinbrenner & Sandmann, 2006; Kathiresan & Sarada, 2009). Recently, a stable nuclear transformation method was reported by Sharon-Gojman et al. (2015). A novel shuttle-vector was developed including the mutated *pds* as a selection marker (based on the description of Steinbrenner & Sandmann (2006)). Two additional transgenes could be simultaneously expressed using this novel vector (Sharon-Gojman et al., 2015). Beyond nuclear transformation, stable transformation of the chloroplast genome was achieved resulting in expression of exogenous antibiotic resistance (Gutiérrez et al., 2012).

However, random mutagenesis is frequently used to generate *H. pluvialis* mutants. Ethyl methanesulfonate (EMS) and N-methyl-N-nitro-N-nitrosoguanidine (MNNG) are the most applied chemical mutagens for this purpose (Tjahjono et al., 1994b; Chumpolkulwong et al., 1997; Tripathi et al., 2001; Chen et al., 2003; Hu et al., 2008; Hong et al., 2012; Gomez et al., 2013). Herbicides are often used as inhibitors of the carotenoid biosynthetic pathway to screen for resistant, astaxanthin overproducing mutants. It is assumed that herbicides like diphenylamine (DPA), norflurazon, nicotin or compactin directly or indirectly interfere with key regulatory enzymes of the carotenoid biosynthetic pathway by competing for the binding site of corresponding cofactors. For instance, norflurazon interferes with PDS in a direct manner and competes probably with the cofactor PTOX for the binding site. Thus, only the

carotenoid biosynthetic pathway of herbicide resistant mutants remains unaffected under stress conditions and in the presence of corresponding herbicide, whereas the carotenoid biosynthetic pathway of non-resistant mutants will be interrupted.

In this study, EMS was applied as a chemical agent for random mutagenesis of *H. pluvialis* CCAC 0125. EMS alkylates keto groups in nucleotides, predominantly guanine bases of DNA molecules. As a result, 6-ethylguanine acts as an adenine analog and pairs with thymine. Thus, EMS leads to A-T \leftrightarrow G-C transition mutations. EMS efficiency is basically similar at all phases of mitosis, efficiency is slightly increased at the G1/S phase (Klug et al., 2011). The dosage of the mutagen is usually adapted to low survival rates ranging from 5 to 15% (Shah et al., 2016). According to Flynn et al. (2002), the rate of multiple mutations decreases with the rate of lethal mutations. Although the mutation rate of EMS cannot be forecasted, multiple mutations can be minimized by choosing a lethal dose of 50% for mutagenesis. Furthermore, unique mutations per genome can be aimed from a statistical point of view when the number of cells exposed to EMS corresponds to the genome size. Based on this information, *H. pluvialis* CCAC 0125 was mutagenized with EMS according to Flynn et al. (2002). For this, wild type and EMS treated samples were plated on several agar plates and consecutively cultivated at 24.28 ± 6.02 (LI₂₅) and 91.34 ± 24.98 (LI₉₀) $\mu\text{mol photons m}^{-2} \text{s}^{-1}$ for three weeks and eleven days, respectively. The number of single colony forming units (cfu) was determined (Figure 23). Although an EMS exposition time of 15 minutes was selected to aim a survival rate of 50% (Figure 7), only $38.77 \pm 2.59\%$ survival was achieved for EMS samples. Putative EMS mutants were screened based on colony diameter and/ or pigmentation due to astaxanthin accumulation. Variations in colony size were significantly different between WT and EMS samples, and between the two applied light intensities. 118 putative EMS mutants were re-analyzed based on colony diameter. Analysis of colony diameter bears the risk of artefacts since on the one hand the analysis is two-dimensional excluding the colony height and on the other hand it cannot be excluded that cfu were formed by two or more cells instead of one single cell. This might explain why only 24% of 118 re-analyzed mutants yielded in reproducible results (Figure 26). Another reason for the low level of reproducibility might be that in the first analysis of colony diameter a mutation was actually present, but was reverted until the second analysis by DNA repair mechanisms. This is also quite realistic since mutagen dosage was relatively low when compared to literature.

Five verified EMS mutants were further analyzed with respect to their growth pattern in suspension. Four of the five mutants had been pre-selected due to bigger colony sizes than WT expecting more efficient growth. However, suspension cultures of selected mutants did not grow better than WT; growth efficiency of all mutants were significantly lower than in WT with a AUC_{exp}/AUC_{total} ratio of 19% (Figure 28).

In an industrial-scale, natural astaxanthin production using *H. pluvialis* in a two-step approach requires optimal growth conditions before exposing cells to suboptimal conditions. This is due to the fact that under suboptimal conditions astaxanthin production will be induced, but cell growth will cease. However, Kiperstok et al. (2016) showed that cultivating and stressing *H. pluvialis* in an immobilized state within TL-PBSR overcomes this issue. At high light intensities, the outer layer of immobilized cells can function as a shield protecting the inner layer of cells from stress. Thus, promoting growth in the inner green layers and astaxanthin production in the outer layers at the same time is possible. The two-step approach for biomass and astaxanthin production from Kiperstok (2016) was adopted for *H. pluvialis* CCAC 0125 WT and derivative EMS mutant E1-16 col-4. The experiment was conducted in two steps exposing samples first to 90 and then to 1,000 $\mu\text{mol photons m}^{-2} \text{ s}^{-1}$ for eight days, respectively. Development of biomass and astaxanthin kinetics was monitored (Figure 29). Under favorable light conditions, biomass and total astaxanthin of WT and mutant E1-16 col-4 were not significantly different with average productivities of 5 and 0.035 $\text{g m}^{-2} \text{ day}^{-1}$, respectively. Unfortunately, results of WT and EMS mutant were not really comparable under light stress due operational problems affecting the WT samples. However, results for E1-16 col-4 were compared with the data sets from Kiperstok (2016) designated as WT_{K-Ref} (Figure 31).

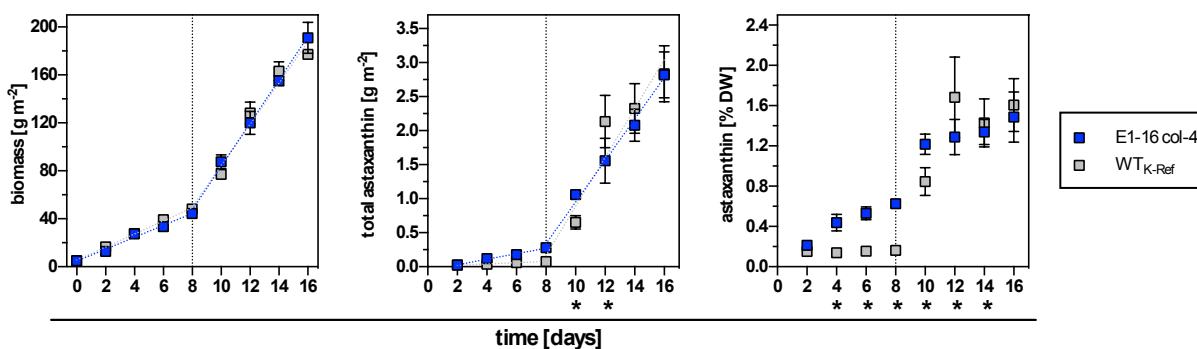


Figure 31 Comparison of biomass and astaxanthin kinetics of immobilized *H. pluvialis* CCAC 0125 WT_{K-Ref} taken from Kiperstok (2016) with EMS mutant E1-16 col-4. Samples were cultivated in a two-step approach according to Kiperstok (2016) using 90 and 1,000 $\mu\text{mol photons m}^{-2} \text{s}^{-1}$ for the first and last eight days of cultivation, respectively. Time point of light switch is represented by vertical dotted line. Biomass, total astaxanthin and astaxanthin content were analyzed. Productivities were calculated from linear regression indicated by colored dotted lines. Significant differences are marked with an asterisk at corresponding time points. *Mean* \pm *SD*; *n* = 3.

Biomass production rates of E1-16 col-4 mutant perfectly matched the results of WT_{K-Ref} without any significant differences: 5.0 vs. 5.5 $\text{g m}^{-2} \text{day}^{-1}$ for the first eight days and 18.0 vs. 17.2 $\text{g m}^{-2} \text{day}^{-1}$ for the last eight days, respectively. Total astaxanthin increase was similar in the first eight days of cultivation for the mutant and WT with 0.04 and 0.01 $\text{g m}^{-2} \text{day}^{-1}$, respectively. Total astaxanthin increase in the last eight days showed significant differences between the mutant and WT with productivities of 0.31 and 0.36 $\text{g m}^{-2} \text{day}^{-1}$, respectively. However, final total astaxanthin was not significantly different with 2.8 g m^{-2} . Astaxanthin content showed the most significant differences between mutant and WT. Astaxanthin content in E1-16 col-4 mutant was predominantly higher than in WT. However, final astaxanthin content of 1.5% was not significantly different from WT. E1-16 col-4 mutant seemed to have a slightly elevated astaxanthin accumulation rate under favorable conditions when compared to WT.

Overall, no striking hyper-growing or hyper-astaxanthin accumulating EMS mutants could be detected within this study. Nevertheless, EMS mutagenesis is a good approach for strain improvement. Major advantages comprise the high efficiency for mutations, the generation of a large pool of mutants and particularly, the status 'non-transgenic' since no exogenous DNA is introduced into the organism. To improve the efficiency of mutations, molecular breeding could be coupled to other random mutagenesis approaches. For instance, Sun et al. (2008) first generated an EMS mutant with 20% increased biomass capability and subjected this mutant to UV irradiance generating a new mutant with increased capabilities for biomass (+68%),

cellular astaxanthin content (+28%) and astaxanthin productivities (+120%). Recently, Wang et al. (2016) generated an astaxanthin-overproducing mutant in three stages. First, a mutant yielding in high biomass was generated with UV irradiation. Secondly, this mutant was further mutated with EMS for improvement of growth cycle length. Thirdly, astaxanthin-overproducing mutants were screened in the presence of the carotenogenesis inhibitor diphenylamine (DPA). Finally, a DPA-resistant UV-EMS mutant was generated this way with the capability for 1.7-fold increased astaxanthin production and a maximum astaxanthin content of 4.7% of DW. Generating mutants with higher capacity for astaxanthin accumulation is the major goal of molecular breeding. However, other types of mutants might be of biotechnological interest, too. For instance, Wang et al. (2005) generated two thin-walled MNNG mutants (WM#537 and WM'2978); this feature might reduce costs for downstream processing of commercial astaxanthin production and increase bioavailability in case of whole cell consumption.

5

Conclusion and outlook

H. pluvialis is already applied as a natural source for biotechnological astaxanthin production, yet the natural product cannot compete with the synthetic analogue on the carotenoid market, e.g. due to high operating costs. In addition to technical improvements for reduction of production costs, competitiveness of natural astaxanthin can be elevated by improvements on a biological level. Since the efficiency for growth and astaxanthin accumulation in *H. pluvialis* depends on various factors and the analysis is generally time- and space-consuming, an efficient short-time, microscale screening method was successfully developed and applied in this study as an alternative approach.

Selecting the optimal strain for growth efficiency or choosing the most efficient stress condition for astaxanthin production or even improving strains via mutagenesis are important factors for future biotechnological progresses. However, emphasis should be taken on genetic stability of strains as well. Algal culture collections generally maintain their wide range of microalgal strains by serial subculturing in numerous culture vessels. This long-term method is not only labor- and space-intensive, but also harbors the risk of phenotypic and genotypic shift in microalgal strains due to spontaneous mutations over time. Thus, cryopreservation constitutes an attractive alternative to long-term maintenance minimizing issues of labor and space and ensuring genetic stability (Saks, 1978; Day et al., 2000; Mori et al., 2002; Rhodes et al., 2006). Unfortunately, a universal protocol for microalgal cryopreservation is not available yet since taxonomically and morphologically diverse microalgae show distinct responses to cryogenic stresses (Day et al., 1997; Harding et al., 2006). However, cryopreservation of biotechnological important microalgae like *H. pluvialis* should be a future goal to assure genetic stability of WT and mutant strains and thus, to provide reproducibility of discoveries from several research projects.

6

References

- ACD/Labs (2013).** ACD/ChemSketch for academic and personal use. <http://www.acdlabs.com/resources/freeware/chemsketch/>. Accessed 20 Jan 2013
- Aflalo C, Meshulam Y, Zarka A, & Boussiba S (2007).** On the relative efficiency of two-vs. one-stage production of astaxanthin by the green alga *Haematococcus pluvialis*. *Biotechnology and bioengineering* **98**: 300–305. doi: 10.1002/bit
- Andersen RA, & Kawachi M (2005).** Traditional microalgae isolation techniques. In: Andersen R. (ed) *Algal culturing techniques*. Elsevier Academic Press, pp 83–100
- Ausich RL (1997).** Commercial opportunities for carotenoid production by biotechnology. *Pure and Applied Chemistry* **69**: 2169–2174. doi: 10.1351/pac199769102169
- BCC Research (2015).** The global market for carotenoids (report code: FOD025E). <http://www.bccresearch.com/market-research/food-and-beverage/carotenoids-global-market-report-fod025e.html>. Accessed 12 Dec 2015
- Benstein RM, Çebi Z, Podola B, & Melkonian M (2014).** Immobilized growth of the peridinin-producing marine dinoflagellate *Symbiodinium* in a simple biofilm photobioreactor. *Marine Biotechnology*. doi: 10.1007/s10126-014-9581-0

- Boussiba S (2000)**. Carotenogenesis in the green alga *Haematococcus pluvialis*: cellular physiology and stress response. *Physiologia Plantarum* **108**: 111–117.
- Boussiba S, Bing W, Yuan JP, et al. (1999)**. Changes in pigments profile in the green alga *Haematococcus pluvialis* exposed to environmental stresses. *Biotechnology Letters* **21**: 601–604. doi: 10.1023/A:1005507514694
- Boussiba S, & Vonshak A (1991)**. Astaxanthin accumulation in the green alga *Haematococcus pluvialis*. *Plant Cell Physiol* **32**: 1077–1082. doi: 10.1111/j.1744-7909.2007.00468.x
- Britton G (1976)**. Biosynthesis of carotenoids. In: Goodwin TW (ed) Chemistry and biochemistry of plant pigments, 2nd edn. Academic Press, pp 262–327
- Buchheim M a., Sutherland DM, Buchheim J a., & Wolf M (2013)**. The blood alga: phylogeny of *Haematococcus* (Chlorophyceae) inferred from ribosomal RNA gene sequence data. *European Journal of Phycology* **48**: 318–329. doi: 10.1080/09670262.2013.830344
- Caisová L, Marin B, & Melkonian M (2013)**. A consensus secondary structure of ITS2 in the Chlorophyta identified by phylogenetic reconstruction. *Annals of Anatomy* **164**: 482–496. doi: 10.1016/j.protis.2013.04.005
- Caisová L, Marin B, & Melkonian M (2011)**. A close-up view on ITS2 evolution and speciation - a case study in the Ulvophyceae (Chlorophyta, Viridiplantae). *BMC Evolutionary Biology* **11**: 262. doi: 10.1186/1471-2148-11-262
- Cardozo KHM, Guaratini T, Barros MP, et al. (2007)**. Metabolites from algae with economical impact. *Comparative Biochemistry and Physiology - C Toxicology and Pharmacology* **146**: 60–78. doi: 10.1016/j.cbpc.2006.05.007
- Chacon-Lee TL, & Gonzalez-Marino GE (2010)**. Microalgae for “healthy” foods - possibilities and challenges. *Comprehensive Reviews in Food Science and Food Safety* **9**: 655–675. doi: 10.1111/j.1541-4337.2010.00132.x

- Chandi GK, & Gill BS (2011).** Production and characterization of microbial carotenoids as an alternative to synthetic colors: a review. *International Journal of Food Properties* **14**: 503–513. doi: 10.1080/10942910903256956
- Chen Y, Li D, Lu W, et al. (2003).** Screening and characterization of astaxanthin-hyperproducing mutants of *Haematococcus pluvialis*. *Biotechnology Letters* **25**: 527–529. doi: 10.1023/A:1022877703008
- Chumpolkulwong N, Kakizono T, Handa T, & Nishio N (1997).** Isolation and characterization of compactin resistant mutants of an astaxanthin synthesizing green alga *Haematococcus pluvialis*. *Biotechnology Letters* **19**: 299–302. doi: 10.1023/A:1018330329357
- Cordero BF, Couso I, León R, et al. (2011).** Enhancement of carotenoids biosynthesis in *Chlamydomonas reinhardtii* by nuclear transformation using a phytoene synthase gene isolated from *Chlorella zofingiensis*. *Applied Microbiology and Biotechnology* **91**: 341–351. doi: 10.1007/s00253-011-3262-y
- Couso I, Vila M, Rodriguez H, et al. (2011).** Overexpression of an exogenous phytoene synthase gene in the unicellular alga *Chlamydomonas reinhardtii* leads to an increase in the content of carotenoids. *Biotechnology Progress* **27**: 54–60. doi: 10.1002/btpr.527
- Damiani MC, Leonardi PI, Pieroni OI, & Cáceres EJ (2006).** Ultrastructure of the cyst wall of *Haematococcus pluvialis* (Chlorophyceae): wall development and behaviour during cyst germination. *Phycologia* **45**: 616–623. doi: 10.2216/05-27.1
- Day JG, Fleck R a, & Benson EE (2000).** Cryopreservation-recalcitrance in microalgae: novel approaches to identify and avoid cryo-injury. *Journal of Applied Phycology* **12**: 369–377. doi: 10.1023/A:1008107229005
- Day JG, Watanabe MM, Morris GJ, et al. (1997).** Long-term viability of preserved eukaryotic algae. *Journal of Applied Phycology* **9**: 121–127. doi: 10.1023/A:1007991507314

- Del Campo J a., García-González M, & Guerrero MG (2007).** Outdoor cultivation of microalgae for carotenoid production: current state and perspectives. *Applied Microbiology and Biotechnology* **74**: 1163–1174. doi: 10.1007/s00253-007-0844-9
- Droop M (1953).** On the ecology of flagellates from some brackish and fresh water rockpools of Finland. *Acta botanica Fennica* **51**: 1–52.
- Droop MR (1954).** Conditions governing haematochrome formation and loss in the alga *Haematococcus pluvialis* Flotow. *Archiv für Mikrobiologie* **20**: 391–397. doi: 10.1007/BF00690882
- Droop MR (1955).** Carotenogenesis in *Haematococcus pluvialis*. *Nature* **175**: 42–42. doi: 10.1038/175042a0
- Elliott AM (1934).** Morphology and life history of *Haematococcus pluvialis*. *Archiv für Protistenkunde* **82**: 250–272.
- Fan L, Vonshak A, & Boussiba S (1994).** Effect of temperature and irradiance on growth of *Haematococcus pluvialis* (Chlorophyceae). *Journal of Phycology* **30**: 829–833. doi: 10.1111/j.0022-3646.1994.00829.x
- Flotow J (1844).** Über *Haematococcus pluvialis*. *Verhandlungen der Kaiserlichen Leopoldinisch-Carolinischen Deutschen Akademie der Naturforscher* **12**: 413–606.
- Flynn T, Ghirardi ML, & Seibert M (2002).** Accumulation of O₂-tolerant phenotypes in H₂-producing strains of *Chlamydomonas reinhardtii* by sequential applications of chemical mutagenesis and selection. *International Journal of Hydrogen Energy* **27**: 1421–1430. doi: 10.1016/S0360-3199(02)00117-9
- Gomez PI, Inostroza I, Pizarro M, & Perez J (2013).** From genetic improvement to commercial-scale mass culture of a Chilean strain of the green microalga *Haematococcus pluvialis* with enhanced productivity of the red ketocarotenoid astaxanthin. *AoB Plants* **5**: plt026-plt026. doi: 10.1093/aobpla/plt026

- Gong Y, Hu H, Gao Y, et al. (2011).** Microalgae as platforms for production of recombinant proteins and valuable compounds: progress and prospects. *Journal of Industrial Microbiology and Biotechnology* **38**: 1879–1890. doi: 10.1007/s10295-011-1032-6
- Good NE, Winget GD, Winter W, et al. (1966).** Hydrogen ion buffers for biological research. *Biochemistry* **5**: 467–477. doi: 10.1021/bi00866a011
- Goodwin TW (1961).** Biosynthesis and function of carotenoids. *Annual Review of Plant Physiology* **12**: 219–244. doi: 10.1146/annurev.pp.12.060161.001251
- Grünewald K, & Hagen C (2000).** Extrusion of secondary carotenoid containing vesicles from flagellates of *Haematococcus pluvialis* (Volvocales; Chlorophyceae). *Journal of Applied Botany – Angewandte Botanik* **74**: 141–144.
- Grünewald K, Hagen C, & Braune W (1997).** Secondary carotenoid accumulation in flagellates of the green alga *Haematococcus lacustris*. *European Journal of Phycology* **32**: 387–392. doi: 10.1017/S0967026297001443
- Grünewald K, Hirschberg J, & Hagen C (2001).** Ketocarotenoid biosynthesis outside of plastids in the unicellular green alga *Haematococcus pluvialis*. *Journal of Biological Chemistry* **276**: 6023–6029. doi: 10.1074/jbc.M006400200
- Guedes AC, Amaro HM, & Malcata FX (2011).** Microalgae as sources of carotenoids. *Marine Drugs* **9**: 625–644. doi: 10.3390/md9040625
- Guerin M, Huntley ME, & Olaizola M (2003).** *Haematococcus* astaxanthin: applications for human health and nutrition. *Trends in Biotechnology* **21**: 210–216. doi: 10.1016/S0167-7799(03)00078-7
- Gutiérrez CL, Gimpel J, Escobar C, et al. (2012).** Chloroplast genetic tool for the green microalgae *Haematococcus pluvialis* (Chlorophyceae, Volvocales). *Journal of Phycology* **48**: 976–983. doi: 10.1111/j.1529-8817.2012.01178.x

- Hagen C, Grünwald K, Schmidt S, & Müller J (2000).** Accumulation of secondary carotenoids in flagellates of *Haematococcus pluvialis* (Chlorophyta) is accompanied by an increase in per unit chlorophyll productivity of photosynthesis. *European Journal of Phycology* **35**: 75–82. doi: 10.1080/09670260010001735651
- Hagen C, Siegmund S, & Braune W (2002).** Ultrastructural and chemical changes in the cell wall of *Haematococcus pluvialis* (Volvocales, Chlorophyta) during aplanospore formation. *European Journal of Phycology* **37**: 217–226. doi: 10.1017/S0967026202003669
- Harding K, Benson EE, Müller J, et al. (2006).** Cryopreservation of storage recalcitrant algae through fundamental studies of thermal behaviour and oxidative stress physiology. *Cryobiology* **53**: 399–400. doi: 10.1016/j.cryobiol.2006.10.077
- Holm-Hansen O (1969).** Algae: amounts of DNA and organic carbon in single cells. *Science* **163**: 87–88. doi: 10.1126/science.163.3862.87
- Hong ME, Choi SP, Park Y II, et al. (2012).** Astaxanthin production by a highly photosensitive *Haematococcus* mutant. *Process Biochemistry* **47**: 1972–1979. doi: 10.1016/j.procbio.2012.07.007
- Hou Y, & Lin S (2009).** Distinct gene number-genome size relationships for eukaryotes and non-eukaryotes: gene content estimation for dinoflagellate genomes. *PLoS ONE* **4**: e6978. doi: 10.1371/journal.pone.0006978
- Hu Z, Li Y, Sommerfeld M, et al. (2008).** Enhanced protection against oxidative stress in an astaxanthin-overproduction *Haematococcus* mutant (Chlorophyceae). *European Journal of Phycology* **43**: 365–376. doi: 10.1080/09670260802227736

- Huang JC, Wang Y, Sandmann G, & Chen F (2006).** Isolation and characterization of a carotenoid oxygenase gene from *Chlorella zofingiensis* (Chlorophyta). *Applied Microbiology and Biotechnology* **71**: 473–479. doi: 10.1007/s00253-005-0166-8
- Industry Experts (2015).** Global astaxanthin market – sources, technologies and applications (report code: PH009). <http://industry-experts.com/verticals/healthcare-and-pharma/global-astaxanthin-market-sources-technologies-and-applications>. Accessed 12 Dec 2015
- Kang CD, An JY, Park TH, & Sim SJ (2006).** Astaxanthin biosynthesis from simultaneous N and P uptake by the green alga *Haematococcus pluvialis* in primary-treated wastewater. *Biochemical Engineering Journal* **31**: 234–238. doi: 10.1016/j.bej.2006.08.002
- Kang CD, & Sim SJ (2008).** Direct extraction of astaxanthin from *Haematococcus* culture using vegetable oils. *Biotechnology Letters* **30**: 441–444. doi: 10.1007/s10529-007-9578-0
- Kapraun DF (2007).** Nuclear DNA content estimates in green algal lineages: Chlorophyta and Streptophyta. *Annals of Botany* **99**: 677–701. doi: 10.1093/aob/mcl294
- Kathiresan S, Chandrashekar A, Ravishankar G a., & Sarada R (2015).** Regulation of astaxanthin and its intermediates through cloning and genetic transformation of β -carotene ketolase in *Haematococcus pluvialis*. *Journal of Biotechnology* **196–197**: 33–41. doi: 10.1016/j.jbiotec.2015.01.006
- Kathiresan S, Chandrashekar A, Ravishankar G a, & Sarada R (2009).** Agrobacterium-mediated transformation in the green alga *Haematococcus pluvialis* (Chlorophyceae, Volvocales). *Journal of Phycology* **45**: 642–649. doi: 10.1111/j.1529-8817.2009.00688.x

- Kathiresan S, & Sarada R (2009).** Towards genetic improvement of commercially important microalga *Haematococcus pluvialis* for biotech applications. *Journal of Applied Phycology* **21**: 553–558. doi: 10.1007/s10811-009-9414-0
- Katsuda T, Lababpour A, Shimahara K, & Katoh S (2004).** Astaxanthin production by *Haematococcus pluvialis* under illumination with LEDs. *Enzyme and Microbial Technology* **35**: 81–86. doi: 10.1016/j.enzmictec.2004.03.016
- Kiperstok AC (2016).** Optimizing immobilized cultivation of *Haematococcus pluvialis* for astaxanthin production. University of Cologne
- Kiperstok AC, Sebestyen P, Podola B, & Melkonian M (2016).** Biofilm cultivation of *Haematococcus pluvialis* enables a highly productive one-phase process for astaxanthin production using high light intensities. *Algal Research* in press.
- Klug WS, Cummings MR, Spencer CA, & Palladino MA (2011).** Concepts of genetics, 10th edn. Pearson
- Kodym A, & Afza R (2003).** Physical and chemical mutagenesis. *Methods in molecular biology (Clifton, NJ)* **236**: 189–204. doi: 10.1385/1-59259-413-1:189
- Lee RE (2008).** Phycology, 4th edn. Cambridge University Press
- Lee YK, & Ding SY (1994).** Cell cycle and accumulation of astaxanthin in *Haematococcus lacustris* (Chlorophyta). *Journal of Phycology* **30**: 445–449. doi: 10.1111/j.0022-3646.1991.00575.x
- Lemoine Y, & Schoefs B (2010).** Secondary ketocarotenoid astaxanthin biosynthesis in algae: a multifunctional response to stress. *Photosynthesis research* **106**: 155–177. doi: 10.1007/s11120-010-9583-3
- Li Y, Miao F, Geng Y, et al. (2012).** Accurate quantification of astaxanthin from *Haematococcus* crude extract spectrophotometrically. *Chinese Journal of Oceanology and Limnology* **30**: 627–637. doi: 10.1007/s00343-012-1217-5

- Li Y, Sommerfeld M, Chen F, & Hu Q (2008).** Consumption of oxygen by astaxanthin biosynthesis: a protective mechanism against oxidative stress in *Haematococcus pluvialis* (Chlorophyceae). *Journal of Plant Physiology* **165**: 1783–1797. doi: 10.1016/j.jplph.2007.12.007
- Li Y, Sommerfeld M, Chen F, & Hu Q (2010).** Effect of photon flux densities on regulation of carotenogenesis and cell viability of *Haematococcus pluvialis* (Chlorophyceae). *Journal of Applied Phycology* **22**: 253–263. doi: 10.1007/s10811-009-9453-6
- Lohr M (2011).** Carotenoid metabolism in phytoplankton. In: Roy S, Llewellyn C, Egeland ES, Johnsen G (eds) *Phytoplankton pigments - characterization, chemotaxonomy and applications in oceanography*, 1st edn. Cambridge University Press, Cambridge, pp 113–161
- Lorenz RT, & Cysewski GR (2000).** Commercial potential for *Haematococcus microalgae* as a natural source of astaxanthin. *Trends in Biotechnology* **18**: 160–167. doi: 10.1016/S0167-7799(00)01433-5
- Marin B (2012).** Nested in the Chlorellales or independent class? Phylogeny and classification of the Pedinophyceae (Viridiplantae) revealed by molecular phylogenetic analyses of complete nuclear and plastid-encoded rRNA operons. *Protist* **163**: 778–805. doi: 10.1016/j.protis.2011.11.004
- Marin B, Palm A, Klingberg M a. x., & Melkonian M (2003).** Phylogeny and taxonomic revision of plastid-containing Euglenophytes based on SSU rDNA sequence comparisons and synapomorphic signatures in the SSU rRNA secondary structure. *Protist* **154**: 99–145. doi: 10.1078/143446103764928521
- Merchant SS, Prochnik SE, Vallon O, et al. (2007).** The *Chlamydomonas* genome reveals the evolution of key animal and plant functions. *Science* **318**: 245–250. doi: 10.1126/science.1143609
- Mori F, Erata M, & Watanabe MM (2002).** Cryopreservation of cyanobacteria and green algae in the NIES collection. *Microbiol. Cult. Collect.* **18**:45–55.

-
- Naumann T, Çebi Z, Podola B, & Melkonian M (2013).** Growing microalgae as aquaculture feeds on twin-layers: a novel solid-state photobioreactor. *Journal of Applied Phycology* **25**: 1413–1420. doi: 10.1007/s10811-012-9962-6
- Nowack ECM, Podola B, & Melkonian M (2005).** The 96-well twin-layer system: a novel approach in the cultivation of microalgae. *Protist* **156**: 239–251. doi: 10.1016/j.protis.2005.04.003
- Olaizola M (2003).** Commercial development of microalgal biotechnology: from the test tube to the marketplace. *Biomolecular Engineering* **20**: 459–466. doi: 10.1016/S1389-0344(03)00076-5
- Pocock M a. (1960).** *Haematococcus* in Southern Africa. *Transactions of the Royal Society of South Africa* **36**: 5–55. doi: 10.1080/00359196009519031
- Podola B, & Melkonian M (2003).** A long-term operating algal biosensor for the rapid detection of volatile toxic compounds. *Journal of Applied Phycology* **15**: 415–424. doi: 10.1023/A:1026051700261
- Pringsheim EG (1946).** Pure cultures of algae. Cambridge University Press, London
- Pröschold T (1998).** Gametogenese bei einzelligen Grünalgen. Cuvillier Publishers
- Pulz O, & Gross W (2004).** Valuable products from biotechnology of microalgae. *Applied Microbiology and Biotechnology* **65**: 635–648. doi: 10.1007/s00253-004-1647-x
- Rhaese HJ, & Boetker NK (1973).** The molecular basis of mutagenesis by methyl and ethyl methanesulfonates. *European journal of biochemistry / FEBS* **32**: 166–172. doi: 10.1111/j.1432-1033.1973.tb02593.x
- Rhodes L, Smith J, Tervit R, et al. (2006).** Cryopreservation of economically valuable marine micro-algae in the classes Bacillariophyceae, Chlorophyceae, Cyanophyceae, Dinophyceae, Haptophyceae, Prasinophyceae, and Rhodophyceae. *Cryobiology* **52**: 152–156. doi: 10.1016/j.cryobiol.2005.10.003

-
- Rogers SO, & Bendich AJ (1985).** Extraction of DNA from milligram amounts of fresh, herbarium and mummified plant tissues. *Plant Molecular Biology* **5**: 69–76. doi: 10.1007/BF00020088
- Saiki RK, Gelfand DH, Stoffel S, et al. (1988).** Primer-directed enzymatic amplification of DNA with a thermostable DNA polymerase. *Science (New York, NY)* **239**: 487–491. doi: 10.1126/science.2448875
- Saks NM (1978).** The preservation of salt marsh algae by controlled liquid nitrogen freezing. *Cryobiology* **15**: 563–568.
- Schultze LKP, Simon M, Li T, et al. (2015).** High light and carbon dioxide optimize surface productivity in a Twin-Layer biofilm photobioreactor. *Algal Research* **8**: 37–44. doi: 10.1016/j.algal.2015.01.007
- Shah MMR, Liang Y, Cheng JJ, & Daroch M (2016).** Astaxanthin-producing green microalga *Haematococcus pluvialis*: from single cell to high value commercial products. *Frontiers in Plant Science* **7**: 531. doi: 10.3389/fpls.2016.00531
- Sharon-Gojman R, Maimon E, Leu S, et al. (2015).** Advanced Methods for genetic engineering of *Haematococcus pluvialis* (Chlorophyceae, Volvocales). *Applied Microbiology and Biotechnology* **10**: 8–15. doi: 10.1016/j.algal.2015.03.022
- Shi J, Podola B, & Melkonian M (2007).** Removal of nitrogen and phosphorus from wastewater using microalgae immobilized on twin layers: an experimental study. *J Appl Phycol* **19**: 417–423. doi: 10.1007/s10811-006-9148-1
- Specht E, Miyake-Stoner S, & Mayfield S (2010).** Micro-algae come of age as a platform for recombinant protein production. *Biotechnology Letters* **32**: 1373–1383. doi: 10.1007/s10529-010-0326-5
- Stanier RY, Kunisawa R, Mandel M, & Cohen-Bazire G (1971).** Purification and properties of unicellular blue-green algae (order Chroococcales). *Bacteriological reviews* **35**: 171–205.

- Steinbrenner J, & Linden H (2001).** Regulation of two carotenoid biosynthesis genes coding for phytoene synthase and carotenoid hydroxylase during stress-induced astaxanthin formation in the green alga *Haematococcus pluvialis*. *Plant physiology* **125**: 810–817. doi: 10.1104/pp.125.2.810
- Steinbrenner J, & Sandmann G (2006).** Transformation of the green alga *Haematococcus pluvialis* with a phytoene desaturase for accelerated astaxanthin biosynthesis. *Applied and Environmental Microbiology* **72**: 7477–7484.
- Sun Y, Liu J, Zhang X, & Lin W (2008).** Strain H2-419-4 of *Haematococcus pluvialis* induced by ethyl methanesulphonate and ultraviolet radiation. *Chinese Journal of Oceanology and Limnology* **26**: 152–156.
- Tjahjono a. E, Kakizono T, Hayama Y, et al. (1994a).** Isolation of resistant mutants against carotenoid biosynthesis inhibitors for a green alga *Haematococcus pluvialis*, and their hybrid formation by protoplast fusion for breeding of higher astaxanthin producers. *Journal of Fermentation and Bioengineering* **77**: 352–357. doi: 10.1016/0922-338X(94)90003-5
- Tjahjono AE, Hayama Y, Kakizono T, et al. (1994b).** Hyper-accumulation of astaxanthin in a green alga *Haematococcus pluvialis* at elevated temperatures. *Biotechnology Letters* **16**: 133–138. doi: 10.1007/BF01021659
- Triki A, Maillard P, & Gudin C (1997).** Gametogenesis in *Haematococcus pluvialis* Flotow (Volvocales, Chlorophyta). *Phycologia* **36**: 190–194.
- Tripathi U, Venkateshwaran G, Sarada R, & Ravishankar GA (2001).** Studies on *Haematococcus pluvialis* for improved production of astaxanthin by mutagenesis. *World Journal of Microbiology and Biotechnology* **17**: 143–148.
- Veldhuis MJW, Cucci TL, & Sieracki ME (1997).** Cellular DNA content of marine phytoplankton using two new fluorochromes: taxonomic and ecological implications. *Journal of Phycology* **33**: 527–541. doi: 10.1111/j.0022-3646.1997.00527.x

Wang C, Hu Z, Zhao C, & Mao X (2012). Isolation of the β -carotene ketolase gene promoter from *Haematococcus pluvialis* and expression of *ble* in transgenic *Chlamydomonas*. *Journal of Applied Phycology* 1–8.

Wang N, Guan B, Kong Q, et al. (2016). Enhancement of astaxanthin production from *Haematococcus pluvialis* mutants by three-stage mutagenesis breeding. *Journal of Biotechnology* **236**: 71–77. doi: 10.1016/j.jbiotec.2016.08.009

Wang SB, Chen F, Sommerfeld M, & Hu Q (2005). Isolation and proteomic analysis of cell wall-deficient *Haematococcus pluvialis* mutants. *Proteomics* **5**: 4839–4851.

7

Appendix

7.1 Chemical index

Table 13 Chemical index

Chemical	Molecular formula	Company	Application
2-[4-(2-hydroxyethyl) piperazin-1-yl] ethanesulfonic acid [HEPES]	$C_8H_{18}N_2O_4S$	Roth	BG-11 culture medium
Agar (plant tissue grade)		AppliChem	agar plates
Agarose		Biozym	molecular analyses; gel electrophoresis
Astaxanthin certified (98.6%)	$C_{40}H_{52}O_4$	Ehrenstorfer GmbH	pigment analysis
Beef extract		Merck	sterility test; bacterial standard medium
Bidistilled water	H_2O	TKA X-Cad	general
Biotin (Vitamin B ₇)	$C_{10}H_{16}N_2O_3S$	Serva	BG-11 culture medium
Boric acid	H_3BO_3	Roth	BG-11 culture medium
Calcium chloride dihydrate	$CaCl_2 \times 2 H_2O$	Merck	BG-11 culture medium
Cetyltrimethylammonium bromide [CTAB]	$C_{19}H_{42}BrN$	Sigma-Aldrich	molecular analyses; CTAB-DNA extraction
Chloroform	$CHCl_3$	Roth	molecular analyses; CTAB-DNA extraction
Cobalt (II) nitrate hexahydrate	$Co(NO_3)_2 \times 6 H_2O$	Merck	BG-11 culture medium
Copper (II) sulfate pentahydrate	$CuSO_4 \times 5 H_2O$	Merck	BG-11 culture medium
Cyanocobalamin (Vitamin B ₁₂)	$C_{63}H_{88}CoN_{14}O_{14}P$	Serva	BG-11 culture medium
D(+)-glucose monohydrate	$C_6H_{12}O_6 \cdot H_2O$	Merck	sterility test; bacterial standard medium
Deoxyribonucleoside triphosphate (2mM) [dNTPs]		Fermentas	molecular analyses; PCR
Dimethyl sulfoxide [DMSO]	C_2H_6OS	Merck	pigment analysis

Table 13 (continuation) Chemical index

Chemical	Molecular formula	Company	Application
Dipotassium phosphate trihydrate	$K_2HPO_4 \times 3 H_2O$	Merck	BG-11 culture medium
DreamTaq™ buffer (10x)		Fermentas	molecular analyses; PCR
DreamTaq™ DNA polymerase (5 units μL^{-1})		Thermo Scientific	molecular analyses; PCR
Ethanol (99.8%)	C_2H_6O	Roth	molecular analyses; CTAB-DNA extraction
Ethidium bromide (1%) [EtBr]	$C_{21}H_{20}BrN_3$	AppliChem	molecular analyses; gel electrophoresis
Ethyl methanesulfonate [EMS]	$CH_3SO_3C_2H_5$	Sigma-Aldrich	mutagenesis/ DNA ethylating agent
Ethylenediaminetetraacetic acid [EDTA; Titriplex II]	$C_{10}H_{16}N_2O_8$	Merck	BG-11 culture medium
Ethylenediaminetetraacetic acid disodium salt dihydrate [NA ₂ EDTA; Titriplex III]	$C_{10}H_{14}N_2Na_2O_8 \times 2 H_2O$	Merck	molecular analyses; CTAB-DNA extraction; gel electrophoresis
GeneRuler™ 1 kb DNA ladder		Thermo Scientific	molecular analyses; gel electrophoresis
Glacial acetic acid [Acetate]	$C_2H_4O_2$	Roth	molecular analyses; gel electrophoresis
Glutaraldehyde (25%)	$C_5H_8O_2$	Agar Scientific	cell fixation for microscopy
Green GoTaq™ loading dye (5x)		Promega	molecular analyses; gel electrophoresis
Hydrogen chloride (37%)	HCl	Roth	molecular analyses; CTAB-DNA extraction
Iron (II) sulfate heptahydrate	$FeSO_4 \times 7 H_2O$	Merck	BG-11 culture medium
Isoamyl alcohol	$C_5H_{12}O$	Merck	molecular analyses; CTAB-DNA extraction
Isopropyl alcohol	C_3H_8O	Roth	molecular analyses; CTAB-DNA extraction
Magnesium sulfate heptahydrate	$MgSO_4 \times 7 H_2O$	Merck	BG-11 culture medium
Manganese (II) chloride tetrahydrate	$MnCl_2 \times 4 H_2O$	Sigma	BG-11 culture medium
Niacinamide	$C_6H_6N_2O$	Sigma	BG-11 culture medium
Nuclease-free water	H_2O	AppliChem	molecular analyses; PCR; sequencing
Peptone (from casein)		Merck	sterility test; bacterial standard medium
Potassium hydroxide	KOH	Merck	BG-11 culture medium
Proteinase K (2.5 units mg^{-1})		Macherey-Nagel	molecular analyses; CTAB-DNA extraction

Table 13 (continuation) Chemical index

Chemical	Molecular formula	Company	Application
RNAseA (120 units mg ⁻¹)		Macherey-Nagel	molecular analyses; CTAB-DNA extraction
Sabouraud 2% glucose agar		Merck	sterility test; fungal test plates
Sea sand		AppliChem	pigment analysis
Sodium carbonate	Na ₂ CO ₃	Merck	BG-11 culture medium
Sodium chloride	NaCl	Merck	molecular analyses; CTAB-DNA extraction
Sodium dodecyl sulfate [SDS]	NaC ₁₂ H ₂₅ SO ₄	Serva	molecular analyses; CTAB-DNA extraction
Sodium hydroxide	NaOH	Merck	BG-11 culture medium
Sodium molybdate dihydrate	Na ₂ MoO ₄ x 2 H ₂ O	Serva	BG-11 culture medium
Sodium nitrate	NaNO ₃	Merck	BG-11 culture medium
Sodium thiosulfate pentahydrate	Na ₂ S ₂ O ₃ x 5 H ₂ O	Roth	mutagenesis; EMS inactivator
Thiamine hydrochloride (Vitamin B ₁) [Thiamine-HCl]	C ₁₂ H ₁₈ Cl ₂ N ₄ OS	Serva	BG-11 culture medium
Tris (hydroxymethyl) aminomethane [Tris]	C ₄ H ₁₁ NO ₃	MP Biomedicals	molecular analyses; CTAB-DNA extraction; gel electrophoresis
Yeast extract		MP Biomedicals	sterility test; bacterial standard medium
Zinc sulfate heptahydrate	ZnSO ₄ x 7 H ₂ O	Merck	BG-11 culture medium

7.2 Micrographs of *H. pluvialis* CCAC 0125

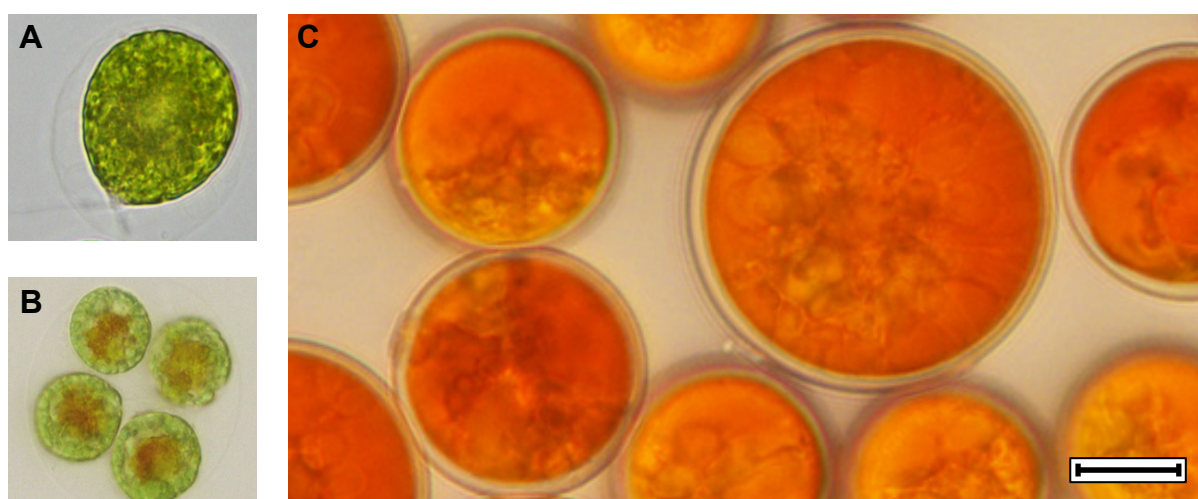


Figure 32 Micrographs of *H. pluvialis* CCAC 0125. Different cell types were captured microscopically with 1,000 x magnification: **[A]** a biflagellate with the protoplast clearly detached from the cell wall, **[B]** a sporangium with 4 palmelloid cells accumulating astaxanthin and **[C]** several mature akinetes of different size. *scale bar* = 8 μ m.

7.3 Set-up of microscale experiments

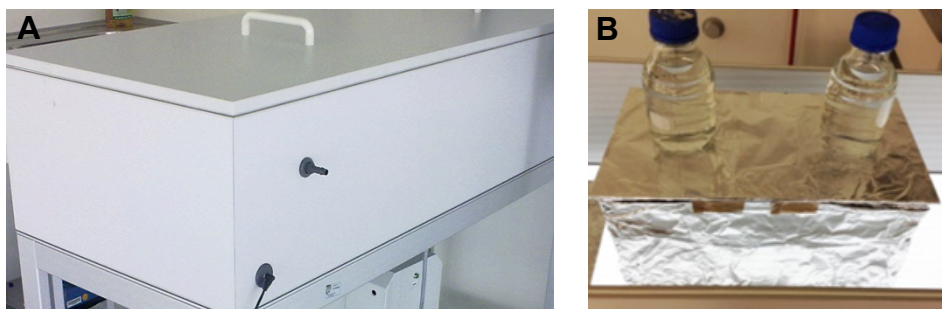


Figure 33 Set-up of microscale experiments. Pictures show **[A]** the custom-made cultivation box with the possibility of adjustable LED illumination from the bottom and **[B]** a humid chamber (containing the samples) placed within the cultivation box.

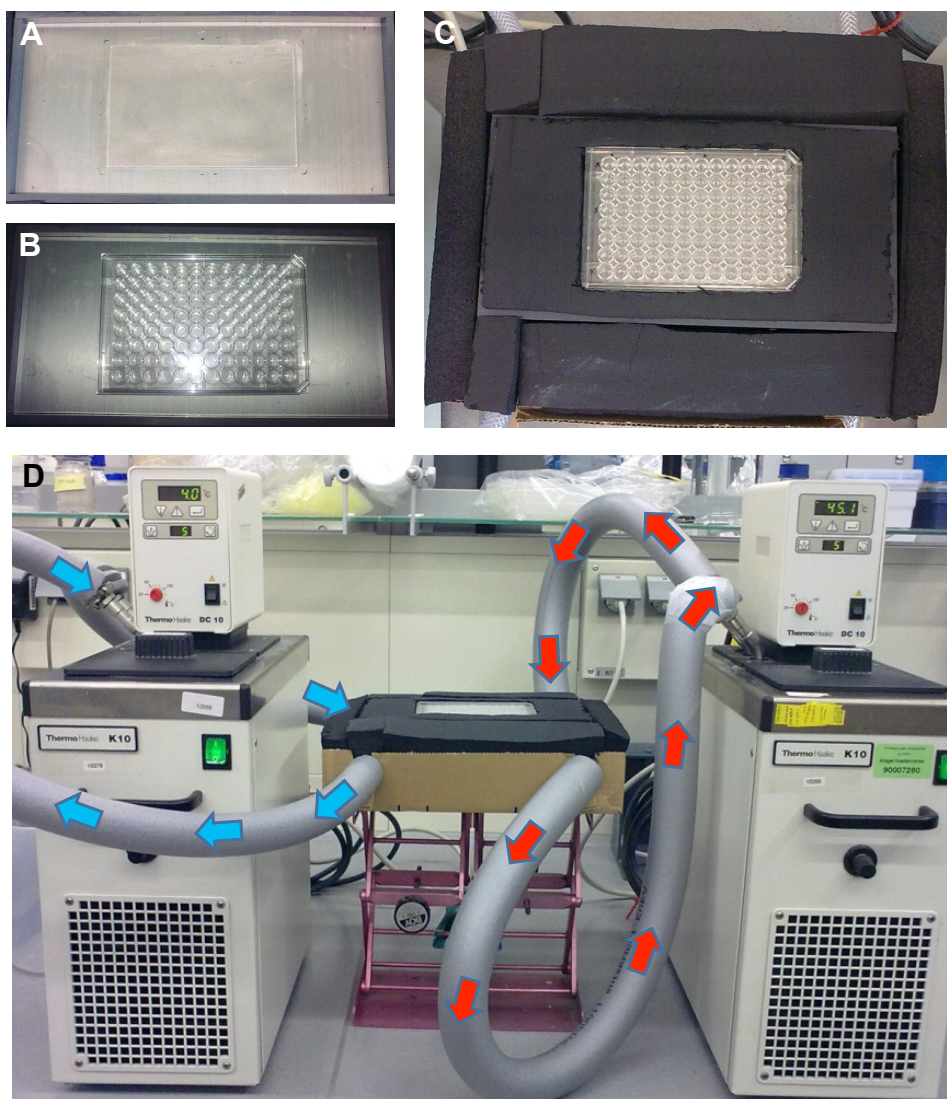


Figure 34 Prototype of the temperature gradient device. Pictures show **[A]** a metal plate used to establish a temperature gradient with **[B]** a 96-well plate on top and **[C]** surrounded with isolating material. **[D]** The temperature gradient was generated by two thermostats circulating cool (blue arrows) and warm water (red arrows) underneath the metal plate.

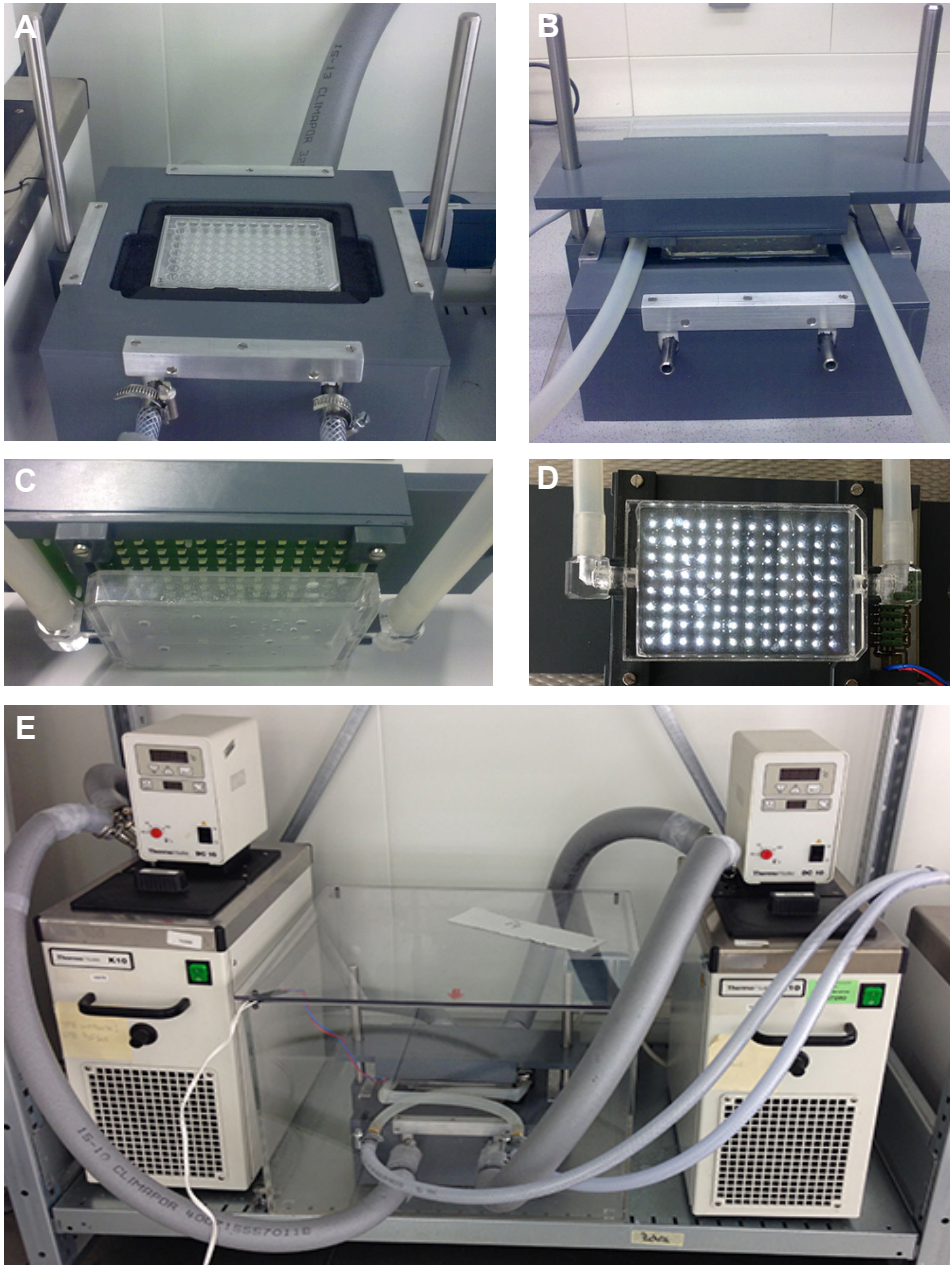


Figure 35 Final temperature gradient device. Pictures show **[A]** the optimized gradient module with **[B]** slidable coverage containing **[C]** the thermolid attached to the LED sheet with **[D]** adjustable light intensities. **[E]** A plastic box, well adapted to the tubings of thermostats, served as a humid chamber in later experiments to prevent evaporation of samples.

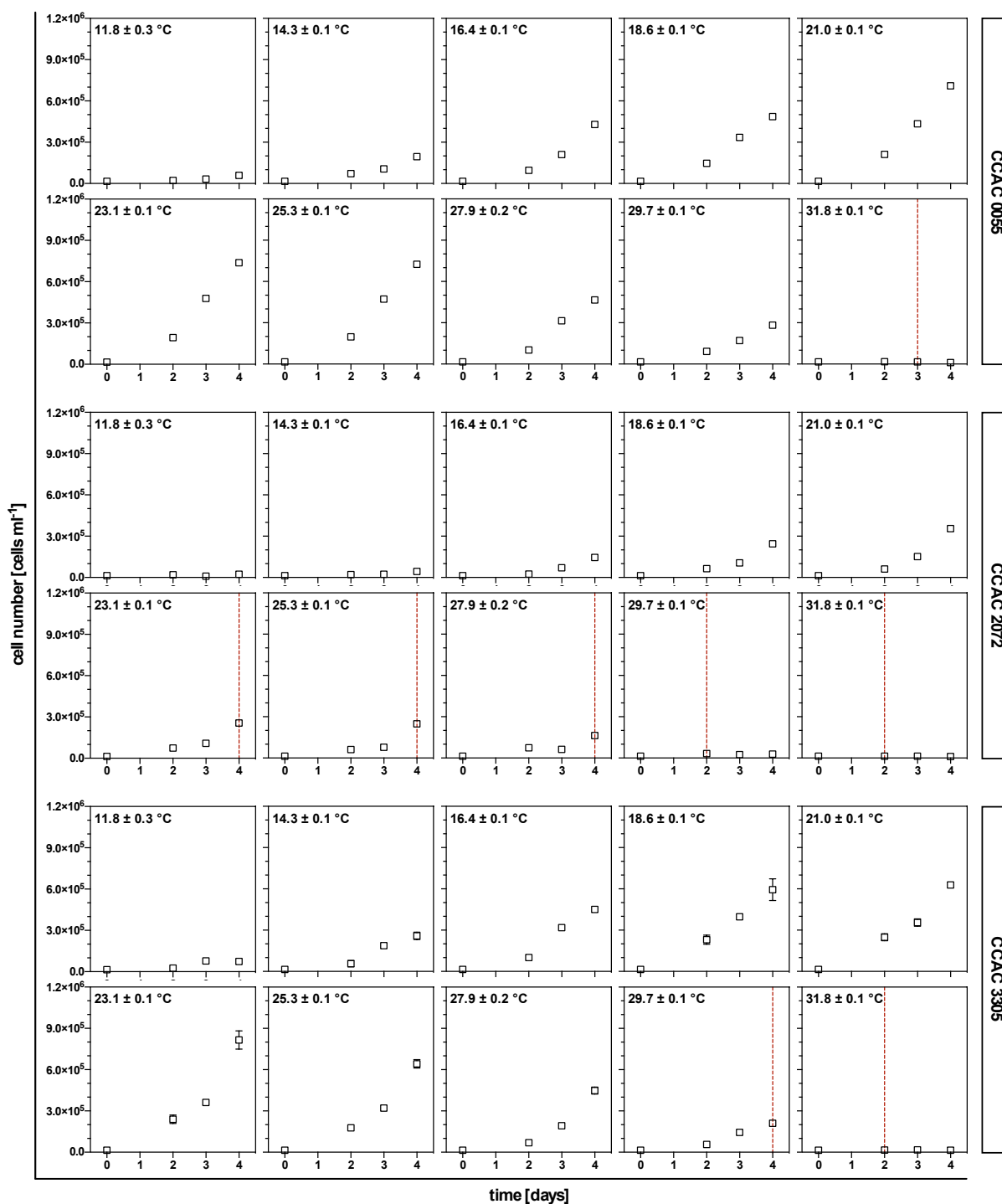


Figure 36 Growth kinetics of CCAC 0055, CCAC 2072 and CCAC 3305 at ten different temperature conditions (11.8 to 31.8°C) and 50 $\mu\text{mol photons m}^{-2} \text{s}^{-1}$. Vertical red, dashed line depicts the first appearance of astaxanthin accumulation. *Mean \pm SE; n=2.*

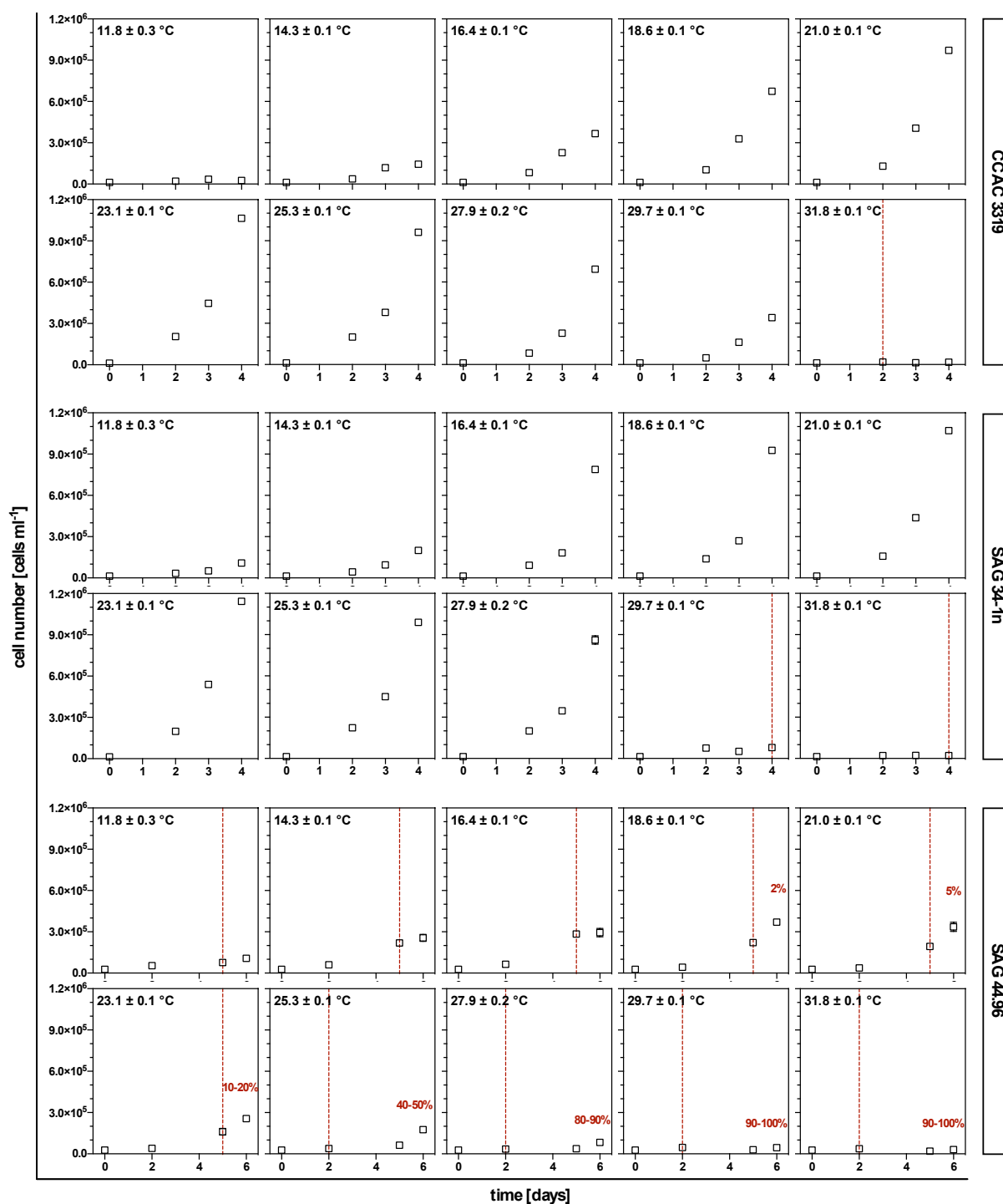


Figure 37 Growth kinetics of CCAC 3319, SAG 34-1n and SAG 44.96 at ten different temperature conditions (11.8 to 31.8 °C) and 50 $\mu\text{mol photons m}^{-2} \text{s}^{-1}$. Vertical red, dashed line depicts the first appearance of astaxanthin accumulation. Bold red values represent the estimated percentage of akinetes. Note that graphs of SAG 44.96 exhibit a different range of the x axis. *Mean \pm SE; n=2.*

7.4 Supplementary data for phylogenetic analyses

7.4.1 IUPAC nucleotide ambiguity code

Table 14 IUPAC nucleotide ambiguity code (www.dnabaser.com)

Code	Represents	Complement
A	Adenine	T
G	Guanine	C
C	Cytosine	G
T	Thymine	A
Y	Pyrimidine (C or T)	R
R	Purine (A or G)	Y
W	weak (A or T)	W
S	strong (G or C)	S
K	keto (T or G)	M
M	amino (C or A)	K
D	A, G, T (not C)	H
V	A, C, G (not T)	B
H	A, C, T (not G)	D
B	C, G, T (not A)	V
X/N	any base	X/N
-	gap	-

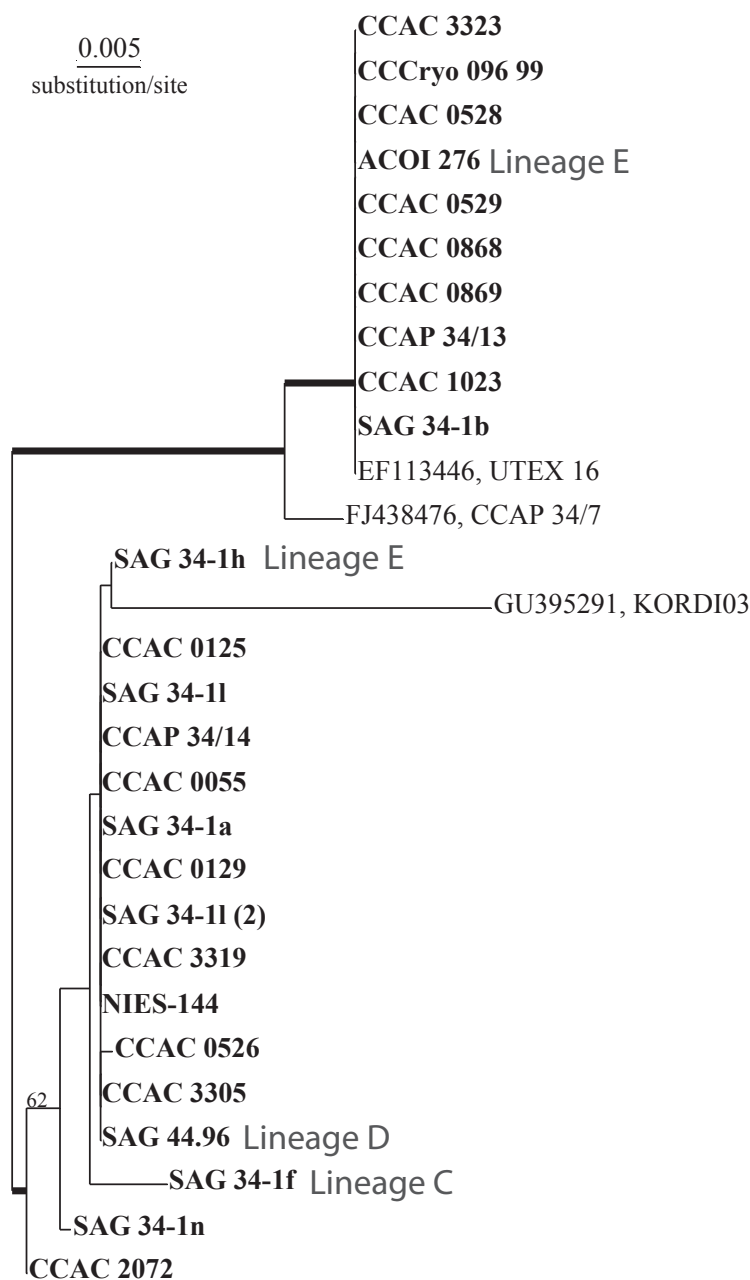
7.4.2 Supplementary data for *rbcL*

Figure 38 Phylogenetic tree from ML analyses of *rbcL* gene. GTR+I+ Γ was used as an evolution model. Values at the branches represent ML-bootstrap from 1,000 pseudo-replicates. Maximum support is indicated by thick branches. Tree comprises 29 taxa. Bold highlighted taxa represent strains subjected in this study. Lineage categories were adapted from Buchheim et al. (2013); unlabeled strains refer to lineage A. Scale bar = 0.005 nucleotide substitutions site⁻¹.

7.4.3 Supplementary data for ITS 2

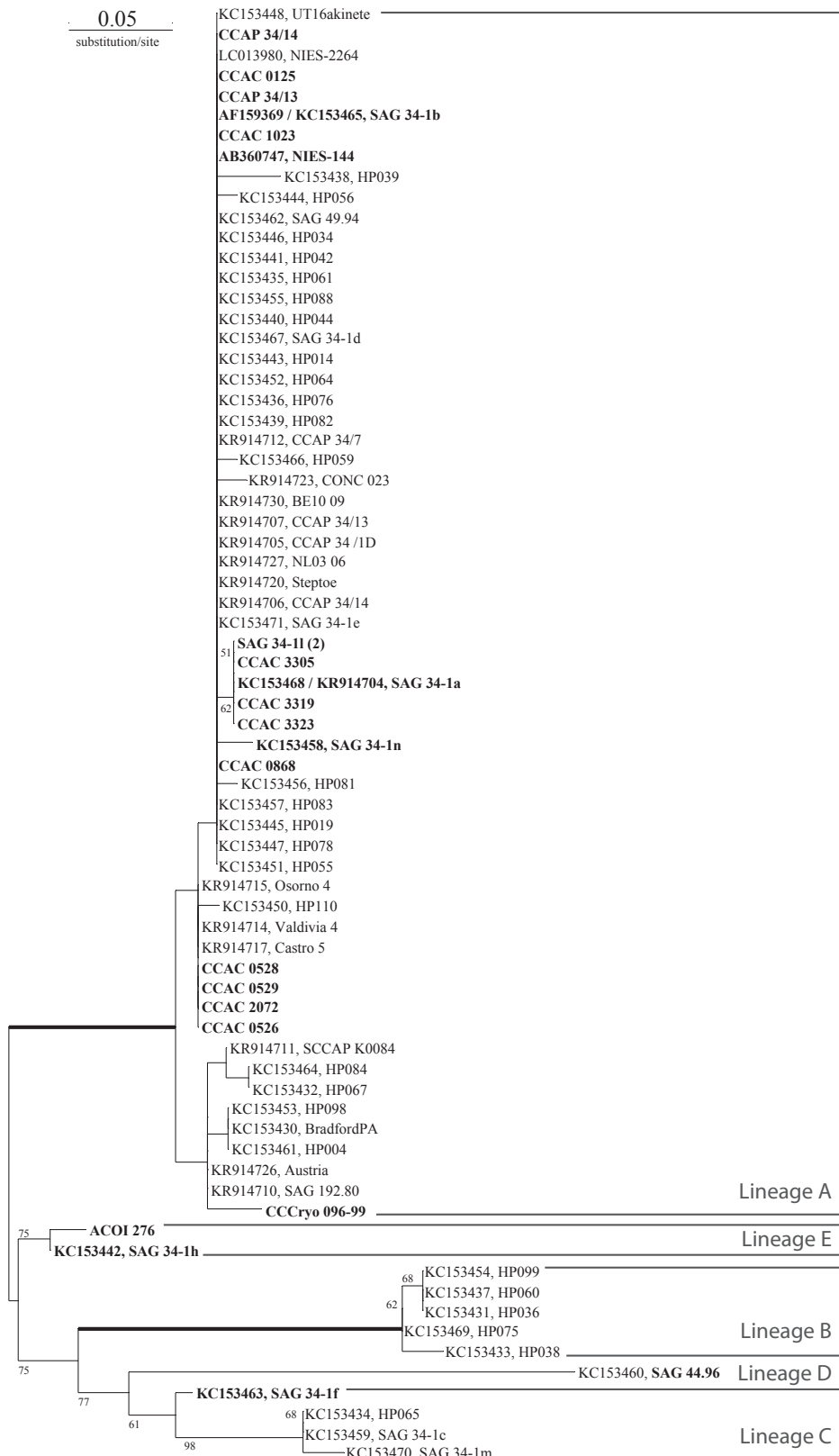


Figure 39 Phylogenetic tree from ML analyses of ITS2 rDNA sequences. GTR+I+ Γ was used as an evolution model. Values at the branches represent ML-bootstrap from 1,000 pseudo-replicates. Maximum support is indicated by thick branches. Tree comprises 72 taxa. Bold highlighted taxa represent strains subjected in this study. Lineage categories were adapted from Buchheim et al. (2013). Scale bar = 0.05 nucleotide substitutions site⁻¹.

7.5 Supplementary information on EMS mutants

7.5.1 Photographs and stereomicrographs of plates



Figure 40 Upside down incubation of agar plates. Plates containing WT and EMS mutants were illuminated with LED light in a custom-made cultivation box. During the experiments the cultivation box was closed with the corresponding lid.

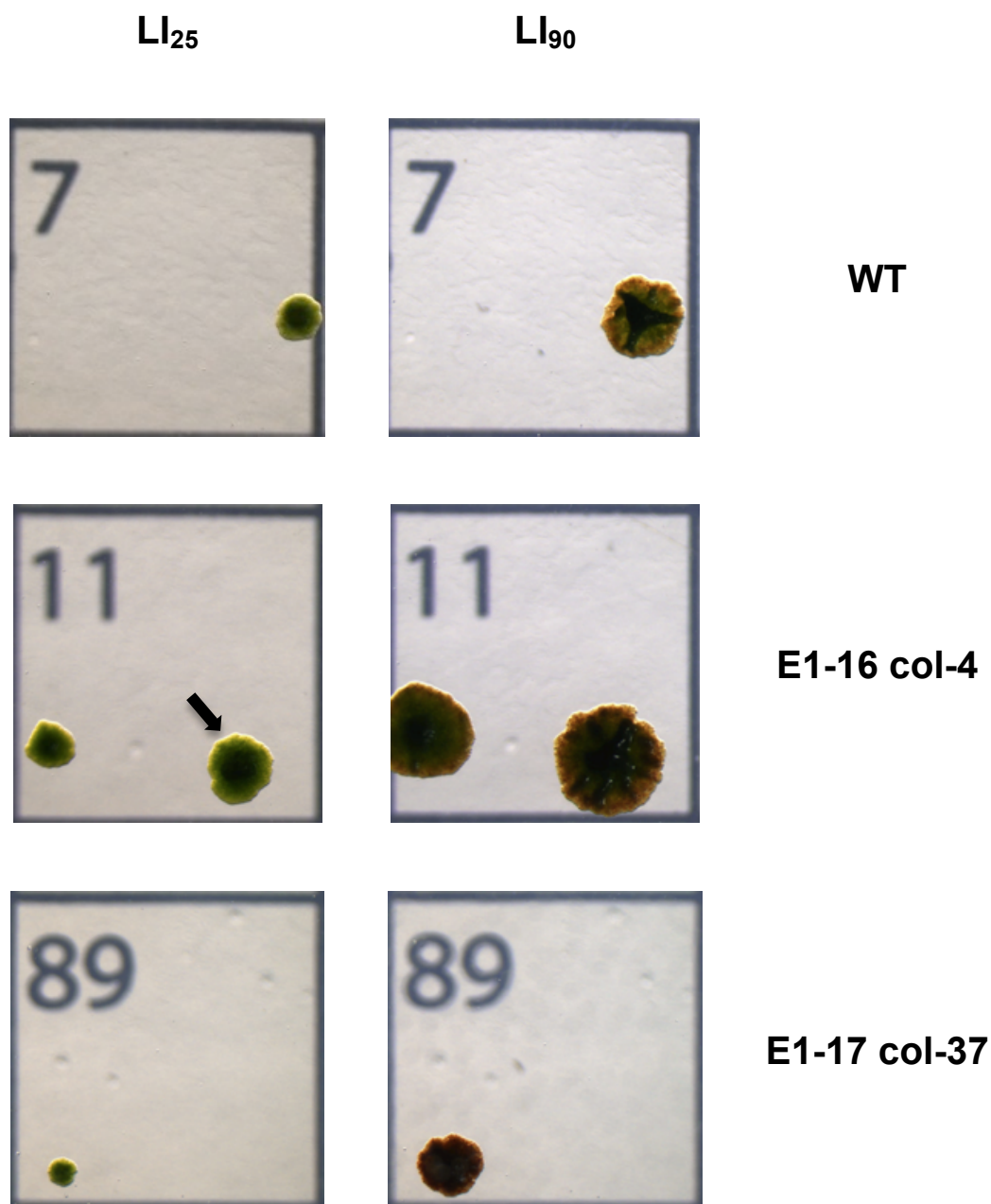


Figure 41 Exemplary stereomicrographs of WT and selected mutants. Cfus consecutively exposed to 25 (LI₂₅) and 90 (LI₉₀) $\mu\text{mol photons m}^{-2} \text{s}^{-1}$ for 3 weeks and eleven days, respectively, were analyzed based on colony diameter and pigmentation. Each square of petri dish grid accounts for 6 mm x 6 mm. Pictures were taken with 7x magnification.

7.5.2 Supplementary data for mutant verification

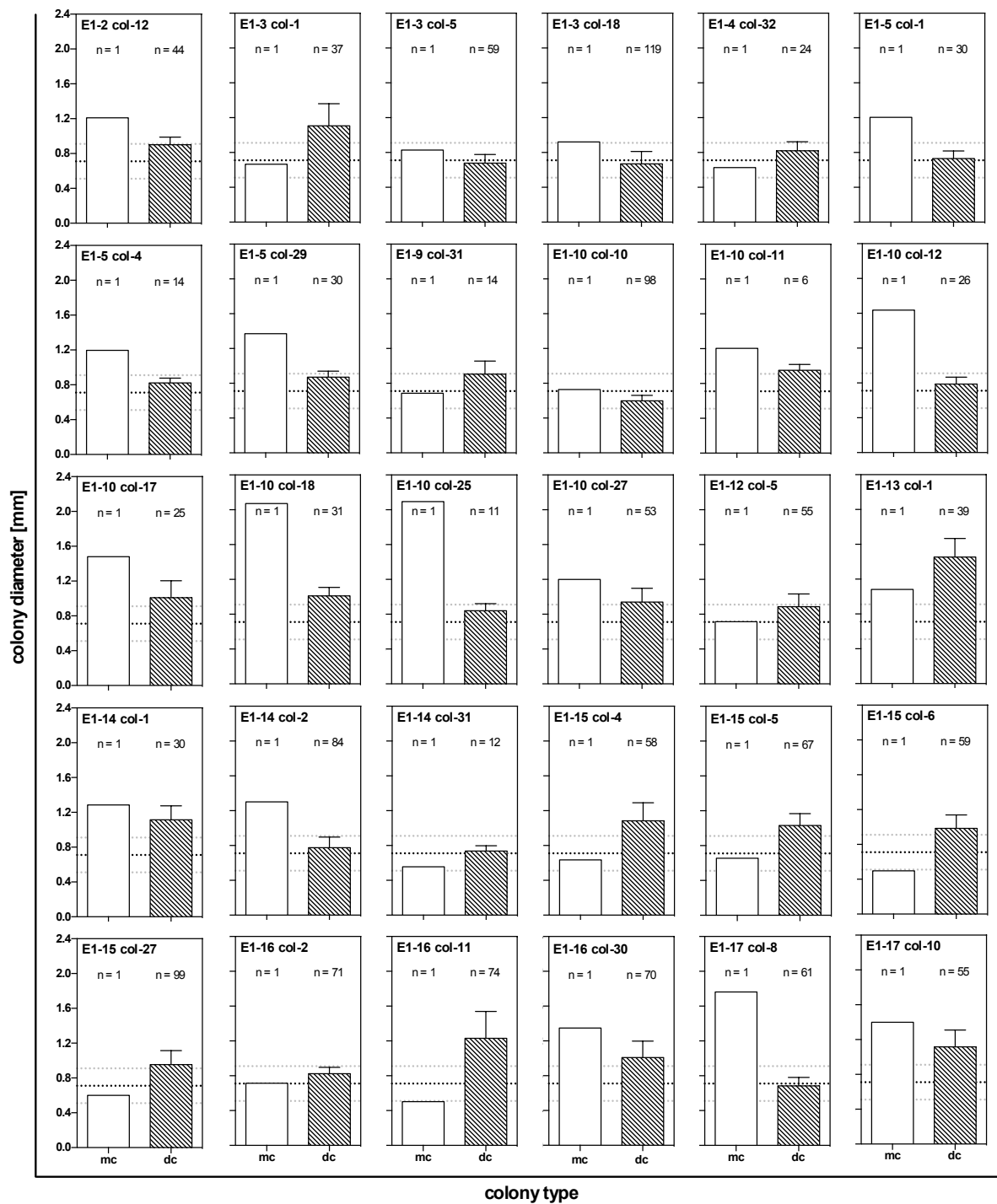


Figure 42 Non-reproducible EMS mutants based on stereomicroscopical analysis of colony diameter. 90 mother colonies (mc) and their corresponding daughter colonies (dc) were not reproducible in colony size. Horizontal dotted lines represent mean (black) and SD (grey) of WT colony diameter.

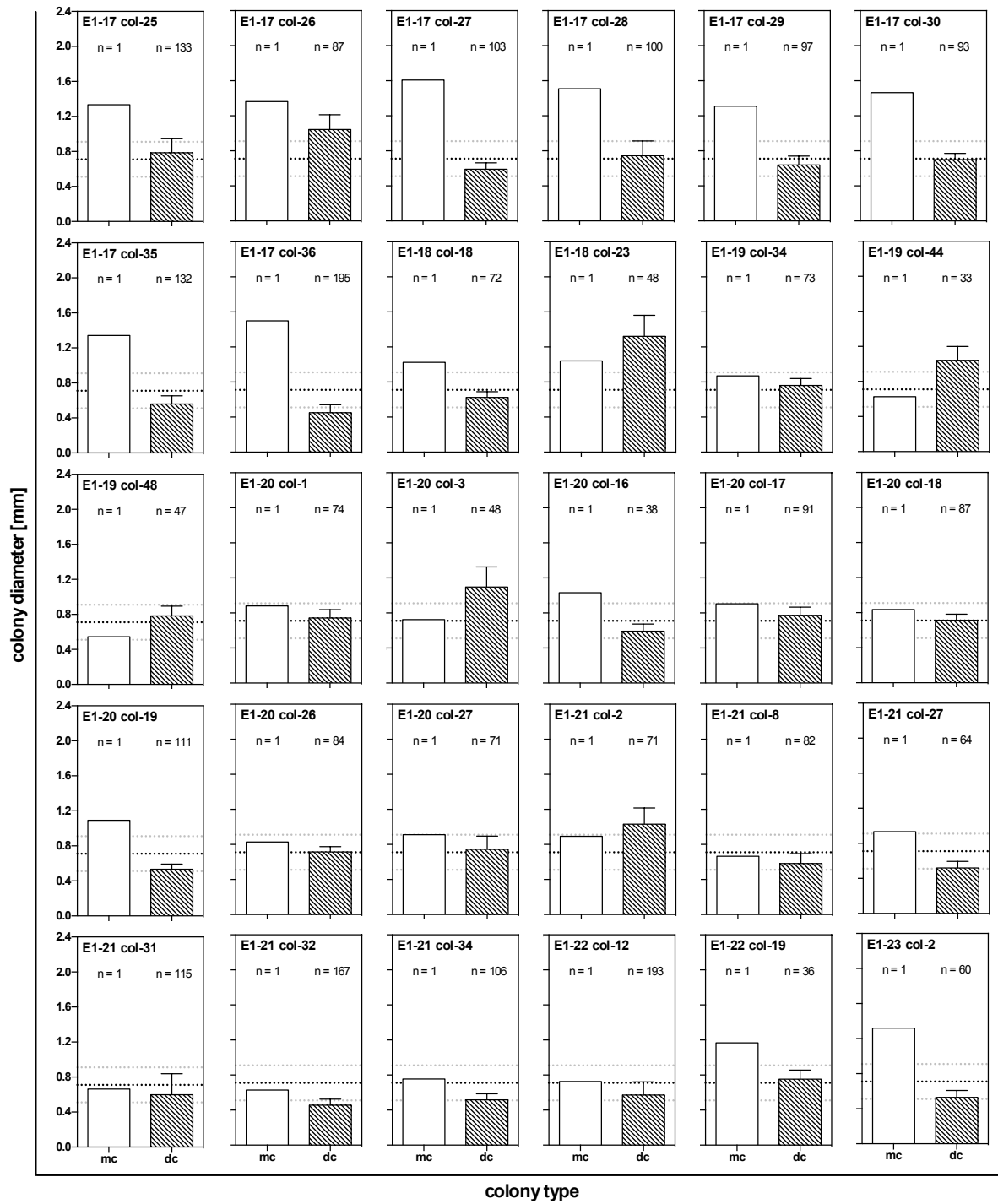


Figure 42 (continuation) Non-reproducible EMS mutants based on stereomicroscopical analysis of colony diameter

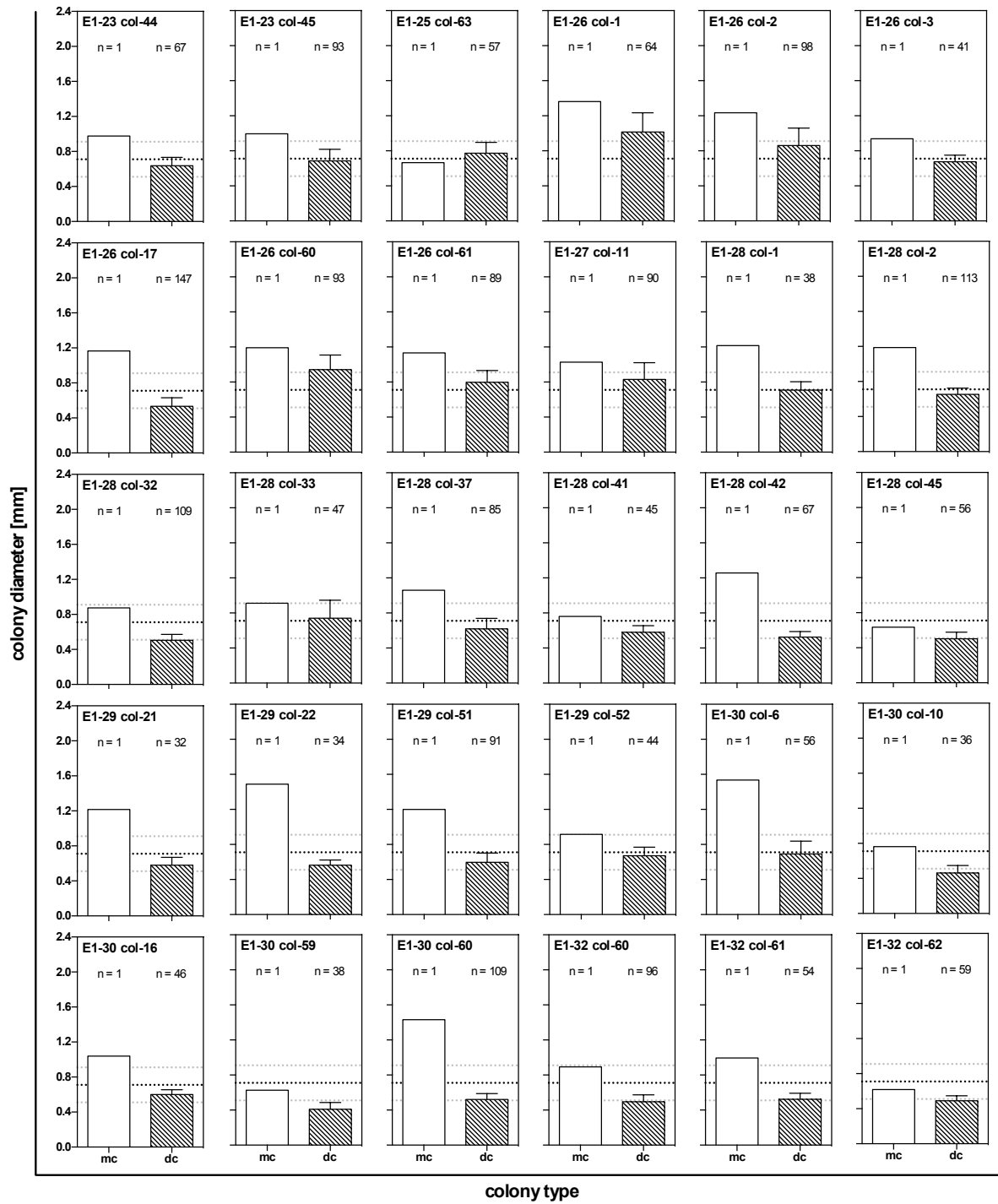


Figure 42 (continuation) Non-reproducible EMS mutants based on stereomicroscopical analysis of colony diameter



Acknowledgements

During my past and present academic studies I had the pleasure to participate in several microalgal research projects within the Melkonian laboratory. Thus, I owe my deepest gratitude to **Prof. Dr. Michael Melkonian** for making all of it possible and for providing me with this challenging PhD project. I am very grateful for his continuous advice and support. I have definitely learned a lot of things broadening both, my theoretical and practical skills.

I would also like to thank **Prof. Dr. Burkhard Becker** (co-examiner) and **Prof. Dr. Siegfried Roth** (chairman) for being part of the examination committee.

Generally, I would like to thank all the **members of the Melkonian lab, Becker lab, CCAC** and especially the **biotech lab** for a pleasant working atmosphere and for their friendly cooperativeness. Furthermore, I would like to thank the **members of the internal workshop** of the Cologne Biocenter; without their competent help, the technical realization of so many ideas wouldn't have been possible.

Special thanks are dedicated to the (formerly) bachelor and master students, **Andreas Franzen, Frederik Koepsell, Irina Maiber and Daniyal Ahmad** who volunteered to participate in my PhD project under my guidance.

Extra thanks are devoted to **Nicole Feja, Dr. Nicole Sausen and Dr. Dorothee Langenbach**. The time with you was always delightful. Thanks for all your motivation and support, also in private.

Last, but not least, I would like to thank my **family and friends** for their continuous support in all kind of situations. Especially, I would like to thank my mother **Ayşe Saliha Çebi**: *Değerli anneciğim, seni sonsuzca seviyorum ve bu doktora tezini sana kalpten ithaf ediyorum!* Thanks to my beloved brothers **Mustafa and Abdulkadir Çebi** for everything you have done for me, all the late night pick-ups from the institute, all the books you have sponsored and all the many other “*abisiii*” things. Finally, thanks to my sister-in-law **Gonca Parlak-Çebi**, you are like a true sister to me and I am very grateful for the association of the Parlak and Çebi clan. Having you all in my life is the greatest gift I can ever imagine 😊



Erklärung

Ich versichere, dass ich die von mir vorgelegte Dissertation selbständig angefertigt, die benutzten Quellen und Hilfsmittel vollständig angegeben und die Stellen der Arbeit – einschließlich Tabellen, Karten und Abbildungen –, die anderen Werken im Wortlaut oder dem Sinn nach entnommen sind, in jedem Einzelfall als Entlehnung kenntlich gemacht habe; dass diese Dissertation noch keiner anderen Fakultät oder Universität zur Prüfung vorgelegen hat; dass sie – abgesehen von unten angegebenen Teilpublikationen – noch nicht veröffentlicht worden ist sowie, dass ich eine solche Veröffentlichung vor Abschluss des Promotionsverfahrens nicht vornehmen werde. Die Bestimmungen der Promotionsordnung sind mir bekannt. Die von mir vorgelegte Dissertation ist von Prof. Dr. Michael Melkonian betreut worden.

Köln, 24. Februar 2017

Zehra Çebi

Zehra Çebi

Lebenslauf

Persönliche Daten

Geburtsdaten	22.12.1982, Köln
Familienstand	Ledig
Nationalität	Türkisch

Bildung

Seit 04/2012	Universität zu Köln – Promotion (Biologie)
	Titel der Dissertation: Efficient microscale screening of various <i>Haematococcus pluvialis</i> strains for growth and astaxanthin production
10/2008 – 03/2011	Universität zu Köln – Master of Science in Biological Sciences
	Titel der Masterarbeit: Cryopreservation of dinoflagellates without the application of cryoprotectants
10/2005 – 09/2008	Universität zu Köln – Bachelor of Science in Biology
	Titel der Bachelorarbeit: Dinoflagellaten als Testsysteme für Ballastwasser
09/2003 – 07/2005	Rheinische Akademie e.V. Köln – staatl. gepr. Biolog.-techn. Assistentin
08/1993 – 06/2002	Dreikönigsgymnasium, Köln – Allgemeine Hochschulreife

Praktika

- 08/2007 – 09/2007 Institut für Luft- und Raumfahrtmedizin, Deutsches Zentrum für Luft- und Raumfahrt (DLR), Köln
- 01/2005 – 02/2005 Institut für Neurophysiologie, Universität zu Köln

Nebentätigkeiten

- 10/2016 – 02/2017 Botanisches Institut, Universität zu Köln – Biolog.-techn. Assistentin
- 07/2013 – 09/2015 Botanisches Institut, Universität zu Köln – Biolog.-techn. Assistentin
- 07/2012 – 03/2013 Botanisches Institut, Universität zu Köln – Wissenschaftliche Mitarbeiterin
- 04/2011 – 07/2011 Botanisches Institut, Universität zu Köln – Wissenschaftliche Hilfskraft
- 05/2009 – 03/2011 Botanisches Institut, Universität zu Köln – Studentische Hilfskraft
- 11/2008 – 03/2009 ALPHA COM Deutschland GmbH, Köln – Büroaushilfe
- 09/2008 – 10/2008 Botanisches Institut, Universität zu Köln – Studentische Hilfskraft
- 10/2007 – 06/2008 ALPHA COM Deutschland GmbH, Köln – Büroaushilfe
- 04/2006 – 06/2006 Institut für Genetik, Universität zu Köln – Studentische Hilfskraft

Publikationen

Benstein, R.M., **Çebi, Z.**, Podola, B., Melkonian, M. (2014). Immobilized growth of the peridinin-producing marine dinoflagellate *Symbiodinium* in a simple biofilm photobioreactor. *Marine Biotechnology* 16: 621-628.

Naumann, T., **Çebi, Z.**, Podola, B., Melkonian, M. (2013). Growing microalgae as aquaculture feeds on twin-layers: a novel solid-state photobioreactor. *Journal of Applied Phycology* 25: 1413-1420.

Köln, 28.11.2016